

NQ

7 7 0 5 7

U M I
MICROFILMED 2003

INFORMATION TO USERS

This manuscript has been reproduced from the microfilm master. UMI films the text directly from the original or copy submitted. Thus, some thesis and dissertation copies are in typewriter face, while others may be from any type of computer printer.

The quality of this reproduction is dependent upon the quality of the copy submitted. Broken or indistinct print, colored or poor quality illustrations and photographs, print bleedthrough, substandard margins, and improper alignment can adversely affect reproduction.

In the unlikely event that the author did not send UMI a complete manuscript and there are missing pages, these will be noted. Also, if unauthorized copyright material had to be removed, a note will indicate the deletion.

Oversize materials (e.g., maps, drawings, charts) are reproduced by sectioning the original, beginning at the upper left-hand corner and continuing from left to right in equal sections with small overlaps.

**ProQuest Information and Learning
300 North Zeeb Road, Ann Arbor, MI 48106-1346 USA
800-521-0600**

UMI[®]

LAMINAR AND TURBULENT FLOW AND HEAT TRANSFER CHARACTERISTICS OF CONFINED IMPINGING STREAMS

Sakamon Devahastin

Department of Chemical Engineering
McGill University
Montreal, Quebec, Canada



**A thesis submitted to the Faculty of Graduate Studies and Research in partial fulfillment
of the requirements for the degree of Doctor of Philosophy**

© Sakamon Devahastin, June 2001



**National Library
of Canada**

**Acquisitions and
Bibliographic Services**

**395 Wellington Street
Ottawa ON K1A 0N4
Canada**

**Bibliothèque nationale
du Canada**

**Acquisitions et
services bibliographiques**

**395, rue Wellington
Ottawa ON K1A 0N4
Canada**

Your file Votre référence

Our file Notre référence

The author has granted a non-exclusive licence allowing the National Library of Canada to reproduce, loan, distribute or sell copies of this thesis in microform, paper or electronic formats.

The author retains ownership of the copyright in this thesis. Neither the thesis nor substantial extracts from it may be printed or otherwise reproduced without the author's permission.

L'auteur a accordé une licence non exclusive permettant à la Bibliothèque nationale du Canada de reproduire, prêter, distribuer ou vendre des copies de cette thèse sous la forme de microfiche/film, de reproduction sur papier ou sur format électronique.

L'auteur conserve la propriété du droit d'auteur qui protège cette thèse. Ni la thèse ni des extraits substantiels de celle-ci ne doivent être imprimés ou autrement reproduits sans son autorisation.

0-612-77057-5

Canada

PREFACE

The author, Sakamon Devahastin, of this thesis chooses the manuscript-based thesis option according to the following thesis preparation guideline given by the Faculty of Graduate Studies and Research:

Candidates have the option of including, as part of the thesis, the text of one or more papers submitted, or to be submitted, for publication, or the clearly duplicated text of one or more published papers. These texts must conform to the "Guidelines for Thesis Preparation" with respect to font size, line spacing and margin sizes and must be bound together as an integral part of the thesis.

The thesis must be more than a collection of manuscripts. All components must be integrated into a cohesive unit with a logical progression from one chapter to the next. In order to ensure that the thesis has continuity, connecting texts that provide logical bridges between the different papers are mandatory.

The thesis must conform to all other requirements of the "Guidelines for Thesis Preparation" in addition to the manuscripts. The thesis must include: a table of contents, an abstract in English and French, an introduction which clearly states the rational and objectives of the research, a comprehensive review of the literature, a final conclusion and summary, and a thorough bibliography or reference list.

Additional material must be provided, where appropriate, in sufficient detail to allow a clear and precise judgement to be made of the importance and originality of the research reported in the thesis.

When co-authored papers are included in a thesis the candidate must have made a substantial contribution to all papers included in the thesis. In addition, the candidate is required to make an explicit statement in the thesis as to who contributed to such work and to what extent. The supervisor must attest to the accuracy of such statements at the doctoral oral defense. Since the task of the examiners is made more difficult in these cases, it is in the candidate's interest to clearly specify the responsibilities of all the authors of the co-authored papers.

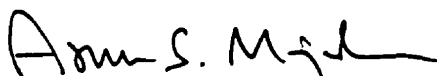
I, Arun S. Mujumdar, hereby give copyright clearance of the following manuscripts of which I am a co-author. The "extent of my contribution" to the following manuscripts is that of a research supervisor. I provided laboratory space, technical consultation as well as general supervision throughout the duration of this Ph.D. thesis.

Chapter 3

- Devahastin, S., Mujumdar, A.S., A numerical study of flow and mixing characteristics of laminar confined impinging streams, to appear in *Chemical Engineering Journal*.
- Devahastin, S., Mujumdar, A.S., A numerical study of mixing in a novel impinging stream in-line mixer, to appear in *Chemical Engineering and Processing*.

Chapter 4

- Devahastin, S., Mujumdar, A.S., A study of turbulent mixing of confined impinging streams using a new composite turbulence model, submitted to *Industrial & Engineering Chemistry Research*.



Arun S. Mujumdar, Professor
Department of Mechanical Engineering
National University of Singapore, Singapore

ABSTRACT

Studies were performed to investigate the flow, heat transfer as well as mixing characteristics of two-dimensional laminar and turbulent confined impinging streams. In the first part numerical simulations were conducted to study the flow and mixing behavior of two-dimensional laminar confined impinging streams. Reynolds numbers beyond which the flow becomes oscillatory and even random were determined for different geometric configurations. Simulations were performed for cases with jet Reynolds numbers in the stable regime to study the mixing characteristics of the system. Numerical simulations were also conducted to study fluid mixing in a novel two-dimensional in-line mixer utilizing multiple impinging stream inlets. Offsetting the top and bottom inlet jets is found effective in improving the quality of mixing due to the presence of intense mixing zones between the inlet jets.

In the second part a study of turbulent flow and heat transfer in two-dimensional confined impinging streams was conducted. A new composite turbulence model is proposed and verified by comparing its predictions with available experimental impingement heat transfer data as well as the experimental velocity and temperature distributions in impinging streams obtained in this work. Better agreement between experimental and numerical results predicted by this new model is noted compared to those predicted by other low-Reynolds number k - ϵ turbulence models tested. The model

was then used to perform a parametric study of the mixing characteristics of two-dimensional turbulent confined impinging streams.

Finally, a numerical study of the gas-particle flow and drying in turbulent two-dimensional confined impinging streams was conducted. Continuous-phase conservation equations are written in the Eulerian frame while the particle equations are written in the Lagrangian frame. Two-way physical coupling between the continuous and particulate phases is taken into account in the governing conservation equations. Monte Carlo stochastic approach is used to model particle dispersion due to the turbulent fluctuations of the continuous-phase velocity. Effects of various operating parameters on the flow and drying behavior of the system are reported and discussed.

RÉSUMÉ

Des études ont été conduites afin d'étudier l'écoulement, le transfert de chaleur ainsi que la façon dont s'effectue le mélange des jets d'air qui se rencontrent tant dans un régime laminaire que turbulent. On a déterminé les nombres de Reynolds en fonction de différentes configurations géométriques y compris dans la région où l'écoulement devient saccadé ou même aléatoire. Des simulations ont été effectuées pour les cas où les nombres de Reynolds correspondent à un régime stable en vue d'étudier le phénomène de mélange des jets. On a ensuite effectué des simulations numériques afin d'étudier la façon dont les fluides se mélangent dans un nouveau type de mélangeur. C'est un système à deux dimensions où plusieurs jets d'air se rencontrent au fur et à mesure. On a ainsi réussi à mettre en évidence, qu'en décalant les parties supérieure et inférieure de l'entrée d'air, il a été possible d'améliorer la qualité du mélange. Ceci a été possible grâce à la présence de zones où le mélange s'effectue d'une façon plus intense. Ces zones se situent entre les entrées des différents jets.

Dans une seconde partie de ce travail, on a étudié le transfert de chaleur dans les écoulements bidimensionnels en régime turbulent, à l'endroit où des jets d'air se rencontrent. Suite à ces études, un nouveau modèle composite a été proposé. Ce modèle a été validé en comparant les prédictions avec les valeurs expérimentales. Parmi les paramètres étudiés figurent le transfert de chaleur, la vitesse ainsi que la distribution de températures mesurées lors de l'interaction des jets d'air. On a trouvé que les valeurs

expérimentales montrent une meilleure corrélation avec le nouveau modèle qu'avec ceux utilisés habituellement. Ces derniers sont valables également en régime turbulent mais pour des nombres de Reynolds peu élevés ainsi que des paramètres $k-\varepsilon$ différents de ceux du nouveau modèle. Par la suite, le nouveau modèle a été utilisé pour effectuer des études spécifiques aux paramètres intervenant dans le phénomène de mélange lors de la rencontre des jets d'air. Ces études ont considéré un système à deux dimensions et un régime turbulent.

Enfin, nous avons effectué une étude numérique du mouvement des particules de gaz et des phénomènes de séchage dans un système à deux dimensions où des jets d'air sont en contact direct en régime turbulent. Les équations représentant la conservation dans la phase continue ont été présentées dans un cadre eulérien tandis que celles représentant le mouvement des particules l'ont été dans un cadre lagrangien. Lors du développement des équations de conservation, on a tenu compte des couplages qui existent entre la phase continue et le comportement des particules individuelles. La méthode stochastique de type Monte Carlo a été employée pour développer le modèle de dispersion des particules due aux variations de vitesse d'air dans la phase continue. On a également observé et décrit les effets des différents paramètres opérationnels sur l'écoulement et sur le déroulement du procédé de séchage dans le système considéré par cette étude.

ACKNOWLEDGEMENTS

First of all I would like to express my sincerest appreciation to my academic advisor, Prof. Arun S. Mujumdar, for his advice, encouragement and support during the past half decade of my master's and doctoral research under his supervision. His mentorship extends, in fact, far beyond the supervision of the theses. The opportunities he gave me to work on and learn from different projects are greatly appreciated.

Several other persons also deserve my appreciation. Brian Kao was very helpful in an early stage of the experimental set-up. Dr. Patrice Nadeau and Jennifer Wu helped with the setting up of a laser Doppler anemometer. Zhi-Yuan Bi was very helpful at various stages of the experimental work. Mrs. Purnima Mujumdar helped tirelessly with the revision of several parts of the text. A friendship of Pattita Suwanruji, Zhi-Yuan Bi, Hongsun Seon, Essau Sanga, Siripon Anantawaraskul and Orasa Tavichai made life much more pleasant and is warmly appreciated. Thanks are also due to the staff of the Chemical Engineering Department, particularly Mr. Walter Greenland and Mr. Lou Cusmich, for their help in the fabrication of the equipment.

Acknowledgement is also due to Dr. George Srzednicki of the University of New South Wales, Australia for his help in the preparation of the French version of the thesis abstract.

Last, but far from least, I am vastly indebted to my parents for their love and endless support without which I would have never reached this stage of accomplishment. The least I could do is to dedicate this thesis to them.

TABLE OF CONTENTS

Preface	i
Abstract	iii
Résumé	v
Acknowledgements	vii
Table of Contents	ix
List of Figures	xii
List of Table	xvii

CHAPTER 1 INTRODUCTION

1.1 General Introduction	1
1.2 Objectives	3
1.3 Thesis Layout	3
References	4

CHAPTER 2 BACKGROUND

2.1 Introduction	6
------------------	---

2.2 General Studies of Impinging Streams	6
2.3 Laminar Impinging Streams	10
2.4 Turbulent Impinging Streams	12
2.5 Gas-Particle Impinging Streams	14
References	17

CHAPTER 3 FLOW AND MIXING CHARACTERISTICS OF TWO-DIMENSIONAL LAMINAR CONFINED IMPINGING STREAMS

3.1 Introduction	23
3.2 Mathematical Formulation	26
3.3 Results and Discussion	30
3.3.1 Flow and Mixing Characteristics of Laminar Confined Impinging Streams	30
3.3.2 Flow and Mixing Characteristics of a Novel Impinging Stream In-line Mixer	42
Closing Remarks	54
Nomenclature	58
References	59

CHAPTER 4 HEAT TRANSFER AND MIXING CHARACTERISTICS OF TWO-DIMENSIONAL TURBULENT CONFINED IMPINGING STREAMS

4.1 Introduction	62
4.2 Experimental Set-Up and Procedure	64
4.3 Mathematical Formulation	72
4.4 Results and Discussion	76
Closing Remarks	88
Nomenclature	89
References	91

CHAPTER 5 FLOW AND DRYING CHARACTERISTICS OF TWO-DIMENSIONAL GAS-PARTICLE IMPINGING STREAMS

5.1 Introduction	94
5.2 Mathematical Formulation	96
5.2.1. Continuous-Phase Equations	96
5.2.2. Disperse-Phase Equations	99
5.2.2.1. Particle Position Equation	99
5.2.2.2. Particle Momentum Equation	99
5.2.2.3. Particle Mass Equation	101
5.2.2.4. Particle Enthalpy Equation	102
5.2.3. Turbulent Dispersion of Particles	102
5.2.4. Calculation of Interactive Source Terms	104
5.2.4.1. Mass Transfer Source	104
5.2.4.2. Momentum Transfer Source	104
5.2.4.3. Enthalpy Transfer Source	104
5.2.5. Particle-Wall Interaction	105
5.2.6. Boundary Conditions	105
5.3 Results and Discussion	107
Closing Remarks	115
Nomenclature	116
References	119

CHAPTER 6 CONCLUSIONS, CONTRIBUTIONS TO KNOWLEDGE AND RECOMMENDATIONS

6.1 Conclusions	122
6.2 Contributions to Knowledge	125
6.3 Recommendations	126

LIST OF FIGURES

CHAPTER 1 INTRODUCTION

1.1	Basic concept of impinging streams	2
-----	------------------------------------	---

CHAPTER 3 FLOW AND MIXING CHARACTERISTICS OF TWO-DIMENSIONAL LAMINAR CONFINED IMPINGING STREAMS

3.1	Schematic diagram of the impinging streams studied in the first part	24
3.2	Schematic diagram of the two-dimensional channel mixer studied in the second part	25
3.3	Schematic diagram of the junction used in model verification	29
3.4	Comparison of dimensionless axial velocity profiles. $Re = U_0 H \rho / \mu$, $X = 5$	29
3.5	Flow regime diagram	31
3.6	Some oscillating patterns of velocity component in y -direction	
	(a) $H/W = 1.0$; $x/W/2 = 1.0$; $Re_j = 4000$	33
	(b) $H/W = 1.0$; $x/W/2 = 50$; $Re_j = 4000$	33
	(c) $H/W = 3.0$; $x/W/2 = 1.0$; $Re_j = 500$	33
	(d) $H/W = 3.0$; $x/W/2 = 50$; $Re_j = 500$	33

3.7	Some fluctuating patterns of velocity component in y -direction	
	(a) $H/W = 1.0$; $x/W/2 = 1.0$; $Re_j = 7500$	34
	(b) $H/W = 1.0$; $x/W/2 = 50$; $Re_j = 7500$	34
	(c) $H/W = 2.0$; $x/W/2 = 1.0$; $Re_j = 3000$	34
	(d) $H/W = 2.0$; $x/W/2 = 50$; $Re_j = 3000$	34
3.8a	Velocity vectors and temperature contours. $H/W = 1.0$; $Re_j = 200$	35
3.8b	Velocity vectors and temperature contours. $H/W = 4.0$; $Re_j = 200$	36
3.9a	Mixing index for $H/W = 1.0$	37
3.9b	Mixing index for $H/W = 2.0$	38
3.9c	Mixing index for $H/W = 3.0$	38
3.9d	Mixing index for $H/W = 4.0$	39
3.10a	Mixing index for $Re_j = 10$	40
3.10b	Mixing index for $Re_j = 50$	40
3.10c	Mixing index for $Re_j = 100$	41
3.10d	Mixing index for $Re_j = 200$	41
3.11a	Velocity vectors. $H/W = 2.0$; $S/W = 2.0$; $Re_j = 50$	43
3.11b	Temperature contours. $H/W = 2.0$; $S/W = 2.0$; $Re_j = 50$	44
3.12	Mixing index	
	(a) $H/W = 1.0$; $S/W = 1.0$	45
	(b) $H/W = 1.0$; $S/W = 2.0$	45
	(c) $H/W = 1.0$; $S/W = 3.0$	45
	(d) $H/W = 2.0$; $S/W = 1.0$	46
	(e) $H/W = 2.0$; $S/W = 2.0$	46
	(f) $H/W = 2.0$; $S/W = 3.0$	46
	(g) $H/W = 3.0$; $S/W = 1.0$	47
	(h) $H/W = 3.0$; $S/W = 2.0$	47
	(i) $H/W = 3.0$; $S/W = 3.0$	47
3.13	Mixing index	
	(a) $H/W = 1.0$; $Re_j = 10$	48
	(b) $H/W = 1.0$; $Re_j = 50$	48
	(c) $H/W = 1.0$; $Re_j = 100$	48

(d) $H/W = 2.0$; $Re_j = 10$	49
(e) $H/W = 2.0$; $Re_j = 50$	49
(f) $H/W = 2.0$; $Re_j = 100$	49
(g) $H/W = 3.0$; $Re_j = 10$	50
(h) $H/W = 3.0$; $Re_j = 50$	50
(i) $H/W = 3.0$; $Re_j = 100$	50
3.14 Mixing index	
(a) $S/W = 1.0$; $Re_j = 10$	51
(b) $S/W = 1.0$; $Re_j = 50$	51
(c) $S/W = 1.0$; $Re_j = 100$	51
(d) $S/W = 2.0$; $Re_j = 10$	52
(e) $S/W = 2.0$; $Re_j = 50$	52
(f) $S/W = 2.0$; $Re_j = 100$	52
(g) $S/W = 3.0$; $Re_j = 10$	53
(h) $S/W = 3.0$; $Re_j = 50$	53
(i) $S/W = 3.0$; $Re_j = 100$	53
3.15 Mixing index in the exit channel	
(a) $H/W = 1.0$; $S/W = 1.0$	55
(b) $H/W = 1.0$; $S/W = 2.0$	55
(c) $H/W = 1.0$; $S/W = 3.0$	55
(d) $H/W = 2.0$; $S/W = 1.0$	56
(e) $H/W = 2.0$; $S/W = 2.0$	56
(f) $H/W = 2.0$; $S/W = 3.0$	56
(g) $H/W = 3.0$; $S/W = 1.0$	57
(h) $H/W = 3.0$; $S/W = 2.0$	57
(i) $H/W = 3.0$; $S/W = 3.0$	57

CHAPTER 4 HEAT TRANSFER AND MIXING CHARACTERISTICS OF TWO-DIMENSIONAL TURBULENT CONFINED IMPINGING STREAMS

4.1a A schematic diagram of the overall heat transfer experimental set-up	65
--	-----------

4.1b	Detailed diagram of the IS used in the heat transfer experiments	66
4.1c	Locations of thermocouples used in the heat transfer experiments	66
4.1d	A photograph of the overall heat transfer experimental set-up	67
4.1e	A photograph of the IS used in the heat transfer experiments	67
4.2a	A schematic diagram of the overall flow experimental set-up	68
4.2b	Detailed diagram of the IS used in the flow experiments	68
4.2c	A photograph of the overall flow experimental set-up (front view)	70
4.2d	A photograph of the overall flow experimental set-up (rear view)	70
4.2e	A photograph of electronic components of an LDV	71
4.2f	A lens mask used in the flow experiments	72
4.3	Impinging jet configuration used in model verification	77
4.4a	Comparison between predicted and experimental local Nusselt number profiles along the impingement surface. $Re_j = 10400$; $H/W = 2.6$	78
4.4b	Comparison between predicted and experimental local Nusselt number profiles along the impingement surface. $Re_j = 5200$; $H/W = 6.0$	78
4.5	Comparison between predicted and experimental normalized temperature	
	(a) $Re_j = 18000-18000$; $I = 2\%$; $\Delta T = 20^\circ \text{C}$; normalized $T = 40^\circ \text{C}$	80
	(b) $Re_j = 20000-10000$; $I = 2\%$; $\Delta T = 10^\circ \text{C}$; normalized $T = 30^\circ \text{C}$	80
4.6a	Comparison between predicted and experimental normalized velocity profiles in IS. $Re_j = 12600$; $I = 15\%$; normalized $U = 0 \text{ m s}^{-1}$	81
4.6b	Comparison between predicted and experimental normalized turbulence intensity profiles in IS. $Re_j = 12600$; $I = 15\%$; normalized $I = 0\%$	82
4.7a	Mixing index for $H/W = 1.0$; $I = 1\%$	84
4.7b	Mixing index for $H/W = 1.0$; $I = 2\%$	85
4.7c	Mixing index for $H/W = 2.0$; $I = 1\%$	85
4.7d	Mixing index for $H/W = 2.0$; $I = 2\%$	86
4.8	Mixing index for $Re_j = 20000$; $I = 1\%$	87
4.9	Mixing index for $H/W = 1.0$; $Re_j = 20000$	88

CHAPTER 5 FLOW AND DRYING CHARACTERISTICS OF TWO-DIMENSIONAL GAS-PARTICLE IMPINGING STREAMS

5.1	Schematic diagram of a one-way exit IS used in the present study	106
5.2	Impinging jet configuration used in model validation	107
5.3	Comparison of gas-phase mean velocity profiles	109
5.4	Profiles of mean gas-phase velocities at $x/W = 1$	110
5.5a	Comparison of gas-phase mean velocity profiles. $Re_j = 10000; I = 1\%; T_0 = 100^\circ\text{C}; D_p = 500 \mu\text{m}; \Gamma_0 = 0.1$	112
5.5b	Comparison of gas-phase mean temperature profiles $Re_j = 10000; I = 1\%; T_0 = 100^\circ\text{C}; D_p = 500 \mu\text{m}; \Gamma_0 = 0.1$	112
5.6	Moisture content profiles in an IS flash dryer $Re_j = 10000; I = 1\%; T_0 = 100^\circ\text{C}; \Gamma_0 = 0.1$	114
5.7	Moisture content profiles in an IS flash dryer $Re_j = 10000; I = 1\%; D_p = 500 \mu\text{m}; \Gamma_0 = 0.1$	115

LIST OF TABLE

CHAPTER 5 FLOW AND DRYING CHARACTERISTICS OF TWO-DIMENSIONAL GAS-PARTICLE IMPINGING STREAMS

5.1	Thermodynamic and Transport Properties of Air-Water System Used in the Present Study	111
------------	---	------------

INTRODUCTION

*The first step to knowledge
is to know that we are ignorant
Socrates*

1.1. GENERAL INTRODUCTION

Impinging streams (IS) constitute a relatively new and unique class of flow configuration. It was first suggested and tested by Elperin (1961) in the early 1960's as a method for intensifying transfer processes in heterogeneous system (Tamir, 1994). Since then a number of engineering unit operations have been successfully conducted in IS (Tamir, 1989; Tamir, 1994). Among other synonyms for IS found in the literature are colliding jets, opposed jets, opposing currents, interacting streams and counterflowing streams.

The basic concept of IS is illustrated in Figure 1.1. Two inlet streams enter the system through two closely spaced inlets along the same axis in opposite directions. As a result of the impingement (or collision) of the opposed streams, a relatively narrow zone, which offers excellent conditions for transport processes is created. The streams then leave the system through the exits situated symmetrically on either side of the impingement region.

For heterogeneous systems particles or droplets can be introduced to either or both of the two fluid streams. The opposed flow of suspensions encourages multiple inter-particle collisions as well as mutual penetration and multiple circulation of particles

from one stream into the other. The penetration of particles into the opposed stream arises due to their inertia whereas deceleration takes place due to drag forces exerted on particles by the opposed stream. At the end of the deceleration path particles are accelerated and once again regain their original stream. After performing several such damped oscillatory motions the particle velocity eventually vanishes and particles are withdrawn from the system. This unique flow configuration results in a significant enhancement of heat and mass transfer processes as reported by several investigators (e.g., Gaddis and Vogelpohl, 1992; Hosseinalipour and Mujumdar, 1995; Hosseinalipour and Mujumdar, 1997; Kleingeld et al., 1999; Berman et al., 2000a,b; Mujumdar et al., 2000).

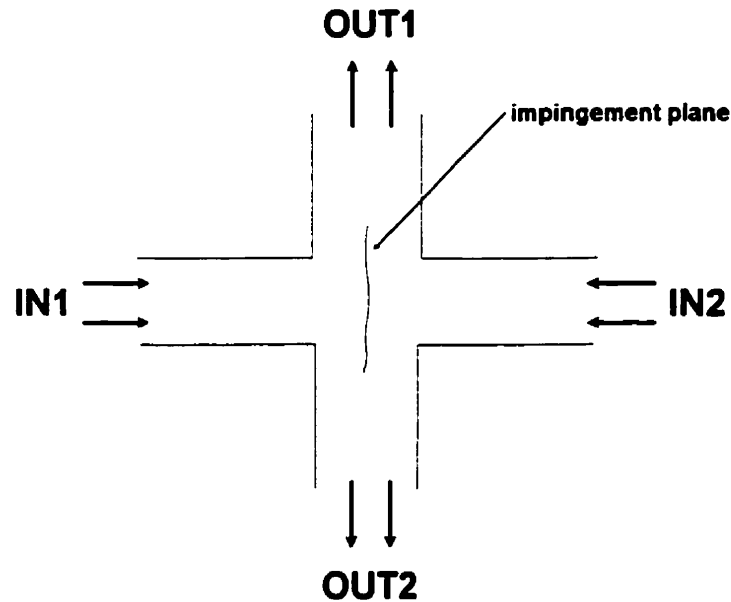


Figure 1.1. Basic concept of impinging streams

Although a number of publications, as partially reviewed in Chapter 2, have reported uses of IS in various applications, very few papers are focused on studies of fundamental transport processes in this flow configuration even in the laminar flow regime. A study of basic transport phenomena along with the development of a reliable model to predict the behavior of the system, as affected by various geometric and

operating parameters, is needed before a smooth design and optimization of the system, which would lead to a wider use of it in industry, can be performed.

1.2. OBJECTIVES

The motivation of this research was to study the fundamental transport processes of both laminar and turbulent confined impinging streams. With a better understanding of the physical characteristics of the system and how various geometric and operating parameters affect the transport behavior of the system, reliable scale-up, design and optimization of various engineering unit operations based on this flow configuration are possible. The objectives of this work were thus:

- To study the effects of various geometric and operating parameters on the fluid mechanics, heat transfer and mixing characteristics of confined impinging streams operated in both laminar and turbulent flow regimes.
- To propose and verify a reliable model for use in the study of turbulent IS.
- To investigate the possibility of employing a novel IS design in some chemical engineering unit operations.
- To extend the model to allow the prediction of gas-particle flow behavior in IS and to investigate the performance of a novel flash dryer based on an IS flow configuration.

1.3. THESIS LAYOUT

This thesis is divided into six chapters of which this introduction is the first. In Chapter 2 a brief review of the literature relevant to the research subject is presented. Chapter 3 discusses the results of the study of flow and mixing characteristics of two-dimensional laminar confined impinging streams. A novel conceptual design of an in-line fluid mixer utilizing multiple impinging stream inlets is also proposed and studied in this chapter. Heat transfer and mixing characteristics of two-dimensional turbulent confined impinging streams is the subject of Chapter 4. A new composite turbulence model is proposed and verified by comparing its predictions with both available

experimental data in the literature and with those obtained in the present study. Thermal mixing characteristics of turbulent confined impinging streams obtained using this newly proposed model is also presented in this chapter. Chapter 5 discusses turbulent gas-particle flow in two-dimensional impinging streams. Drying characteristics of a novel two-dimensional flash dryer based on an impinging stream flow configuration are also illustrated.

Finally, Chapter 6 presents conclusions of this research along with contributions to knowledge and recommendations for future work.

REFERENCES

- Berman, Y., Tanklevsky, A., Oren, Y., Tamir, A., 2000a, Modeling and experimental studies of SO₂ absorption in coaxial cylinders with impinging streams, part I, *Chemical Engineering Science*, 55, pp. 1009-1021.
- Berman, Y., Tanklevsky, A., Oren, Y., Tamir, A., 2000b, Modeling and experimental studies of SO₂ absorption in coaxial cylinders with impinging streams, part II, *Chemical Engineering Science*, 55, pp. 1023-1028.
- Elperin, I.T., 1961, Heat and mass transfer in opposing currents, *Journal of Engineering Physics*, 6, pp. 62-68. Quoted by Tamir (1994).
- Gaddis, E.S., Vogelpohl, A., 1992, The impinging-stream reactor: a high performance loop reactor for mass transfer controlled chemical reactions, *Chemical Engineering Science*, 47, pp. 2877-2882.
- Hosseinalipour, S.M., Mujumdar, A.S., 1995, Flow, heat transfer and particle drying characteristics in confined opposing turbulent jets: a numerical study, *Drying Technology – An International Journal*, 13, pp. 753-781.
- Hosseinalipour, S.M., Mujumdar, A.S., 1997, A model for superheated steam drying of particles in an impinging streams dryer, pp. 537-574, in I. Turner and A.S. Mujumdar (Eds.) *Mathematical Modeling and Numerical Techniques in Drying Technology*, Marcel Dekker, New York.

-
- Kleingeld, A.W., Lorenzen, L., Botes, F.G., 1999, The development and modelling of high-intensity impinging stream jet reactors for effective mass transfer in heterogeneous systems, *Chemical Engineering Science*, 54, pp. 4991-4995.
- Mujumdar, A.S., Hosseinalipour, S.M., Devahastin, S., 2000, A two-dimensional superheated steam impinging stream dryer: a computational model, *Bulletin of the Polish Academy of Sciences: Technical Sciences*, 48, pp. 287-299.
- Tamir, A., 1989, Processes and phenomena in impinging-stream reactors, *Chemical Engineering Progress*, 85, pp. 53-61.
- Tamir, A., 1994, *Impinging-Stream Reactors: Fundamentals and Applications*, Elsevier, Amsterdam.

BACKGROUND

*Knowledge is of two kinds. We know a subject ourselves,
or we know where we can find information upon it*

Samuel Johnson

2.1. INTRODUCTION

This chapter presents a brief review of the literature relevant to the research subject. Various applications of impinging streams (IS) in engineering unit operations are discussed first. More fundamental works related to the fluid mechanics and heat transfer characteristics of both laminar and turbulent IS are then reviewed. Finally, a brief review of the current literature on transport processes in gas-particle flows in impinging stream configurations and their mathematical model is presented.

2.2. GENERAL STUDIES OF IMPINGING STREAMS

Impinging streams constitute a relatively new class of flow configuration, which has proved useful in conducting a wide array of chemical engineering unit operations. Extensive reviews of the applications of impinging streams can be found in Tamir (1989) and Tamir (1994). Only brief discussion of some recent applications of IS will be given here.

Yao et al. (1995) conducted an experimental study of evaporative cooling of air in an impinging stream cooler in which two gas-droplet streams flow in opposite directions and collide in the impingement zone. The air is cooled by evaporation of the water droplets. The heat and mass transfer effectiveness of the impinging streams was evaluated by placing a partition in the impingement zone, which prevented interaction between the streams. Effects of the initial droplet size and velocity as well as atomization and coalescence of droplets on the enhancement effect of impinging streams were also investigated. The effect of atomization or coalescence was found to be negligible up to initial droplet diameters of about 0.004 m. This is due to the fact that atomization increases the surface area for heat transfer but, at the same time, decreases the time the droplet remains in the cooler (due to less inertia). Therefore, the net effect may not be significant. The effect of initial relative velocity between phases on the enhancement factor is found to depend on the size of the droplet.

Berman and Tamir (1996) studied experimentally the collection of dry phosphate dust and coalescence of moistened phosphate dust in an impinging stream dust collector. They reported that the water spray increases the collection efficiency by 5-20% compared to dry collection. It was also found that problems of wet dust accumulation on the collector walls could be alleviated by applying the inclined (instead of coaxial) impinging streams.

Berman et al. (2000a,b) developed a wet-type desulfurization absorber comprising of coaxial cylinders with impinging streams. The effect of the composition of the flue gas, types of the spray nozzle as well as the type of the sorbents on SO₂ absorption in this absorber was experimentally investigated. A semi-empirical model of the flue gas desulfurization process was developed and it was found that the agreement between the predictions and experimental data were within $\pm 15\%$. The absorption efficiency was high, in the range of 93-97%. Kleingeld et al. (1999) confirmed the merit of using an impinging stream contactor in the chemical absorption operation due to very high values of mass transfer coefficient and specific interfacial area. A model for the prediction of the interfacial area production in an impinging stream contactor has also been developed.

Berman and Tamir (2000) studied liquid-liquid extraction in thin circular films formed by collision of two coaxial immiscible liquid streams. The flow of the films

generated is in a direction normal to the initial flow of the jets. Geometrical parameters of the thin film, mass transfer coefficients of the solute between the films as well as power input were determined. It is reported that, for a relatively identical power input, mass transfer coefficients in this novel extractor were higher by a factor of 10-200 compared to those of the conventional devices. It is also noted that the total extraction time is smaller than in conventional devices due to the relatively fast separation in the settler since dispersion between phases is relatively small. Recently, Dehkordi (2001) conducted an experimental study of liquid-liquid extraction of three solutions in impinging streams. Similar conclusions to those obtained by Berman and Tamir (2000) regarding the effectiveness of impinging streams in liquid-liquid extraction processes were derived.

Impinging streams have been used to carry out chemical reactions by several researchers (e.g., Sohrabi and Jamshidi, 1997). Recently, Sohrabi and Marvast (2000) employed a tangential flow impinging stream reactor, which was based on the design first used by Bar and Tamir (1990), to perform the isomerization of D-glucose to D-fructose using the immobilized glucose isomerase. The conversion of glucose in this reactor is found to be much higher than that in conventional reactors. The hydrodynamic behavior of this reactor has also been investigated along with the measurement and modeling of the residence time distribution of solid particles using Markov chains discrete formulation. Enhanced mass transfer performance of the impinging stream reactor over conventional reactors have been validated by several studies (e.g., Gaddis and Vogelpohl, 1992; Sievers et al., 1995). It is noted by Sprehe et al. (1998) that the impinging stream reactor distinguishes itself in comparison with other systems not only through a high mass transfer coefficient but also through a high rate of increase of the mass transfer coefficient with increasing power dissipation.

Drying of particles and pastes in impinging streams is probably the most popular operation conducted with impinging streams. In fact it was one of the earliest operations performed in impinging streams to verify the effectiveness of transport processes in this flow configuration (Elperin, 1961). Tamir et al. (1984) tested a two tangentially fed impinging stream dryer operated in a constant rate period of drying and reported that it has higher efficiency than other commonly used dryers, i.e., spray dryer, spouted bed as well as fluidized bed dryers. The pumping power consumption is also lower than that

required by a fluidized bed dryer. Kitron et al. (1987) studied some hydrodynamics, drying and particle residence time distribution (RTD) behavior of multistage two tangentially fed impinging stream dryers. The use of a four impinging stream dryer, as a means to increase the number of impingement zones per dryer, was also investigated along with its mixing and drying characteristics. Comparing with a single-stage two tangentially fed impinging stream dryer this dryer consumes less energy (by a factor of 4-10). The time to obtain the required mixing state is also reduced. Kitron and Tamir (1988) studied hydrodynamics, holdup of particles and their mean residence time and RTD as well as drying behavior of a coaxial two impinging stream dryer. As expected, it is found that the effective volume of the transfer process is not the actual contactor volume but is a certain volume located between the faces of the inlet streams. This again confirms the merit of using the impinging stream flow configuration in conducting various chemical engineering unit operations.

Scale-up rules and hydrodynamics, mean residence time, RTD as well as heat transfer and drying characteristics of coaxial impinging stream contactors have been reviewed by Kitron and Tamir (1990). A review of hydrodynamics and heat transfer behavior of various variations of impinging stream dryers along with their industrial applications was given by Kudra and Mujumdar (1989).

Hu and Liu (1999) recently performed experiments to study the flow and drying characteristics of a hybrid two-stage impinging stream dryer. The first stage is a coaxial two impinging stream dryer while the second stage is a so-called semi-cyclic impinging stream dryer. The latter configuration is somewhat similar to the two tangentially fed impinging streams of Tamir et al. (1984). The combined unit has shown to overcome the shortcomings of single separate configuration in terms of particles mean residence time and accumulation of wet particles on the contactor walls.

For a detailed discussion of impinging stream dryers including a classification scheme the reader is referred to the first comprehensive review of impinging stream dryers prepared by Kudra and Mujumdar (1995).

2.3. LAMINAR IMPINGING STREAMS

Although a number of works have been devoted to the study of confined impinging jets at low Reynolds numbers (e.g., Baydar, 1999), little is reported about the flow and thermal characteristics of confined impinging streams (or opposed jets). Wood et al. (1991) studied the flow field created by two impinging liquid jets in a single-sided opening cylindrical chamber using particle tracing, laser Doppler velocimeter (LDV) and three-dimensional numerical simulation. The two jets are impinged coaxially near the closed end of a cylindrical mixing chamber. Their results show that there is a threshold value of Reynolds number beyond which the flow exhibits oscillations. It is noted that by taking care to minimize disturbances and vibration the breakdown of the impinging jet structure could be delayed. The flow also displays hysteresis in that once the structure broke down it could only be reestablished by lowering the flow rate to much lower Reynolds number in the stable region.

Roy et al. (1994) studied, both numerically and experimentally, laminar steady two-dimensional mixing flow in a junction (one-way exit impinging streams). By using an LDV they were able to obtain the transition Reynolds number (based on the mean velocity in the exit branch) beyond which the flow in the exit branch becomes turbulent. No attempts have been made by these investigators to study the effect of the system geometry on the flow structure, however.

Hosseinalipour and Mujumdar (1997a,b) used temperature as a passive tracer to monitor mixing of two fluid streams in their numerical study of flow and thermal characteristics of steady two-dimensional confined laminar opposing jets. They found that by increasing the jet Reynolds number the attainment of uniformity of temperature profile (and hence complete mixing of the two streams) is delayed. This is due to the increase in the momentum of the fluid in the exit channel (and hence shorter residence time of the fluid in the system) due to the additional mass coming into the system.

Unger et al. (1998) studied flow and mixing in a semi-confined impinging jet contactor at low jet Reynolds numbers ($Re_j < 80$) using flow visualization techniques, particle image velocimetry and three-dimensional numerical simulations. They reported that two steady-state flow regimes are found to exist. At low jet Reynolds numbers (Re_j

< 10) the jets do not impinge and the velocity field scales linearly with Re_j . For $Re_j > 10$, the jets begin to impinge and recirculation regions form above and below the impingement point. They also reported substantially improvement in the mixing by a slight modification of the impinging jet geometry that disrupts geometric symmetry.

Johnson (2000a) performed flow visualization, LDV measurements as well as steady and unsteady three-dimensional finite volume simulations to study flow field created by impingement of laminar liquid jets of unequal momentum in a confined cylindrical chamber very similar to the one studied by Wood et al. (1991). Based on the video analysis of the flow field, this investigator has found that the impingement area and the structure of the flow are more stable at high jet Reynolds number than comparable equal flow rate cases. Unsteady numerical simulations of the flow field predicted the delay of unidirectional flow (in the downstream direction of the inlet jets) until large value of the downstream distance has elapsed. This leads to longer fluid residence time and hence poorer mixing as compared to the equal flow cases.

Johnson (2000b) proposed alternative schemes to reduce negative effects of flow imbalance (which is sometimes required by stoichiometry of the reactions conducted in the equipment) such as nozzle plugging due to high pressure region (impingement plane) near the lower momentum jet outlet. Three schemes have been proposed and tested and it is possible to shift the impingement point toward the geometric center of the chamber by these simple modifications of the inlet nozzles. Mixing is not improved, however.

Johnson and Wood (2000) studied the flow field of opposed axisymmetric jets in confined cavities of square and cylindrical cross-section experimentally and numerically. The geometries are again similar to the one studied earlier by Wood et al. (1991) and Johnson (2000a,b). As expected, the onset of oscillations and the upper limit of finite oscillations were found to be a function of the jet Reynolds number and the nozzle diameter to chamber dimension ratio. The oscillating flow field is classified as self-sustaining oscillations where instabilities in the jet shear layer are amplified because of feedback from pressure disturbances in the impingement region. Above the limit values no regular oscillations were observed since the jets no longer impinge directly. At this point the impingement pressure distribution is significantly altered and feedback from the

interface would no longer exist. As a design consideration it is suggested that the onset conditions (geometry and flow) should be considered the minimum for jet interaction.

2.4. TURBULENT IMPINGING STREAMS

As mentioned in the previous section not many papers appear in the literature devoted to the study of the fundamental transport processes in impinging streams even in the laminar flow regime. The available information on turbulent transport processes in this flow configuration is equally scarce, if not even more difficult to find. Again, a number of papers have recently been published on the modeling of turbulent flow and heat transfer behavior of impinging jets, which has characteristics somewhat similar to those of impinging streams. Seyedein et al. (1994) used both low-Reynolds and high-Reynolds number versions of $k-\varepsilon$ turbulence model to study the flow field and heat transfer impingement due to a turbulent single slot jet discharging normally into a confined channel. Better agreement between numerical results obtained using low-Reynolds number models and the available experimental data is noted compared to those results obtained using high-Reynolds number model. Morris et al. (1996) modified the converged solution obtained from a commercial finite-volume code via the application of different turbulent Prandtl number functions in the post-processing program. The predicted heat transfer results were then compared with experimental data; the predicted stagnation and average heat transfer coefficients agree with experiments to within a maximum deviation of 16-20 percent.

To avoid using a full second moment closure, which may be the solution to modelling the flow with recirculation and streamline curvature (Dianat et al., 1996; Morris et al., 1999), some investigators have recently employed simplified models which combined computational robustness and efficiency of linear eddy viscosity models (e.g., $k-\varepsilon$ models) with improved model accuracy of second moment closures (e.g., Behnia et al., 1999; Bauer et al., 2000). Modeling of semi-confined turbulent impinging and opposing jet flows is expected to be a complex problem due to the current lack of detailed experimental characterization of the hydrodynamic flow field.

Champion and Libby (1993) analyzed the flow field arising from two closely spaced unconfined turbulent opposed jets in both two-dimensional and axisymmetric configurations. The diameter of the jets was large compared to their separation distance. The ratio of the integral scale of the turbulence and the separation distance of the jets as well as the turbulence intensity of the incoming jets are assumed to be small to enable the use of an asymptotic technique. The mean velocity components are given by the mean Euler equations except in an impingement layer within which discontinuities in the flow from each jet occur. Outside this layer the turbulence characteristics in a known mean velocity field are determined in terms of a Reynolds stress description. The temperature in the two streams is assumed to be slightly different so that there is also a thermal layer at the stagnation plane. Comparison was made with the available experimental data for the mean velocity and turbulence intensities with good and reasonable agreement, respectively.

Kostiuk and Libby (1993) compared experimental mean axial velocity and the intensity of the radial and axial velocity components on the axis of axisymmetric turbulent opposed jets with those obtained from the Reynolds stress theory of Champion and Libby (1993) mentioned above. The agreement is found to be satisfactory although some improvements might be achieved by adjustments of some empirical coefficients in the model equation.

Hosseinalipour and Mujumdar (1995) used five low-Reynolds number k - ϵ models and the standard high-Reynolds number model to study the fluid flow and heat transfer characteristics of two-dimensional turbulent confined impinging and opposing jet flows. The so-called "Yap correction" was also tested with low-Reynolds number models to investigate its effect on the heat transfer predictions for the impinging jet case. Experimental data and numerical predictions by different turbulence models were compared for the impinging jet case. Due to lack of experimental data, however, only the numerical results of the opposing jet case were presented.

A number of new turbulence models for predicting fluid flow and heat transfer in separating and reattaching flows have been proposed and studied in recent years (e.g., Abe et al., 1994a,b; Park and Sung, 2001). They may be worth consideration when modeling the fluid mechanics and heat transfer in impinging and opposed jets. Recently

proposed models for turbulent heat transfer in the near-wall region (hence are applicable for confined jet configurations as well) include those of Hwang and Lin (1999) and Deng et al. (2001).

For comprehensive reviews of various turbulence modeling techniques the reader may refer to Wilcox (1993) and Chen and Jaw (1998).

2.5. GAS-PARTICLE IMPINGING STREAMS

Although a number of papers have been published on gas-particle and gas-droplet contacting operations in impinging streams (e.g., Tamir et al., 1984; Kitron and Tamir, 1988; Kudra and Mujumdar, 1989; Kudra and Mujumdar, 1995; Hu and Liu, 1999), very few papers have attempted modeling of these operations from first principles. A large pool of literature on gas-particle flows in other configurations is available, however. Only closely related publications are reviewed here. It should be noted also that although two major transport models for particles, i.e., Eulerian (Spalding, 1980) and Lagrangian approaches, are widely used in the study of gas-particles flows, the latter technique, which is based on the particle-source-in cell (PSI-CELL) model of Crowe et al. (1977), is used in the present research.

Yoshida et al. (1990) conducted experiments to study the flow and heat transfer mechanisms of a two-dimensional gas-solid impinging jet via the use of an LDV. They reported the presence of particles rebounding from the impingement plate and the gas-phase reverse flow caused by those particles. This leads to a significant heat transfer enhancement near the stagnation point due to the production of turbulence in the viscous sublayer by particles. However, the turbulence structure undergoes only a slight change in the wall jet region where the gas-solid interaction is smaller.

Yokomine and Shimizu (1999) studied experimentally the heat transfer behavior of a gas-solid impinging jet for divertor cooling of the fusion power reactor. Effects of various operating and geometric parameters on the heat transfer coefficient were investigated. It is found that by changing the particle from hard glassy carbon to soft and fine graphite the heat transfer coefficient increases markedly. This is due to the reduced erosion of the impingement plate, which enables the use of higher solid mass flow rate,

and increased heat capacity of the particle. Turbulence augmentation by particles also promotes heat transfer. However, increasing the solid loading beyond the optimum value leads to the saturation of the heat transfer enhancement effect and indeed to the attenuation of the turbulence.

Niu and Tsai (2000) used the Lagrangian approach to numerically study the effects of various operating parameters on erosion of the impingement plate by particle impact in a two-dimensional turbulent impinging jet flow. The effects of turbulence and particle-wall interaction were included in their work. It is found that the turbulence intensity, particle size, inlet flow velocity as well as temperature have significant effects on erosion. The agreement between numerical and experimental data is better than those obtained in the previous models that did not include the effects of particle-wall interaction and two-way coupling between phases.

Hosseinalipour (1996) and Hosseinalipour and Mujumdar (1997c) studied numerically the flow, heat transfer and drying characteristics in confined turbulent opposing jets using superheated steam as the drying medium. They computed particle trajectories as well as temperature and moisture content histories of particles (up to 2000 entering the contactor through one inlet nozzle). Both continuous-phase and particle equations were solved to study the aforementioned. Effects of various operating and geometric parameters on various transport processes were investigated in detail. This is by far the most extensive study on mathematical modeling of gas-particle flows with heat and mass transfer in two-dimensional confined impinging streams. They developed a computer code to solve the coupled equations that included effects of the restitution coefficient and turbulence modulation by the presence of particles. They computed the residence time distributions in the contactor and examined the effects of both flow and geometric parameters on the mean residence time as well as its distribution according to particle size and its initial location at entry into the contactor. Extremely large computing times limited their parametric studies, unfortunately.

Berman and Tamir (1996) studied coalescence of particles in coaxial impinging streams and proposed a coalescence model, which is based on equation expressing the condition for inter-particle collision rate as well as the equation of motion of a single particle. The model assumes coalescence only between small and large particles. It also

assumes that the probability of inter-particle collisions between large particles is negligible when comparing with the collisions between small and large particles.

Wu and Wu (1997) studied experimentally and theoretically the pressure drop across the impinging stream contactor (ISC) resulted from the acceleration of particles as well as the impingement of two inlet streams. It is found that a large proportion of the power (more than 80%) used for the operation of ISC is being consumed in the acceleration of particles while the pressure drop due to the impingement of inlet streams is independent of the presence of particles. The proposed model for the total pressure drop predicts the experimental results satisfactorily.

Voropayev et al. (2000) conducted a numerical study of the particle behavior in the impingement region and its neighborhood of axisymmetric gas-particle opposing jets as applied to the milling operation. The effects of the particle diameter and restitution coefficient for inter-particle collisions on the particle behavior in the impingement zone were investigated. The results obtained can be used for the new jet milling design as well as for the development of a new milling model, which takes into account the particle breaking kinetics, which can be derived from single particle impact fragmentation experiments.

Chang and Wu (1994) performed a sensitivity study on the stochastic separated flow (SSF) model, which employs the Monte Carlo method to track the drops in the turbulent flow field. They found that the use of no less than 1000 computational particles for each representative size could yield prediction that is statistically stationary for the polydispersed case. In contrast, 200 computational drops for each representative size are adequate to obtain an invariant solution using the deterministic separated flow (DSF) model. Non-uniform discretization of the size spectrum is recommended to save the computer time and storage.

For a review on multiphase flows with droplets and particles the reader is referred to Crowe et al. (1998). For a review on numerical models for two-phase turbulent flows the reader may refer to Crowe et al. (1996). A review of recent developments in the modeling and numerical simulation of turbulent gas-solid flows including the effects of particle-wall and inter-particle collisions is given by Sommerfeld (1998).

REFERENCES

- Abe, K., Kondoh, T., Nagano, Y., 1994a, A new turbulence model for predicting fluid flow and heat transfer in separating and reattaching flows—I. Flow field calculations, *International Journal of Heat and Mass Transfer*, 37, pp. 139-151.
- Abe, K., Kondoh, T., Nagano, Y., 1994b, A new turbulence model for predicting fluid flow and heat transfer in separating and reattaching flows—II. Thermal field calculations, *International Journal of Heat and Mass Transfer*, 38, pp. 1467-1481.
- Bar, T., Tamir, A., 1990, An impinging-stream reactor with two pairs of air feed, *Canadian Journal of Chemical Engineering*, 68, pp. 541-552.
- Bauer, W., Haag, O., Hennecke, D.K., 2000, Accuracy and robustness of nonlinear eddy viscosity models, *International Journal of Heat and Fluid Flow*, 21, pp. 312-319.
- Baydar, E., 1999, Confined impinging air jet at low Reynolds numbers, *Experimental Thermal and Fluid Science*, 19, pp. 27-33.
- Behnia, M., Parneix, S., Shabany, Y., Durbin, P.A., 1999, Numerical study of turbulent heat transfer in confined and unconfined impinging jets, *International Journal of Heat and Fluid Flow*, 20, pp. 1-9.
- Berman, Y., Tamir, A., 1996, Experimental investigation of phosphate dust collection in impinging streams, *Canadian Journal of Chemical Engineering*, 74, pp. 817-821.
- Berman, Y., Tamir, A., 1996, Coalescence model of particles in coaxial impinging streams, *Canadian Journal of Chemical Engineering*, 74, pp. 822-833.
- Berman, Y., Tanklevsky, A., Oren, Y., Tamir, A., 2000a, Modeling and experimental studies of SO₂ absorption in coaxial cylinders with impinging streams, part I, *Chemical Engineering Science*, 55, pp. 1009-1021.
- Berman, Y., Tanklevsky, A., Oren, Y., Tamir, A., 2000b, Modeling and experimental studies of SO₂ absorption in coaxial cylinders with impinging streams, part II, *Chemical Engineering Science*, 55, pp. 1023-1028.
- Berman, Y., Tamir, A., 2000, Extraction in thin liquid films generated by impinging streams, *AIChE Journal*, 46, pp. 769-778.
- Champion, M., Libby, P.A., 1993, Reynolds stress description of opposed and impinging turbulent jets, part I: Closely spaced opposed jets, *Physics of Fluids A*, 5, pp. 203-216.

- Chang, K.-C., Wu, W.-J., 1994, Sensitivity study of Monte Carlo solution procedure of two-phase turbulent flow, *Numerical Heat Transfer, Part B*, 25, pp. 223-244.
- Chen, C.-J., Jaw, S.-Y., 1998, *Fundamentals of Turbulence Modeling*, Taylor & Francis, Washington.
- Crowe, C.T., Sharma, M.P., Stock, D.E., 1977, The particle-source-in cell (PSI-CELL) model for gas-droplet flows, *ASME Journal of Fluids Engineering*, 99, pp. 325-332.
- Crowe, C.T., Troutt, T.R., Chung, J.N., 1996, Numerical models for two-phase turbulent flows, *Annual Review of Fluid Mechanics*, 28, pp. 11-43.
- Crowe, C., Sommerfeld, M., Tsuji, Y., 1998, *Multiphase Flows with Droplets and Particles*, CRC Press, Boca Raton.
- Dehkordi, A.M., 2001, Novel type of impinging streams contactor for liquid-liquid extraction, *Industrial & Engineering Chemistry Research*, 40, pp. 681-688.
- Deng, B., Wu, W., Xi, S., 2001, A near-wall two-equation heat transfer model for wall turbulent flows, *International Journal of Heat and Mass Transfer*, 44, pp. 691-698.
- Dianat, M., Fairweather, M., Jones, W.P., 1996, Reynolds stress closure applied to axisymmetric, impinging turbulent jets, *Theoretical and Computational Fluid Dynamics*, 8, pp. 435-447.
- Elperin, I.T., 1961, Heat and mass transfer in opposing currents, *Journal of Engineering Physics*, 6, pp. 62-68. Quoted by Tamir (1994).
- Gaddis, E.S., Vogelpohl, A., 1992, The impinging-stream reactor: a high performance loop reactor for mass transfer controlled chemical reactions, *Chemical Engineering Science*, 47, pp. 2877-2882.
- Hosseinalipour, S.M., Mujumdar, A.S., 1995, Comparative evaluation of different turbulence models for confined impinging and opposing jet flows, *Numerical Heat Transfer, Part A*, 28, pp. 647-666.
- Hosseinalipour, S.M., 1996, Transport processes in laminar and turbulent opposing jet contactors, Ph.D. Thesis, Department of Chemical Engineering, McGill University, Canada.
- Hosseinalipour, S.M., Mujumdar, A.S., 1997a, Flow and thermal characteristics of steady two-dimensional confined laminar opposing jets: part I. equal jets, *International Communications in Heat and Mass Transfer*, 24, pp. 27-38.

- Hosseinalipour, S.M., Mujumdar, A.S., 1997b, Flow and thermal characteristics of steady two-dimensional confined laminar opposing jets: part II. unequal jets, *International Communications in Heat and Mass Transfer*, 24, pp. 39-50.
- Hosseinalipour, S.M., Mujumdar, A.S., 1997c, A model for superheated steam drying of particles in an impinging streams dryer, pp. 537-574, in I. Turner and A.S. Mujumdar (Eds.) *Mathematical Modeling and Numerical Techniques in Drying Technology*, Marcel Dekker, New York.
- Hu, X., Liu, D., 1999, Experimental investigation on flow and drying characteristics of a vertical and semi-cyclic combined impinging streams dryer, *Drying Technology – An International Journal*, 17, pp. 1879-1892.
- Hwang, C.B., Lin, C.A., 1999, A low Reynolds number two-equation $k_\theta - \epsilon_\theta$ model to predict thermal fields, *International Journal of Heat and Mass Transfer*, 42, pp. 3217-3230.
- Johnson, D.A., 2000a, Experimental and numerical examination of confined laminar opposed jets: part I. momentum imbalance, *International Communications in Heat and Mass Transfer*, 27, pp. 443-454.
- Johnson, D.A., 2000b, Experimental and numerical examination of confined laminar opposed jets: part II. momentum balancing, *International Communications in Heat and Mass Transfer*, 27, pp. 455-463.
- Johnson, D.A., Wood, P.E., 2000, Self-sustained oscillations in opposed impinging jets in an enclosure, *Canadian Journal of Chemical Engineering*, 78, pp. 867-875.
- Kitron, A., Buchmann, R., Luzzatto, K., Tamir, A., 1987, Drying and mixing of solids and particles residence time distribution in four impinging streams and multistage two impinging streams reactors, *Industrial & Engineering Chemistry Research*, 26, pp. 2454-2461.
- Kitron, Y., Tamir, A., 1988, Performance of a coaxial gas-solid two-impinging-streams reactor: hydrodynamics, residence time distribution, and drying heat transfer, *Industrial & Engineering Chemistry Research*, 27, pp. 1760-1767.
- Kitron, Y., Tamir, A., 1990, Characteristics and scale-up of coaxial impinging streams gas-solid contactors, *Drying Technology – An International Journal*, 8, pp. 781-810.

- Kleingeld, A.W., Lorenzen, L., Botes, F.G., 1999, The development and modelling of high-intensity impinging stream jet reactors for effective mass transfer in heterogeneous systems, *Chemical Engineering Science*, 54, pp. 4991-4995.
- Kostiuk, L.W., Libby, P.A., 1993, Comparison between theory and experiment for turbulence in opposed streams, *Physics of Fluids A*, 5, pp. 2301-2303.
- Kudra, T., Mujumdar, A.S., 1989, Impinging stream dryers for particles and pastes, *Drying Technology – An International Journal*, 7, pp. 219-266.
- Kudra, T., Mujumdar, A.S., 1995, Impinging stream dryers, pp. 539-566, in A.S. Mujumdar (Ed.) *Handbook of Industrial Drying, 2nd Edition*, Marcel Dekker, New York.
- Morris, G.K., Garimella, S.V., Amano, R.S., 1996, Prediction of jet impingement heat transfer using a hybrid wall treatment with different turbulent Prandtl number functions, *ASME Journal of Heat Transfer*, 118, pp. 562-569.
- Morris, G.K., Garimella, S.V., Fitzgerald, J.A., 1999, Flow-field prediction in submerged and confined jet impingement using the Reynolds stress model, *ASME Journal of Electronic Packaging*, 121, pp. 255-262.
- Niu, Y.-Y., Tsai, C.-S., 2000, Simulation of erosion by the dilute particulate flow impact, *Numerical Heat Transfer, Part A*, 37, pp. 167-187.
- Park, T.S., Sung, H.J., 2001, Development of a near-wall turbulence model and application to jet impingement heat transfer, *International Journal of Heat and Fluid Flow*, 22, pp. 10-18.
- Roy, J.C., Bertrand, C., Le Palec, G., 1994, Numerical and experimental study of mixed and forced convection in a junction, *International Journal of Heat and Mass Transfer*, 37, pp. 1985-2006.
- Seyedein, S.H., Hasan, M., Mujumdar, A.S., 1994, Modelling of a single confined turbulent slot jet impingement using various k- ϵ turbulence models, *Applied Mathematical Modelling*, 18, pp. 526-537.
- Sievers, M., Gaddis, E.S., Vogelpohl, A., 1995, Fluid dynamics in an impinging-stream reactor, *Chemical Engineering and Processing*, 34, pp. 115-119.

-
- Sohrabi, M., Jamshidi, A.M., 1997, Studies on the behavior and application of the continuous two impinging streams reactors in gas-liquid reactions, *Journal of Chemical Technology and Biotechnology*, 69, pp. 415-420.
- Sohrabi, M., Marvast, M.A., 2000, Application of a continuous two impinging streams reactor in solid-liquid enzyme reactions, *Industrial & Engineering Chemistry Research*, 39, pp. 1903-1910.
- Sommerfeld, M., 1998, Modelling and numerical calculation of turbulent gas-solids flows with the Euler/Lagrange approach, *KONA*, 16, pp. 194-206.
- Spalding, D.B., 1980, Numerical computation of multiphase fluid flow and heat transfer, pp. 139-167, in C. Taylor and K. Morgan (Eds.) *Recent Advances in Numerical Methods in Fluids*, Pineridge Press, Swansea, UK.
- Sprehe, M., Gaddis, E., Vogelpohl, A., 1998, On the mass transfer in an impinging-stream reactor, *Chemical Engineering Technology*, 21, pp. 19-21.
- Tamir, A., 1989, Processes and phenomena in impinging-stream reactors, *Chemical Engineering Progress*, 85, pp. 53-61.
- Tamir, A., 1994, *Impinging-Stream Reactors: Fundamentals and Applications*, Elsevier, Amsterdam.
- Tamir, A., Elperin, I., Luzzatto, K., 1984, Drying in a new two impinging streams reactor, *Chemical Engineering Science*, 39, pp. 139-146.
- Unger, D.R., Muzzio, F.J., Brodkey, R.S., 1998, Experimental and numerical characterization of viscous flow and mixing in an impinging jet contactor, *Canadian Journal of Chemical Engineering*, 76, pp. 546-555.
- Voropayev, S., Vasilkov, O., Dorokhov, I., Eskin, D., 2000, Gas-particles opposed jets interaction simulation, *Proceedings of the 3rd Israeli Conference for Conveying and Handling of Particulate Solids*, Dead Sea, Israel, Vol. 1., pp. 6.18-6.23.
- Wilcox, D.C., 1993, *Turbulence Modeling for CFD*, DCW Industries, Inc., La Cañada, CA.
- Wood, P., Hrymak, A., Yeo, R., Johnson, D., Tyagi, A., 1991, Experimental and computational studies of the fluid mechanics in an opposed jet mixing head, *Physics of Fluids A*, 3, pp. 1362-1368.

-
- Wu, G., Wu, Y., 1997, Resistance of impinging stream contactor to solid-air suspension flow, *Chinese Journal of Chemical Engineering*, 5, pp. 270-279.
- Yao, B., Berman, Y., Tamir, A., 1995, Evaporative cooling of air in impinging streams, *AIChE Journal*, 41, pp. 1667-1675.
- Yokomine, T., Shimizu, A., 1999, Experimental investigation on impingement heat transfer of gas-solid suspension flow, Paper AJTE99-6433, *Proceedings of the 5th ASME/JSME Joint Thermal Engineering Conference*, San Diego, CA.
- Yoshida, H., Suenaga, K., Echigo, R., 1990, Turbulence structure and heat transfer of a two-dimensional impinging jet with gas-solid suspensions, *International Journal of Heat and Mass Transfer*, 33, pp. 859-867.

**FLOW AND MIXING CHARACTERISTICS OF TWO-DIMENSIONAL
LAMINAR CONFINED IMPINGING STREAMS**

*"I could have done it in a much more complicated way"
said the red Queen, immensely proud
Lewis Carroll*

3.1. INTRODUCTION

Although a number of publications, as partially reviewed in the previous chapter, have reported uses of impinging streams (IS) in various applications (e.g., Tamir, 1989; Kudra and Mujumdar, 1989; Tamir, 1994; Hosseinalipour and Mujumdar, 1995; Yao et al., 1995; Berman and Tamir, 1996; Berman et al., 2000a,b; Berman and Tamir, 2000), very few papers (Wood et al., 1991; Hosseinalipour and Mujumdar, 1997a,b; Unger et al., 1998; Johnson and Wood, 2000) are focused on studies of the fundamental transport processes in this flow configuration even in the laminar flow regime which is of practical importance when dealing with high-viscosity fluids, e.g., polymer solutions, polymer melts, liquid foodstuffs, etc. The lack of this fundamental information is the motivation of the study presented in this chapter.

Although a number of works have been devoted to the study of confined impinging jets at low Reynolds numbers (e.g., Baydar, 1999), little is reported about the flow and thermal characteristics of confined impinging streams (or opposing jets). Roy et al. (1994) studied, both numerically and experimentally, laminar steady two-dimensional mixing flow in a junction (one-way exit impinging streams). By using a laser Doppler

velocimeter (LDV) they were able to obtain the transition Reynolds number (based on the mean velocity in the exit branch) beyond which the flow in the exit branch becomes turbulent. This result will be discussed further in a subsequent section.

Hosseinalipour and Mujumdar (1997a,b) used temperature as a passive tracer to monitor mixing of two fluid streams of different temperatures in their numerical study of flow and thermal characteristics of steady two-dimensional confined laminar opposing jets. They found that by increasing the jet Reynolds number the attainment of uniformity of the temperature profile (and hence complete mixing of the two streams) is delayed. This is attributed to the shorter residence time of the fluid in the system due to the increased mean flowrate. Unger et al. (1998) studied flow and mixing in an unconfined impinging jet contactor at low jet Reynolds numbers ($Re_j < 80$) using flow visualization techniques, particle image velocimetry and three-dimensional numerical simulations. They found two steady-state flow regimes. At low jet Reynolds numbers ($Re_j < 10$) the jets do not impinge and the velocity field scales linearly with Re_j . For $Re_j > 10$, the jets begin to impinge and recirculation regions form above and below the impingement plane. They also reported substantial improvement in mixing by a slight modification of the impinging jet geometry that disrupts geometric symmetry.

In this chapter numerical results of the study of laminar flow and mixing in two-dimensional confined impinging streams are presented.

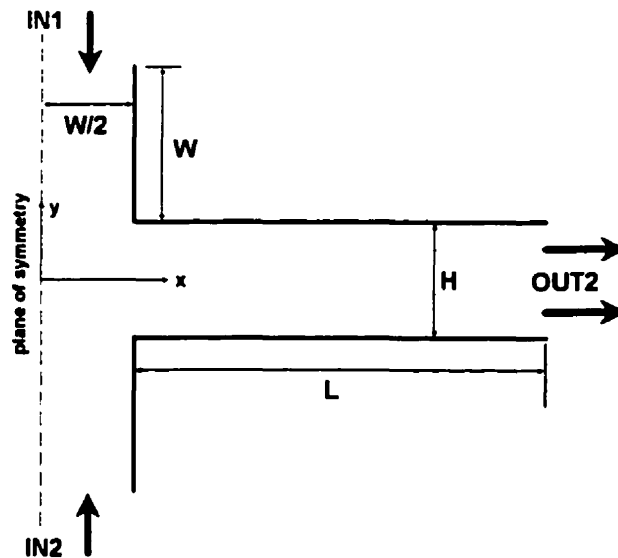


Figure 3.1. Schematic diagram of the impinging streams studied in the first part.

The chapter is divided into two parts. In the first part time-dependent conservation equations for mass, momentum and energy were solved to obtain the flow characteristics of a two-dimensional laminar confined impinging stream geometry (Figure 3.1). The Reynolds numbers (based on an inlet jet hydraulic diameter, which is calculated assuming the aspect ratio of 10 between the width and the height of the exit channel) beyond which the flow displays periodicity and in some cases randomly fluctuates were identified for different geometric configurations. It is found that this transition Reynolds number depends strongly on the geometric parameter viz. the ratio of the height of the exit channel (H) to the width of the inlet jets (W), especially at lower values of this ratio. Simulations were also performed for cases with jet Reynolds numbers in the stable regime to study the mixing characteristics of the system. The effects of inlet jet Reynolds number and geometric configuration on mixing are studied and discussed.

In the second part a new conceptual design for a modified in-line mixer for high-viscosity fluids without the use of mechanical obstructions in the channel, which are potential sources for fouling and also high pressure drop, is proposed. The concept involves dividing one of the fluid streams into a multiplicity of streams, which are injected into the main flow channel as two-dimensional slot jets, which are directed in opposite directions. To evaluate the mixing performance of this device, fluid temperature was used as a passive tracer. Effects of various key parameters viz. inlet jet Reynolds number, the ratio of the height of the mixer exit channel to the width of the inlet jets (H/W) and the ratio of the spacing between the two inlet jets (S) to the width of the inlet jets on the mixing behavior of the system are explained.

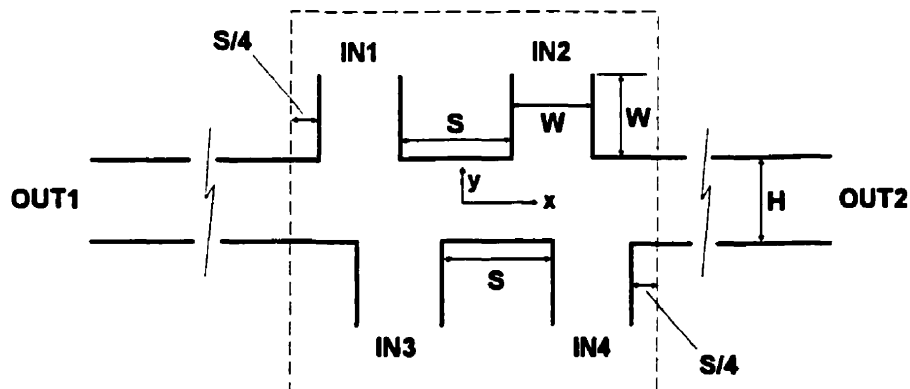


Figure 3.2. Schematic diagram of the two-dimensional channel mixer studied in the second part

Further, it is shown via numerical simulations that the jets perform better if they are offset with respect to each other, i.e., they do not collide normally but are displaced as shown in Figure 3.2.

3.2. MATHEMATICAL FORMULATION

To formulate the mathematical description of the transport processes in impinging streams the following assumptions are made: the flow is laminar, incompressible and the fluid is Newtonian with constant physical properties. In part two, the flow is assumed to be steady and thus the transient terms in equations (3.2) and (3.3) are equal to zero. Viscous dissipation is neglected. The flow is assumed to be fully developed (both hydrodynamically and thermally) at the exits of the IS.

Based on the above assumptions conservation equations for mass, momentum and energy (in tensor form) can be written as follows (Bird et al., 1960):

Continuity equation:

$$\frac{\partial u_i}{\partial x_i} = 0 \tag{3.1}$$

Momentum equation:

$$\rho \left(\frac{\partial u_j}{\partial t} + u_i \frac{\partial u_j}{\partial x_i} \right) = - \frac{\partial p}{\partial x_j} + \mu \frac{\partial}{\partial x_i} \left(\frac{\partial u_j}{\partial x_i} \right) + \rho g_j \tag{3.2}$$

Energy equation:

$$\rho c_p \left(\frac{\partial T}{\partial t} + u_i \frac{\partial T}{\partial x_i} \right) = k \frac{\partial}{\partial x_i} \left(\frac{\partial T}{\partial x_i} \right) \tag{3.3}$$

in which i and j take on the values 1 and 2.

These equations were solved numerically subject to the following initial and boundary conditions (see Figures 3.1 and 3.2 for the description of symbols used in parts 1 and 2, respectively):

Part 1**Initial conditions**

$$\text{At } t = 0 \quad u_i = 0 \text{ and } T = 20^\circ \text{ C} \quad (3.4)$$

Boundary conditions**Inlet 1**

$$(0 < x < W/2; y = W + H/2) \quad u_1 = 0; u_2 = -u_{2,jet} \text{ and } T = T_{inlet 1} \quad (3.5)$$

Inlet 2

$$(0 < x < W/2; y = -(W + H/2)) \quad u_1 = 0; u_2 = u_{2,jet} \text{ and } T = T_{inlet 2} \quad (3.6)$$

Top and bottom walls

$$(W/2 < x < L + W/2) \quad u_i = 0 \text{ and } \frac{\partial T}{\partial y} = 0 \quad (3.7)$$

Outlet

$$(x = L + W/2) \quad \frac{\partial \phi}{\partial x} = 0 \quad (3.8)$$

Along the symmetrical plane

$$(x = 0) \quad \frac{\partial \phi}{\partial x} = 0 \quad (3.9)$$

Part 2**Boundary conditions****Top inlets**

$$u_1 = 0; u_2 = -u_{2,jet} \text{ and } T = T_{top jets} \quad (3.10)$$

Bottom inlets

$$u_1 = 0; u_2 = u_{2,jet} \text{ and } T = T_{bottom jets} \quad (3.11)$$

Top and bottom walls

$$u_i = 0 \text{ and } \frac{\partial T}{\partial y} = 0 \quad (3.12)$$

Outlets

$$\frac{\partial \phi}{\partial x} = 0 \quad (3.13)$$

where ϕ represents all solved variables.

The conservation equations, along with the initial and boundary conditions, were solved numerically using control-volume-based computational fluid dynamic software PHOENICS version 2.2.2 (CHAM, 1997). In this code the convection terms in the momentum and energy equations were discretized using the hybrid scheme (Patankar, 1980). A fully implicit scheme (Patankar, 1980) was used to discretize the transient terms. The discretized equations were solved using the well-known SIMPLEST algorithm (CHAM, 1997). The solution was considered converged when the following criterion is met for all dependent variables:

$$\max \left| \frac{\phi^{n+1} - \phi^n}{\phi_r} \right| \leq 10^{-3} \quad (3.14)$$

between sweeps n and $n+1$; ϕ_r represents the reference value for the dependent variable ϕ . To improve convergence underrelaxation of the false transient type was used for the two velocity components and the temperature. Whole-field residuals were checked to ensure that the converged solution set satisfies the governing equations within a prescribed error.

Due to the large number of cases studied it was not possible to check the grid independence for each individual case. To overcome this problem, as suggested by Hosseinalipour and Mujumdar (1997a), the appropriate number of grids were found through a grid doubling procedure for the “worst” case with the highest Reynolds number for each geometry and applied to all other cases for that particular geometry. This procedure results in longer running times for the lower Reynolds number cases but it was compensated for by the time saving in not running grid doubling runs for each individual case. For details regarding the discretization of the governing equations and various schemes used to solve the discretized equations the reader may refer to Patankar (1980).

The above model was verified by comparison with the experimental and numerical results of Roy et al. (1994) who studied mixing flow in a junction (one-way exit impinging streams). This junction configuration is shown schematically in Figure 3.3; the symmetrical plane in Figure 3.1 is replaced by a solid wall in this case. The width of the inlet channels is half the exit channel height. All walls were specified to be adiabatic (well insulated).

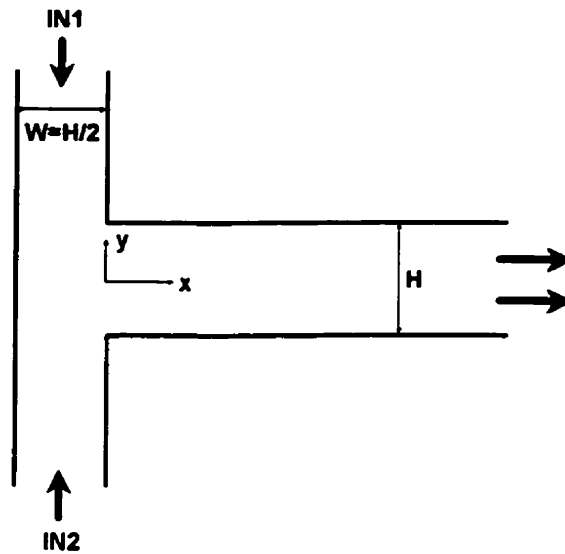


Figure 3.3. Schematic diagram of the junction used in model verification.

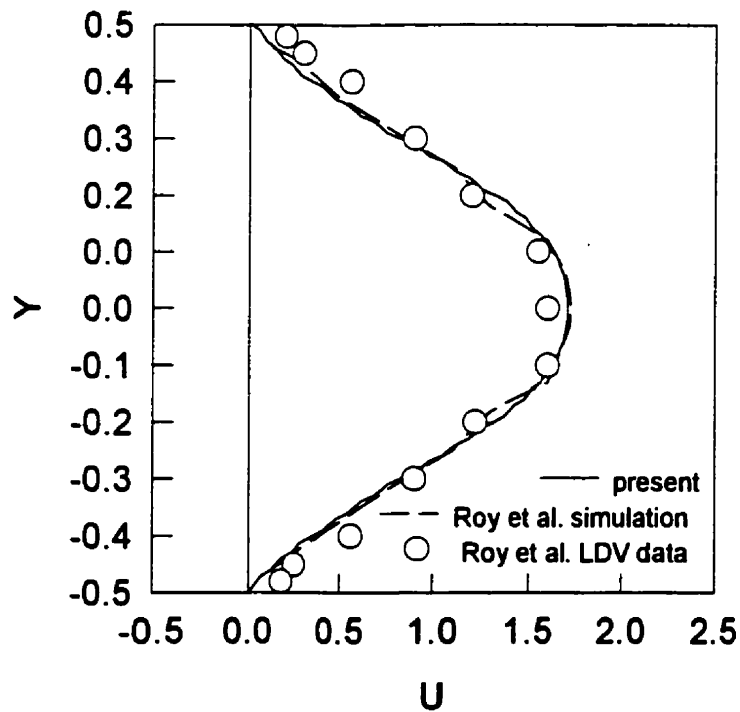


Figure 3.4. Comparison of dimensionless axial velocity profiles.

$Re = U_0 H \rho / \mu = 500$ (based on the mean velocity in the exit branch); $X = x/H = 5$ (where H is the height of the exit branch, see Figure 3.3); $Y = y/H$. $U = u/U_0$ where U_0 is the mean velocity in the exit branch.

Figure 3.4 compares the predicted dimensionless axial velocity profiles using the present simulation with both the numerical and experimental results of Roy et al. (1994). It is seen from this figure that the present results are in good agreement with both sets of data. The small discrepancies may be due to the slight differences in the measuring positions used in the experiment and the simulation. No data are available for temperature fields in similar configurations.

3.3. RESULTS AND DISCUSSION

3.3.1. Flow and mixing characteristics of laminar confined impinging streams

The fluid was injected into the system through the two inlets (see Figure 3.1). The two streams impinged normally against each other and then left the system through the exit channels situated symmetrically on either side of the impingement region. The length of the mixing channel was extended long enough to satisfy the fully developed channel flow assumption. To study mixing of the two fluid streams air of different temperatures was injected through each inlet channel. The ranges of parameters studied are: inlet jet Reynolds number (Re_j) from 500 to 10000 for time-dependent cases and from 10 to 3500 for steady cases; the ratio of the height of the exit channel to the width of the inlet jet (H/W) was varied from 1.0 to 4.0.

By solving the transient conservation equations for mass, momentum and energy it was possible to obtain conditions where the flow begins to shift from laminar to a transitional and then a random flow regime. The velocity components were sampled at each time step at $x = W/2$ and $y = 0$ to determine if the flow was unsteady (either periodic or random oscillatory). These results are shown in Figure 3.5. This figure shows that the transition Reynolds number depends strongly on the geometric configuration viz. H/W , especially at lower values of H/W . A similar study has been reported by Roy et al. (1994) for the transition Reynolds number of the flow in a junction (one-way exit impinging streams). Only one case with $H/W = 2$ is reported in their study, however. They mentioned that the flow in the exit branch becomes turbulent for $Re > 500$ (based on the mean velocity in the exit branch). Using the present computer code the transition Reynolds number is identified to be $Re \approx 700$. The discrepancy between our numerical

and their experimental results may be due to the presence of unavoidable disturbances when conducting the real experiment, which may lead to an earlier onset of instability than the one obtained numerically. Similar trend has been reported by Wood et al. (1991) who studied experimentally and numerically the flow field created by two impinging liquid jets in a cylindrical chamber. They found that the calculations are more stable than the experimental conditions with respect to stability of the flow. This is due to the fact that the computational inlet boundary condition is fixed properly while in the experiments a pressure wave would be fed back into the jet itself, which could create a disturbance and promote oscillations in the mixing chamber. Nevertheless, this shows that the code performs quite satisfactorily in predicting the flow characteristics of impinging streams.

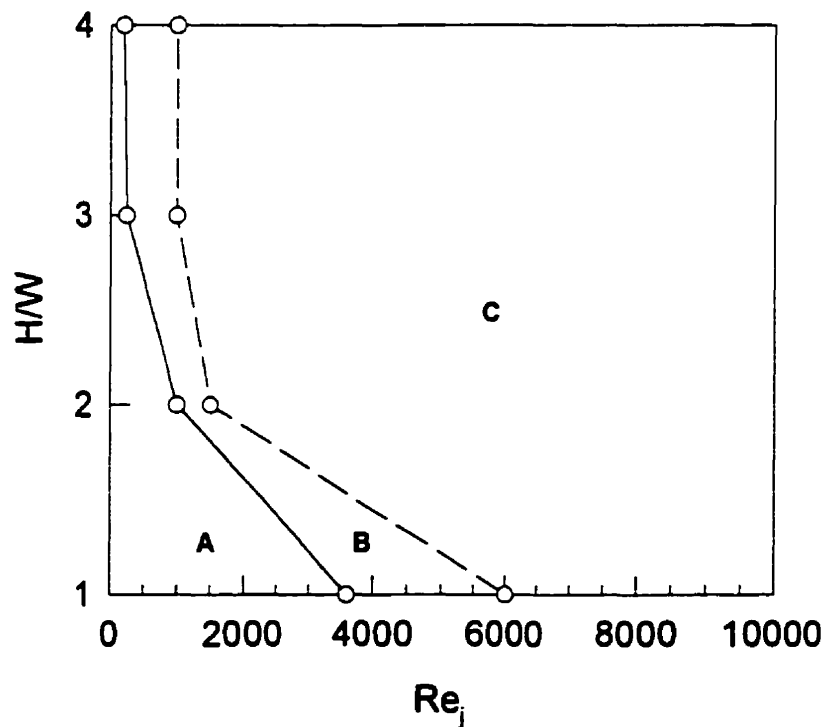


Figure 3.5. Flow regime diagram.

A: stable; B: oscillatory (periodic); C: random oscillatory

Some typical plots of the velocity component in the y -direction are shown in Figures 3.6 and 3.7 where various oscillating and fluctuating patterns can be identified.

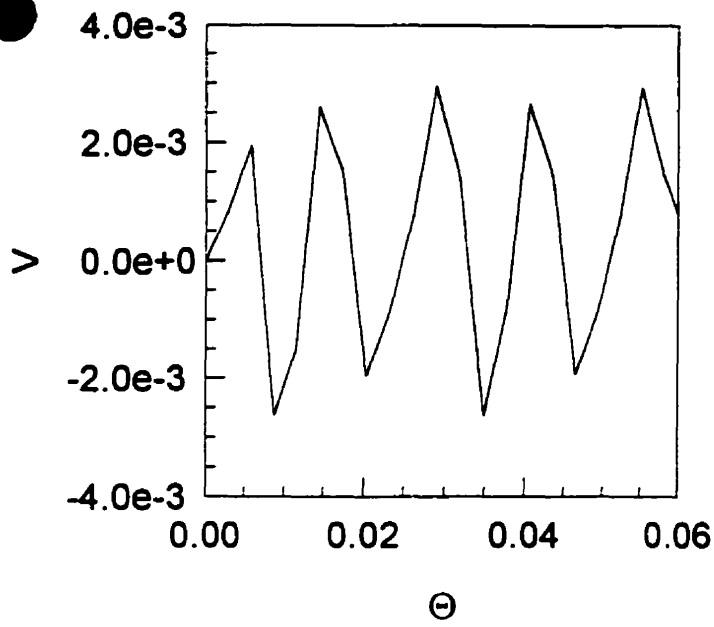
Similar behavior is observed for each case for the velocity component in the x -direction as well. It can be seen in these figures that the oscillations as well as fluctuations diminish as the exit ports are approached. It is seen in Figure 3.6 that the degree of oscillation (amplitude as well as frequency of oscillation) is smaller at lower H/W despite the higher value of Re_j ; the further away from the stable regime the higher is the degree of oscillation. Similar trend is observed for the fluctuating cases shown in Figure 3.7. The diminishing of the fluctuating velocity component is not as clear as can be seen for the oscillating cases, however.

As noted earlier temperature was used as a passive tracer to study mixing of the two fluid streams introduced into the system. As the two streams mix and approach the exit ports the temperature profiles across the exit channel height are flattened; the well-mixed condition is satisfied when no temperature gradient exists across the channel height, i.e., the temperature profile is flat. To quantify the mixing performance of the system at different operating conditions and geometric configurations a mixing index was defined as follows:

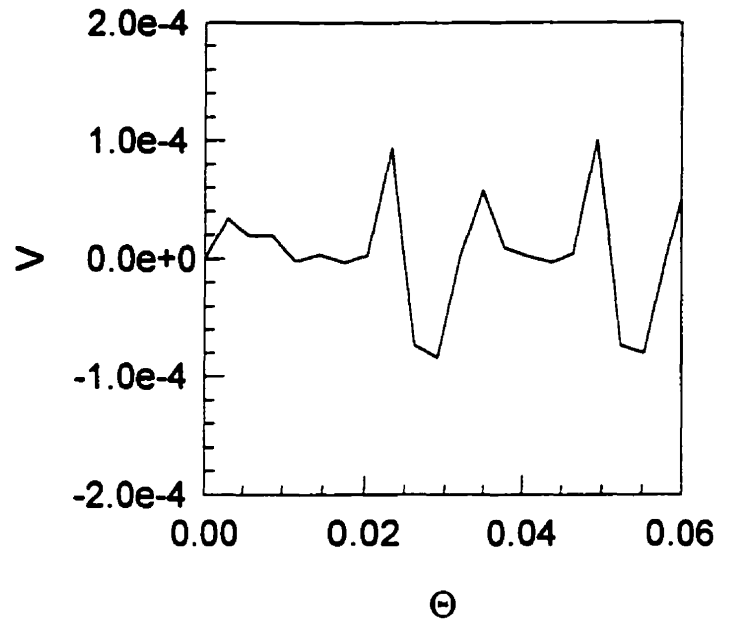
$$\text{Mixing index} = \frac{\sigma_T}{\Delta T} \quad (3.15)$$

where σ_T is the standard deviation of the fluid temperature across the channel height at a specific axial location and ΔT is the temperature difference between the two inlet streams. $\sigma_T = 0$ thus implies well-mixed condition. Note that different criteria for mixing (e.g., the one proposed by Hosseinalipour and Mujumdar (1997a)) may be used but the above criterion is conceptually easier to visualize. Nonetheless, either index should equally predict the channel length required to well mix the two streams.

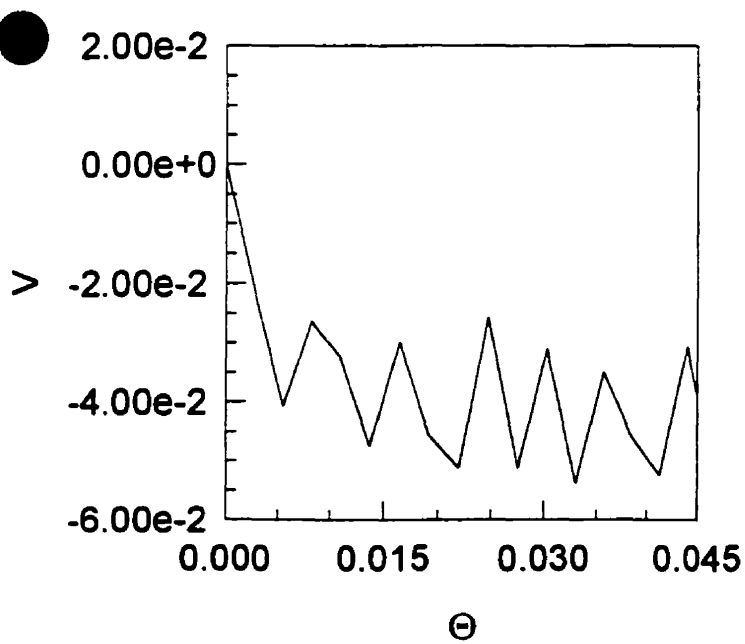
As mentioned earlier simulations were performed for cases with inlet jet Reynolds numbers in the stable regime to study the mixing characteristics of the system. The plots of velocity vectors and temperature isotherms of two representative cases are shown in Figure 3.8. At low H/W , i.e., $H/W = 1$, no recirculating bubble is observed at low Re_j (say $Re_j < 1000$). The flow develops only a short distance downstream of the impingement region. The jet interaction is also weak; the two jets seem to flow parallel to and do not penetrate into each other even in the zone of impingement. This trend continues to hold even at higher Re_j , i.e., $Re_j = 3500$.



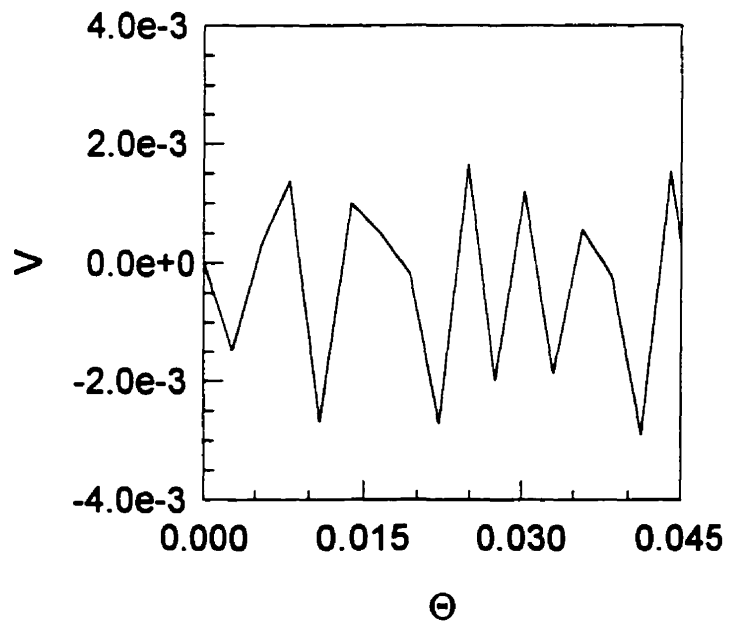
(a)



(b)

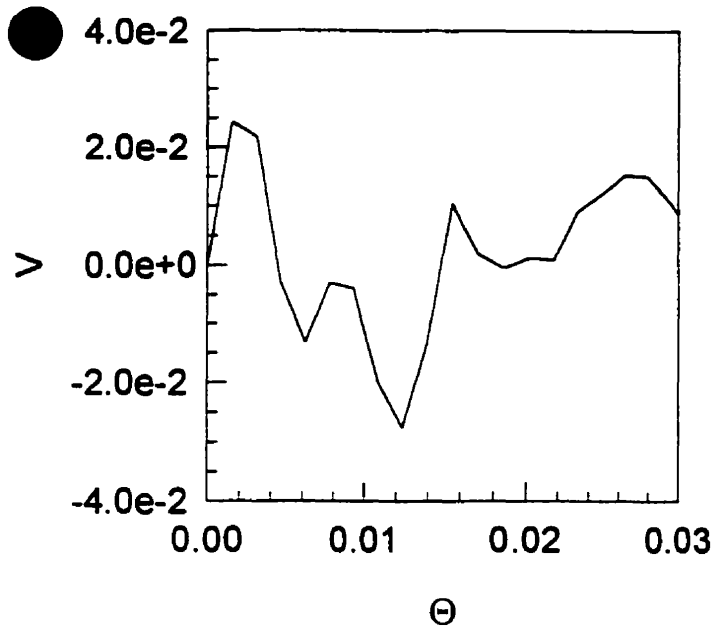


(c)

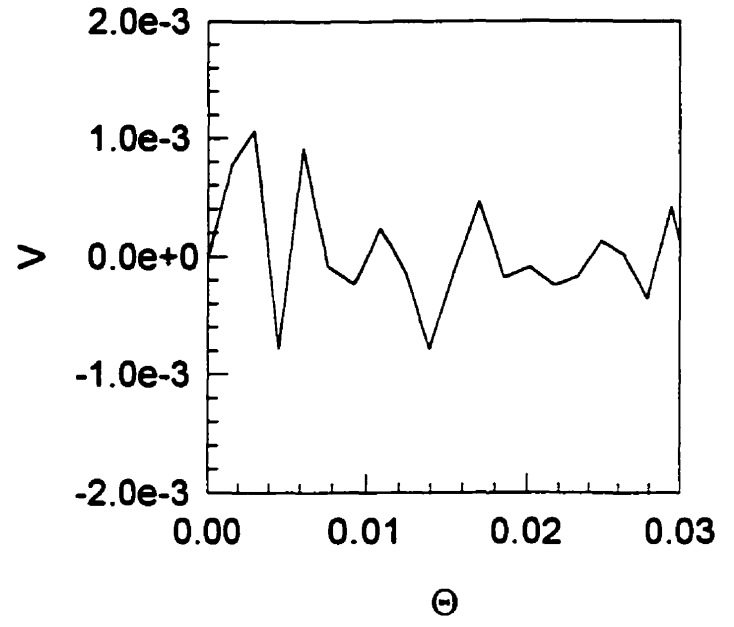


(d)

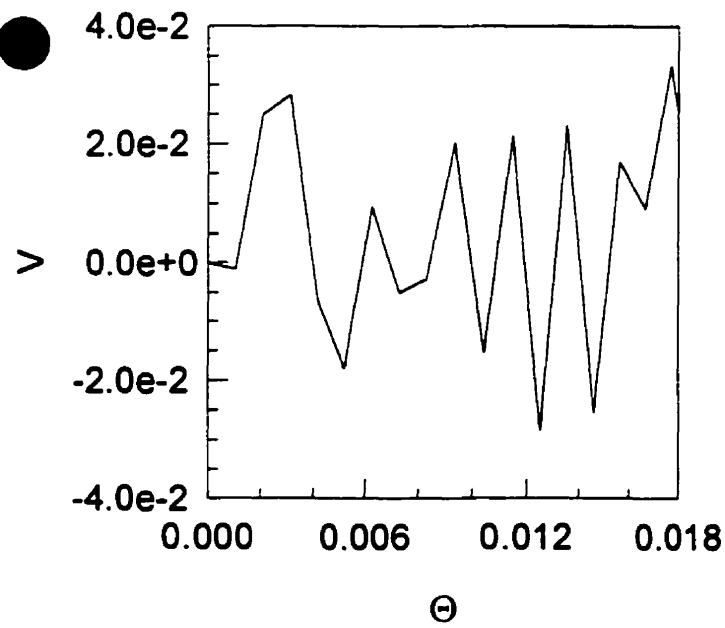
Figure 3.6. Some oscillating patterns of velocity component in y -direction.
 (a) $H/W = 1.0$; $x/W/2 = 1.0$; $Re_j = 4000$ (b) $H/W = 1.0$; $x/W/2 = 50$; $Re_j = 4000$
 (c) $H/W = 3.0$; $x/W/2 = 1.0$; $Re_j = 500$ (d) $H/W = 3.0$; $x/W/2 = 50$; $Re_j = 500$



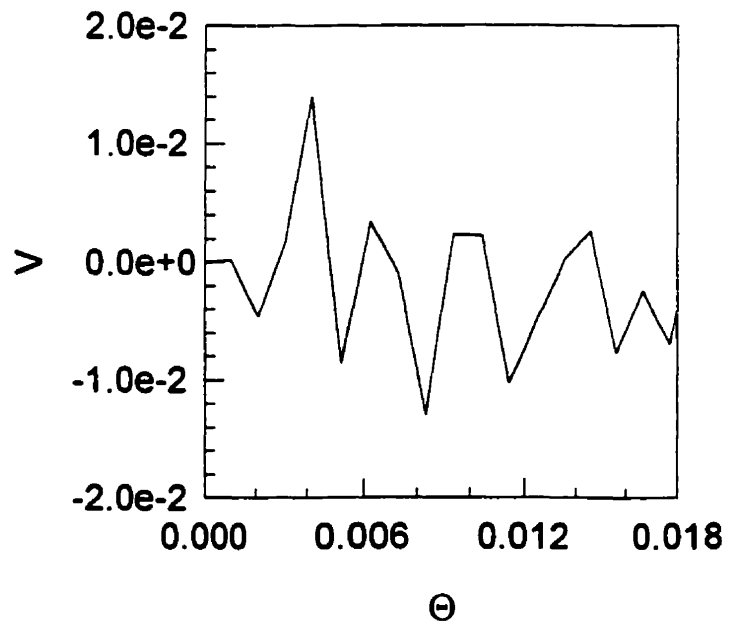
(a)



(b)



(c)



(d)

Figure 3.7. Some fluctuating patterns of velocity component in y-direction.
 (a) $H/W = 1.0$; $x/W/2 = 1.0$; $Re_j = 7500$ (b) $H/W = 1.0$; $x/W/2 = 50$; $Re_j = 7500$
 (c) $H/W = 2.0$; $x/W/2 = 1.0$; $Re_j = 3000$ (d) $H/W = 2.0$; $x/W/2 = 50$; $Re_j = 3000$

As H/W increases recirculating bubbles are observed at much lower Re_j . The vortices size increases with increased Re_j ; this trend is more pronounced at higher values of H/W . The jet interaction is also stronger as H/W increases as is seen in Figure 3.8b. A structure similar to the “pancake” reported by Wood et al. (1991) can also be seen in this figure. The flow develops much later downstream compared to the case shown in Figure 3.8a. Large recirculating bubbles are also seen in this figure. The shape of the temperature profiles is affected by the jet interaction and the presence of the vortices as can be seen in this figure.

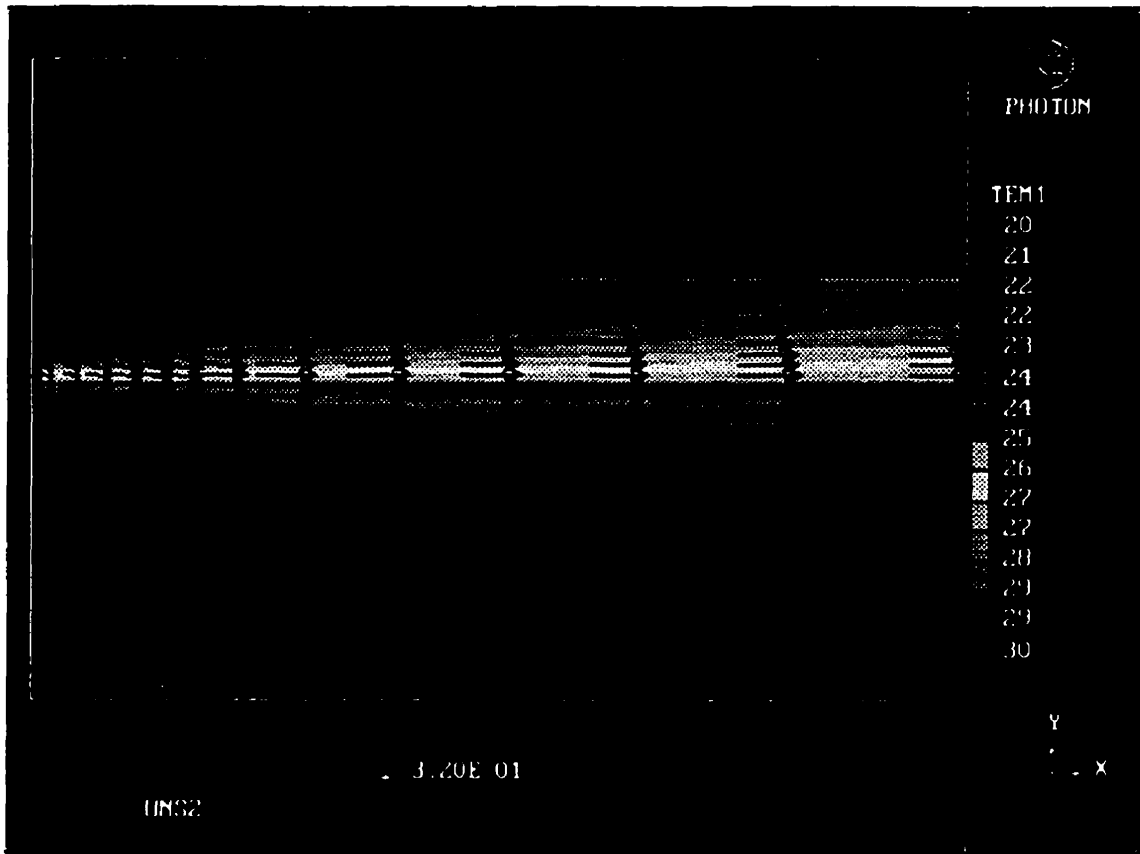


Figure 3.8a. Velocity vectors and temperature contours

$$H/W = 1.0; Re_j = 200$$

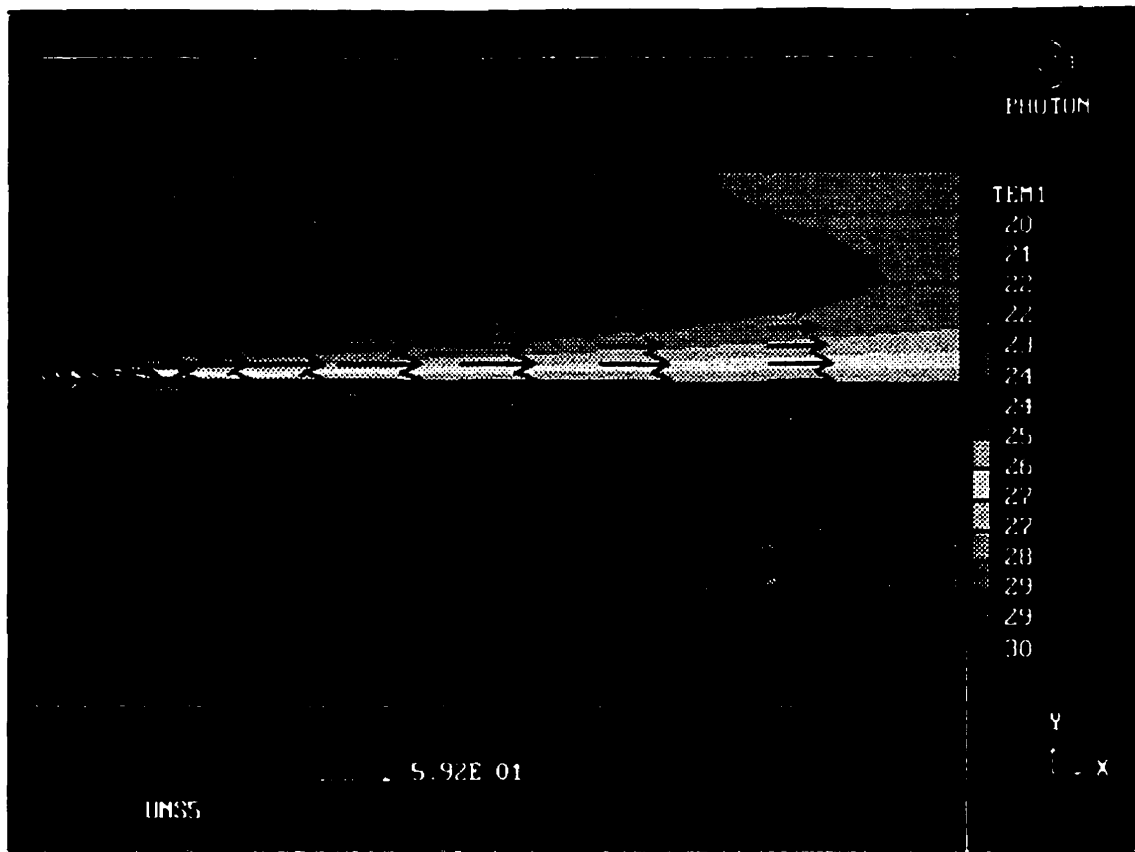


Figure 3.8b. Velocity vectors and temperature contours

$$H/W = 4.0; Re_j = 200$$

The plots of the mixing index versus dimensionless axial distance with the jet Reynolds number as a parameter are shown in Figures 3.9a-3.9d for $H/W = 1-4$, respectively. Both dimensional and dimensionless coordinates are shown in these figures for easy comparison. It should be noted that the upper limit of $x/W/2 = 200$ in these figures was chosen arbitrarily and does not imply that the computational domain ends at that particular value. The fully developed assumption at the exit still holds for all cases reported here.

It can be seen from these figures that a longer exit channel is required for complete mixing as the jet Reynolds number increases. This trend holds for all H/W values studied. This may be ascribed to the increase in momentum of the fluid in the exit

channel (and hence shorter residence time of the fluid in the system) due to the additional mass coming into the system. At low H/W values, i.e., $H/W = 1-2$, the mixing curves scale monotonically with Re_j since very small jet interaction occurs. Thermal mixing is mainly by diffusion. As H/W increases the jet interaction is stronger and hence a better mixing in the impingement zone and its vicinity. For a particular value of the jet Reynolds number the distance to attain well-mixed condition increases in the dimensionless distance but decreases dimensionally with H/W since the transverse diffusive term in the energy equation becomes less dominant as H/W increases. Very good mixing is obtained over a rather short distance for all cases studied, however.

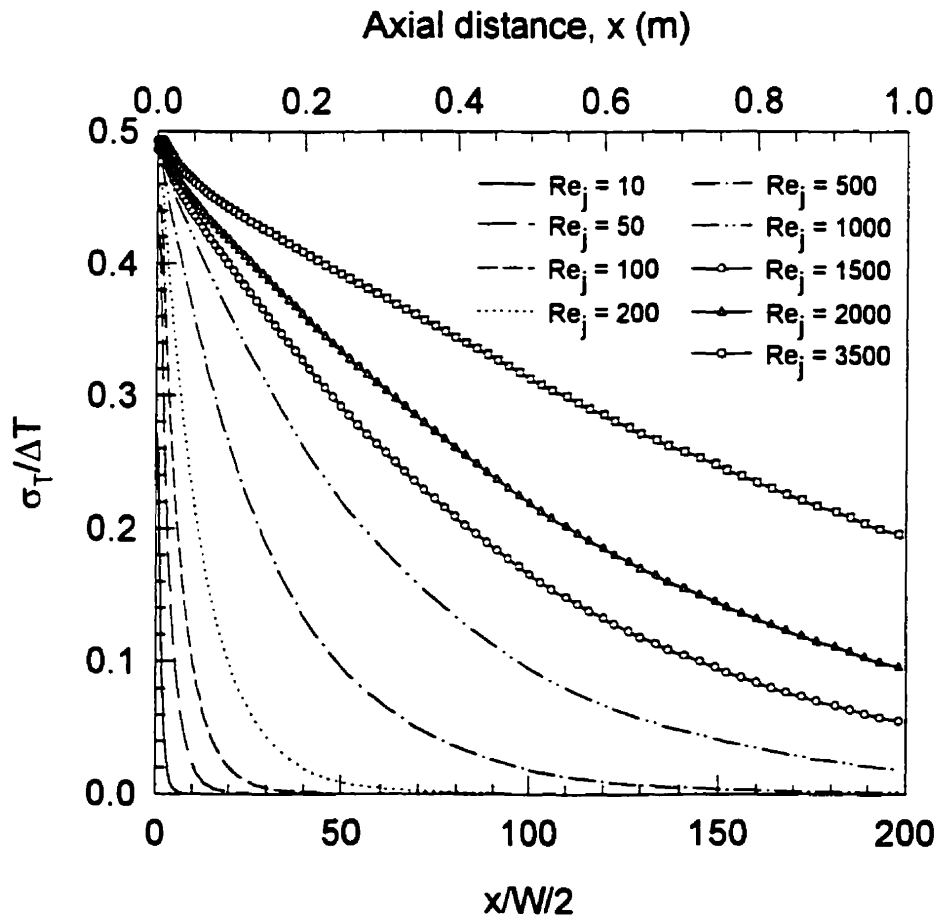
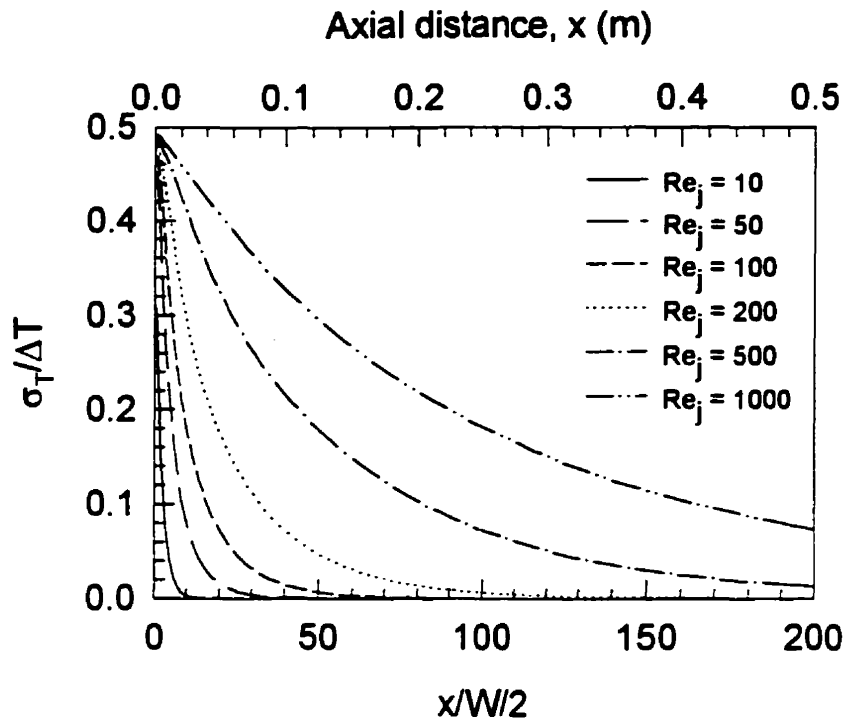
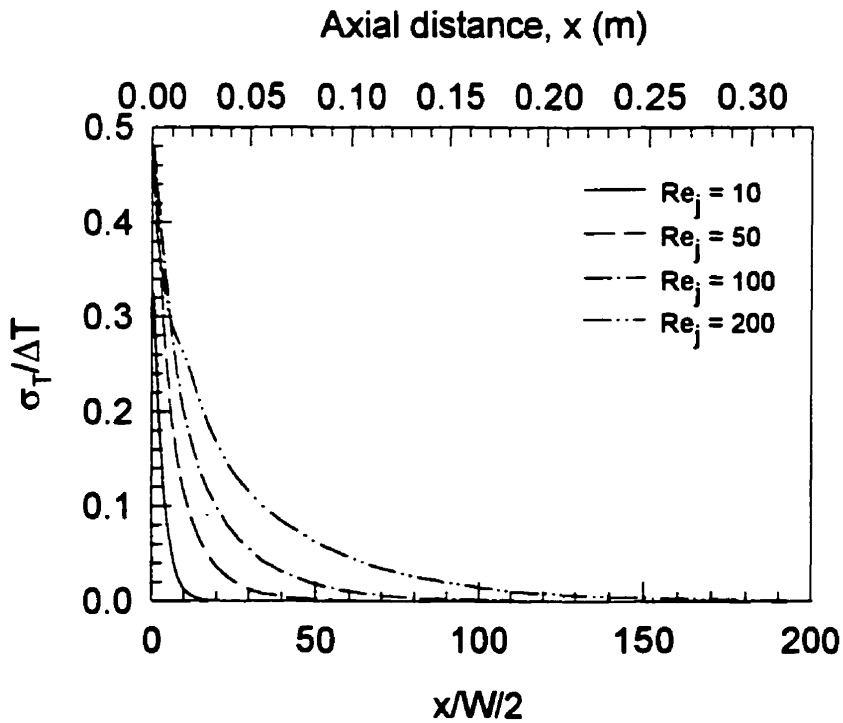


Figure 3.9a. Mixing index for $H/W = 1.0$.

Figure 3.9b. Mixing index for $H/W = 2.0$.Figure 3.9c. Mixing index for $H/W = 3.0$.

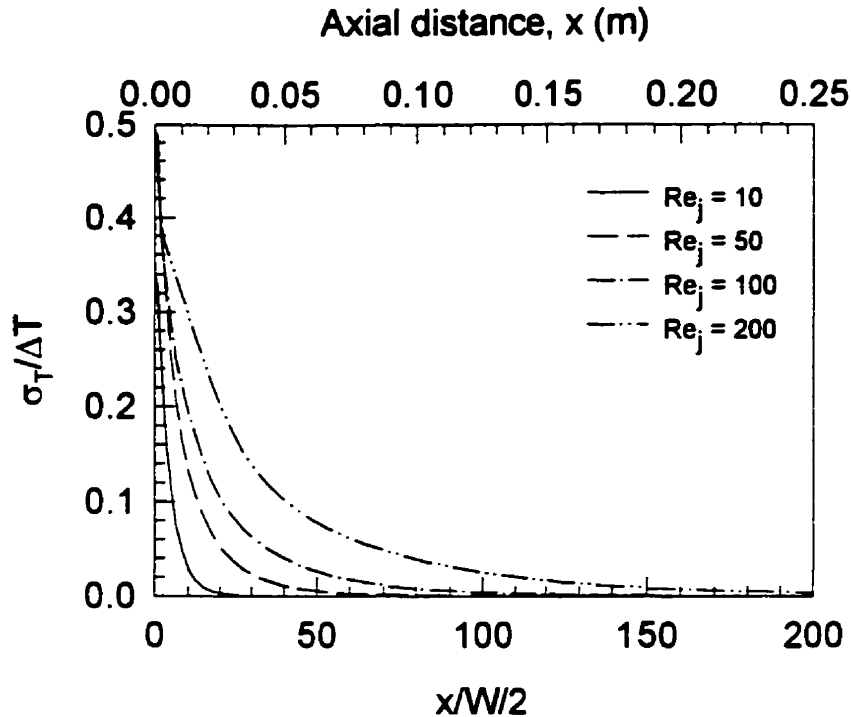
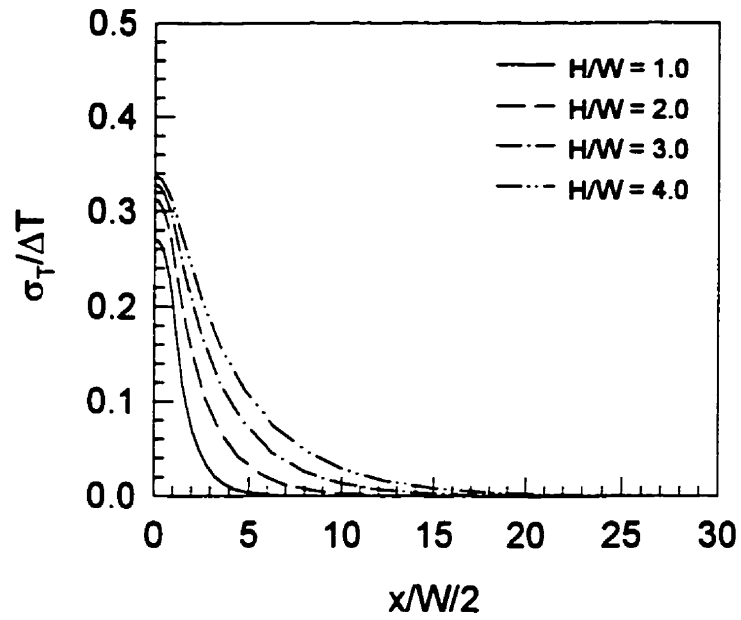
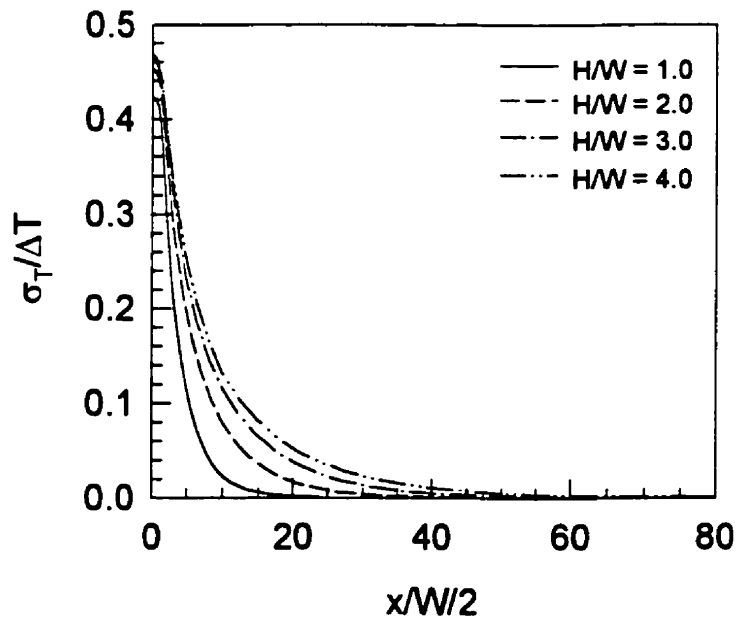
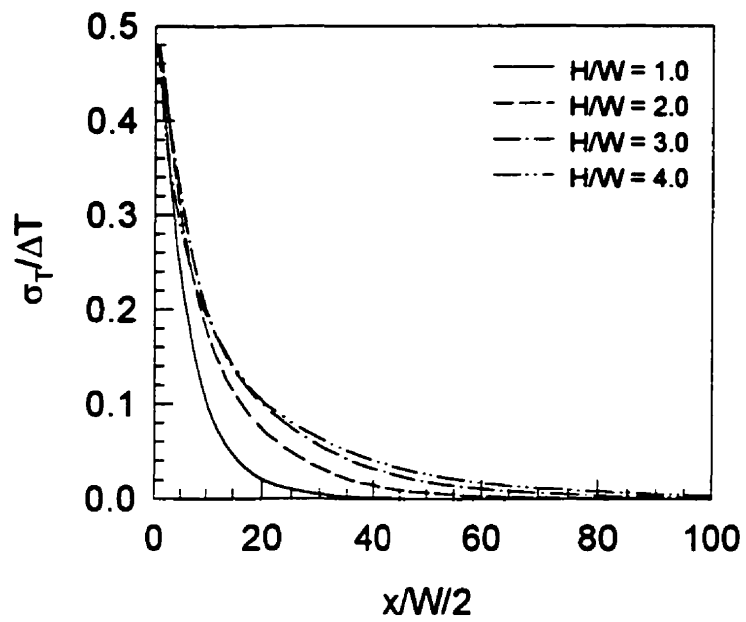
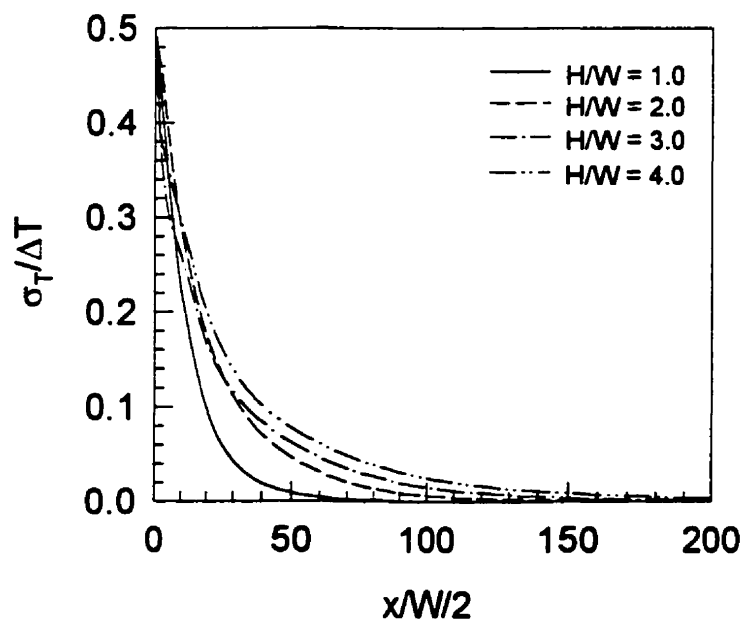


Figure 3.9d. Mixing index for $H/W = 4.0$.

Figure 3.10 shows the plots of the mixing index versus $x/W/2$ with H/W as a parameter. The upper limit of $Re_j = 200$ was chosen here since this is the last point where a laminar steady solution can be obtained for $H/W = 4$ (see Figure 3.5). Again, as H/W increases the dimensionless length of the exit channel required to well mix the two streams increases. This effect of H/W on the mixing length, however, decreases with an increase in H/W . The effect of the jet interaction on the mixing in the impingement region can be seen again in Figures 3.10c and 3.10d. As H/W increases the jet interaction is stronger and hence a better mixing (Figure 3.10c). As H/W becomes higher and hence the higher jet velocity at the same Re_j due to the smaller jet opening the higher lateral momentum tends to push the fluid out of the system faster. This leads to a poorer mixing at high Re_j and H/W as is seen in Figure 3.10d.

Figure 3.10a. Mixing index for $Re_j = 10$.Figure 3.10b. Mixing index for $Re_j = 50$.

Figure 3.10c. Mixing index for $Re_j = 100$.Figure 3.10d. Mixing index for $Re_j = 200$.

3.3.2. Flow and mixing characteristics of a novel impinging stream in-line mixer

The fluid was injected normally into the two-dimensional channel through the top and bottom two-dimensional slot jet inlets (Figure 3.2). These streams impinged against each other and then left the mixing channel through the exits situated on either side of the mixer. The mixing channels were extended long enough to satisfy the fully developed channel flow assumption. The top and bottom jets are offset with respect to each other; the effect of this offset on the mixing performance of the mixer is of interest in this section. The mixing behavior is reported only for the area marked by the dotted line in Figure 3.2 as this area represents an elementary domain of a mixer consisting of an infinite number of inlets. The ranges of parameters studied in this work are: inlet jet Reynolds number (Re_j) from 10 to 100, and H/W and S/W from 1.0 to 3.0.

The plots of velocity vectors and temperature isotherms for one representative case are shown in Figures 3.11a and 3.11b, respectively. It can be seen from the vector plots that there exists a region between the inlet jets where shear-induced mixing (due to large velocity gradients in the flow in this region) occurs. Very good mixing is obtained in this region as can be seen from the isotherms in Figure 3.11b. Recirculation zones are observed only on one side (either near the top or bottom wall) of each pair of top and bottom jets due to the offset; each jet prevents formation of the recirculation bubble on the opposite wall. The absence of these recirculating zones is beneficial as it results in a more uniform mixing in the channel.

Figure 3.12 shows plots of the mixing index versus dimensionless axial distance with the inlet jet Reynolds number as a parameter. For fixed values of H/W and S/W increasing of Re_j leads to a better mixing in the region between the inlet jets due to the higher shear-induced mixing. This trend is less pronounced at higher S/W values (where the region between the jets is more extended). As the spacing between the jets increases the fluid has longer time to exchange momentum and hence better mixing is obtained and overshadows the effect of increased shear at higher Re_j . Away from this zone, however, reduced mixing is indicated at higher Re_j due to the shorter residence time of the fluid in the mixer caused by the increased mean velocity as Re_j increases. Higher values of the

mixing index at both ends of the marked region are due to the difference in temperature of the next pair of incoming jets.

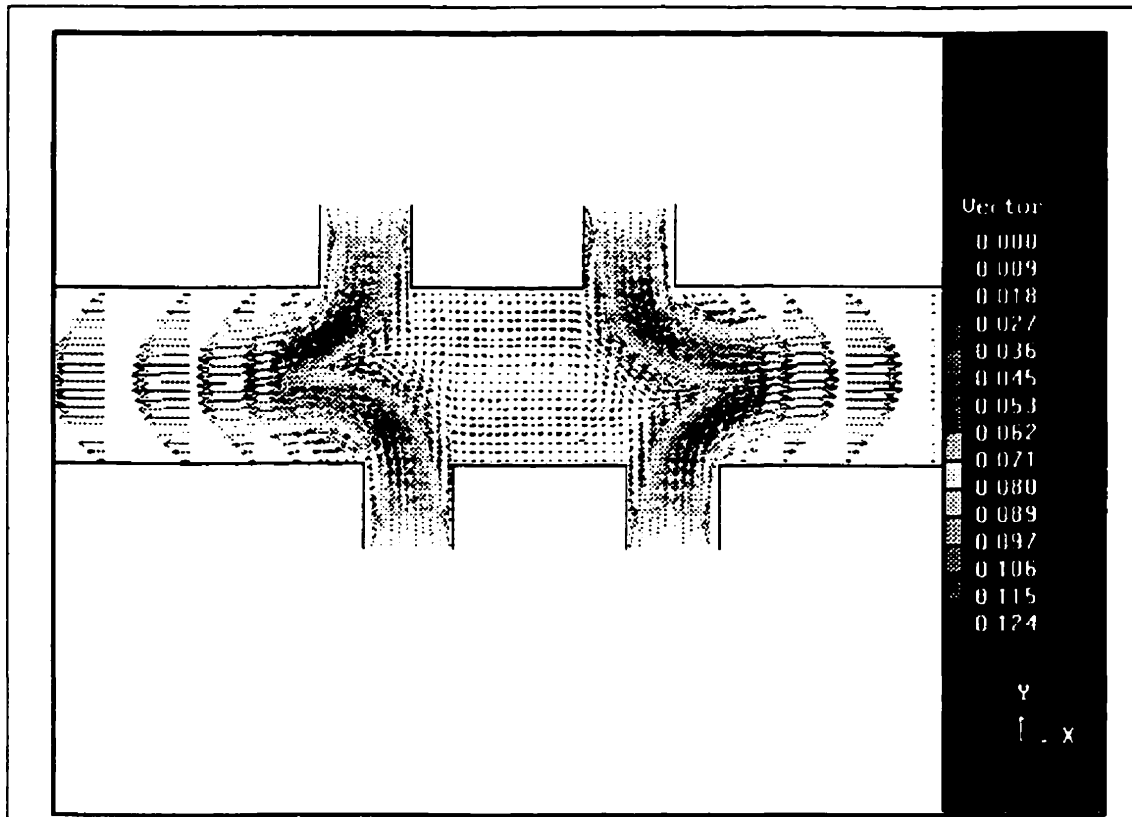


Figure 3.11a. Velocity vectors.

$H/W = 2.0; S/W = 2.0; Re_j = 50$

As can be seen from Figure 3.13, for fixed values of H/W and Re_j ; increasing S/W leads to a better mixing in the region between the jets but yields comparable results in the other regions. Of course, this region of good mixing is longer in axial length at higher S/W . This effect is less pronounced at higher Re_j ; due to the better mixing achievable by higher shear rates.

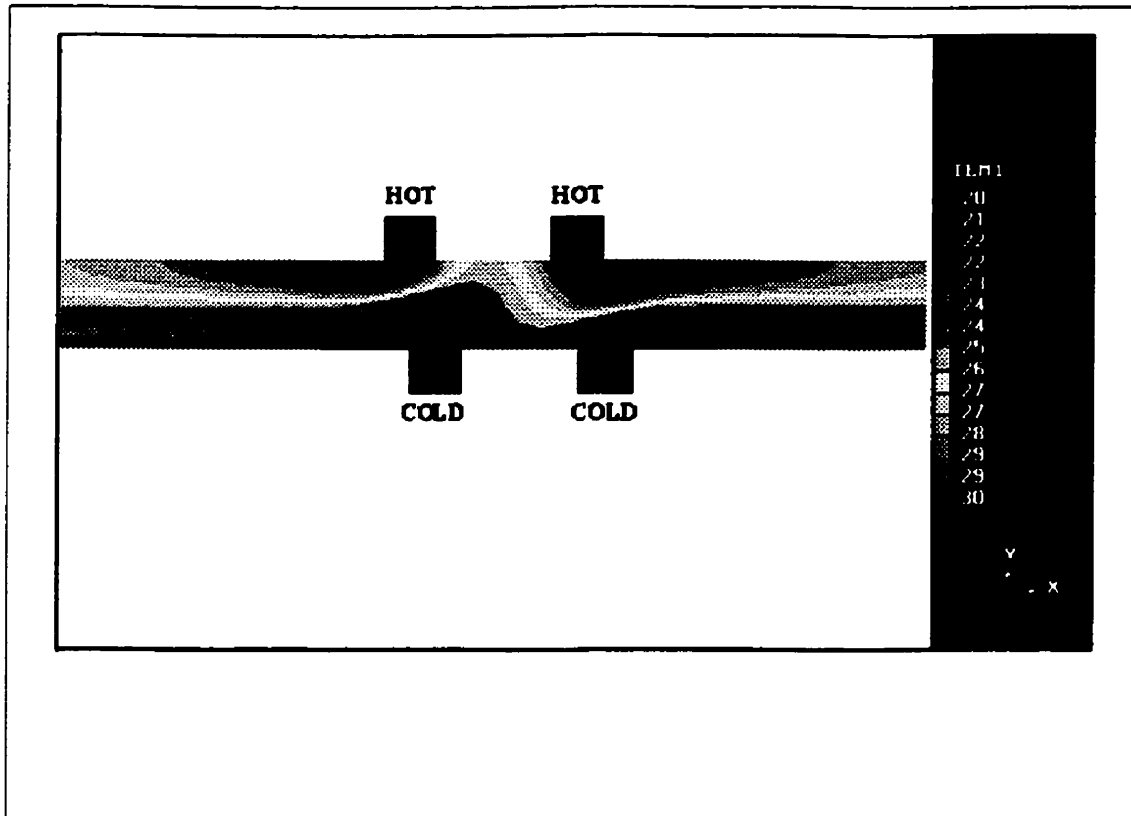
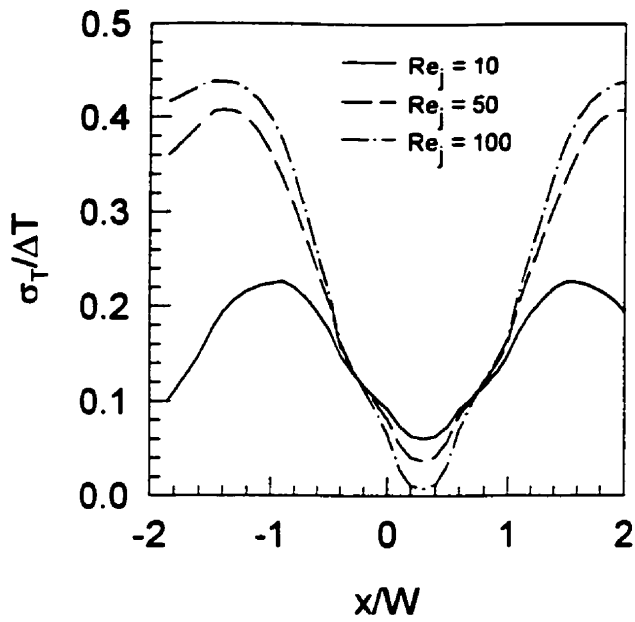


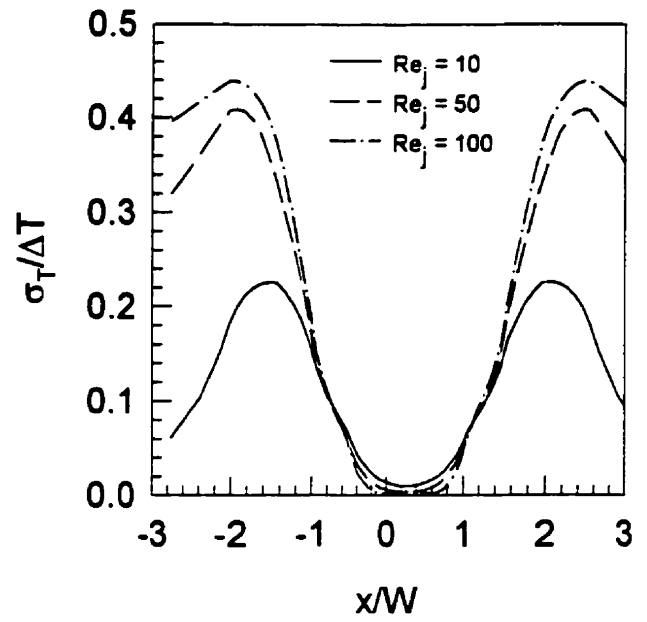
Figure 3.11b. Temperature contours.

$$H/W = 2.0; S/W = 2.0; Re_j = 50$$

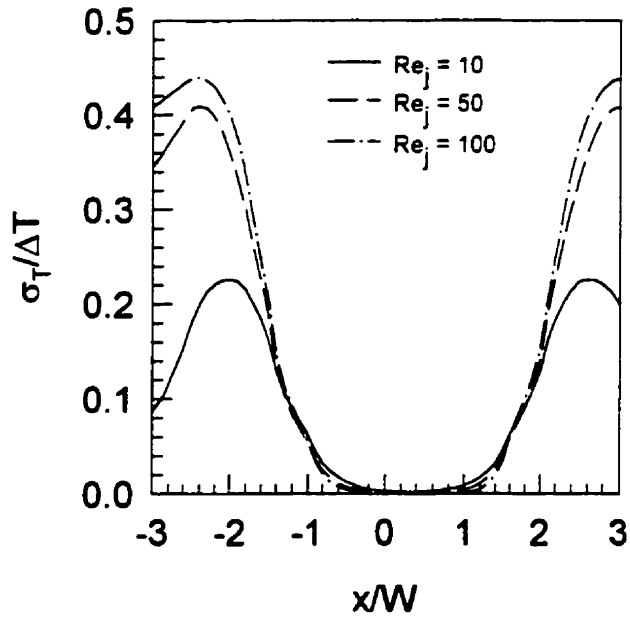
The plots of the mixing index versus dimensionless axial distance with H/W as a parameter are shown in Figure 3.14. As H/W increases more uniform (but poorer) mixing is noted. This effect is especially pronounced at lower values of S/W and Re_j . The reason for this behavior is that as H/W increases the spacing between the inlet jets, S , decreases (since the value of H is fixed). Mixing is thus more uniform across the length of the mixer as there is a shorter region of intense mixing. This effect of H/W is less pronounced as Re_j increases, however.



(a)



(b)

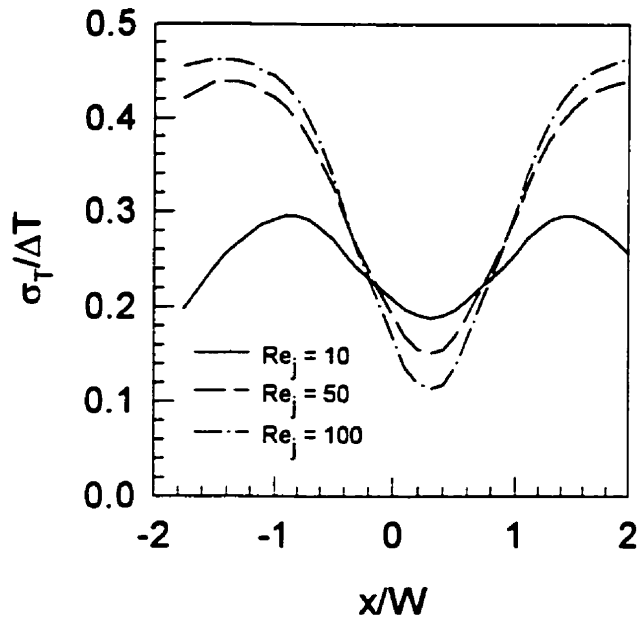


(c)

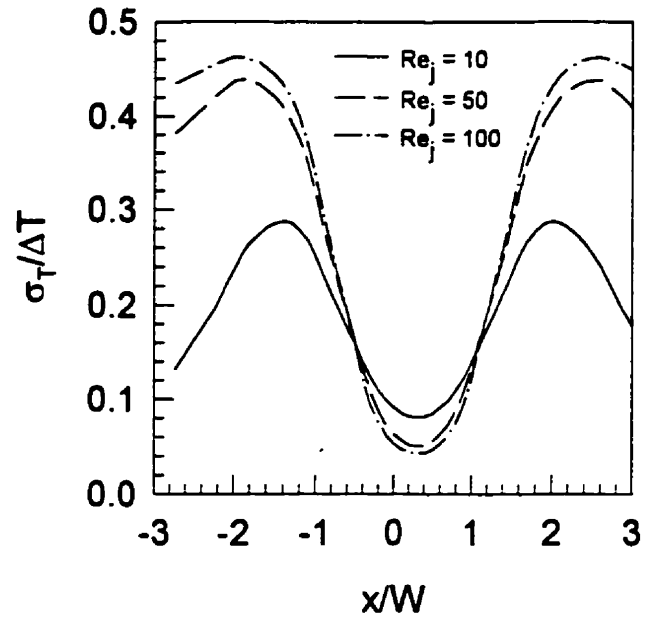
Figure 3.12. Mixing index.

(a) $H/W = 1.0$; $S/W = 1.0$ (b) $H/W = 1.0$; $S/W = 2.0$

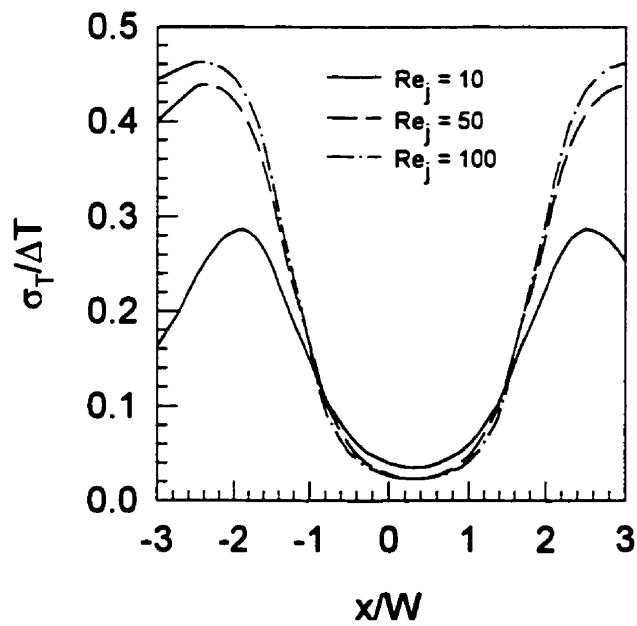
(c) $H/W = 1.0$; $S/W = 3.0$



(d)

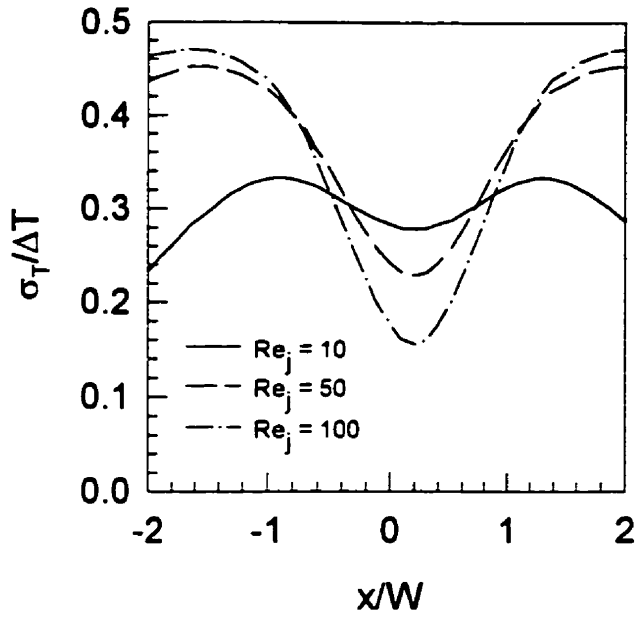


(e)

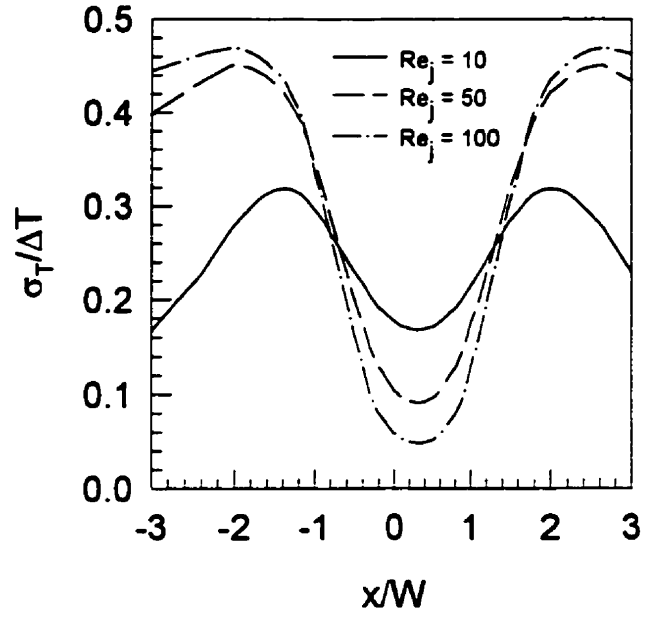


(f)

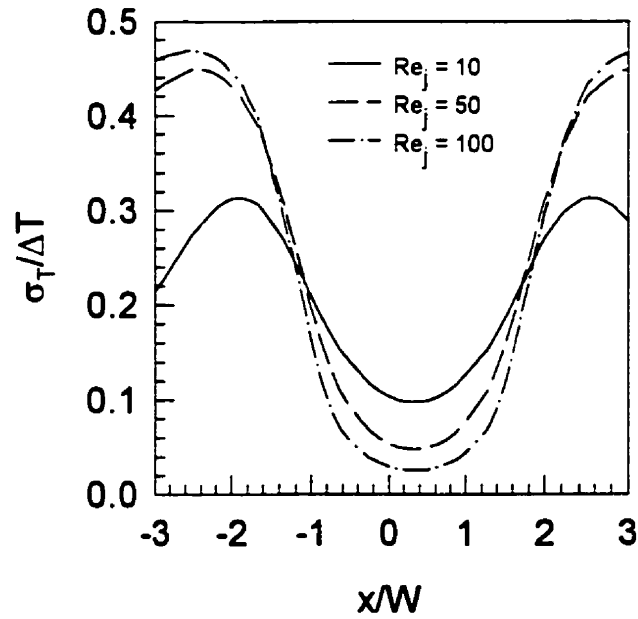
Figure 3.12. Mixing index (cont'd)
 (d) $H/W = 2.0$; $S/W = 1.0$ (e) $H/W = 2.0$; $S/W = 2.0$
 (f) $H/W = 2.0$; $S/W = 3.0$



(g)

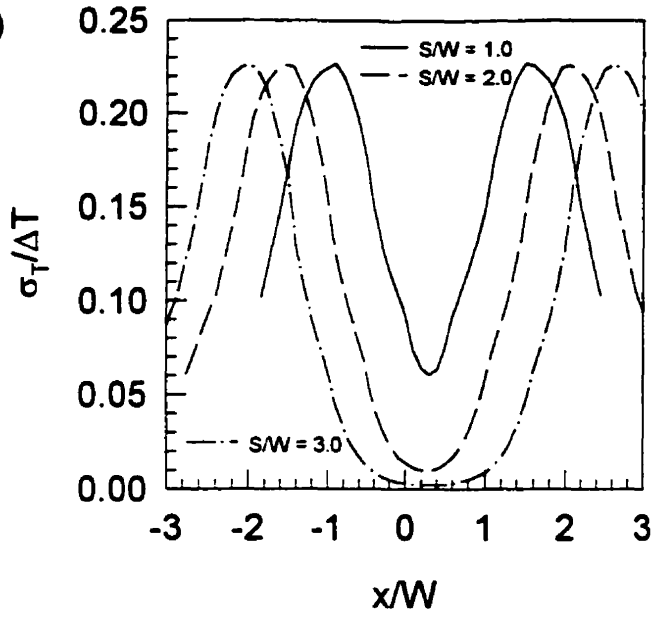


(h)

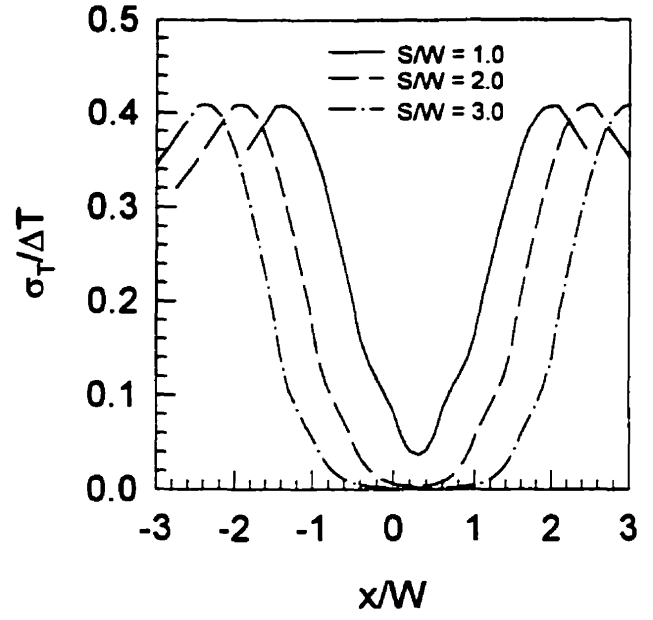


(i)

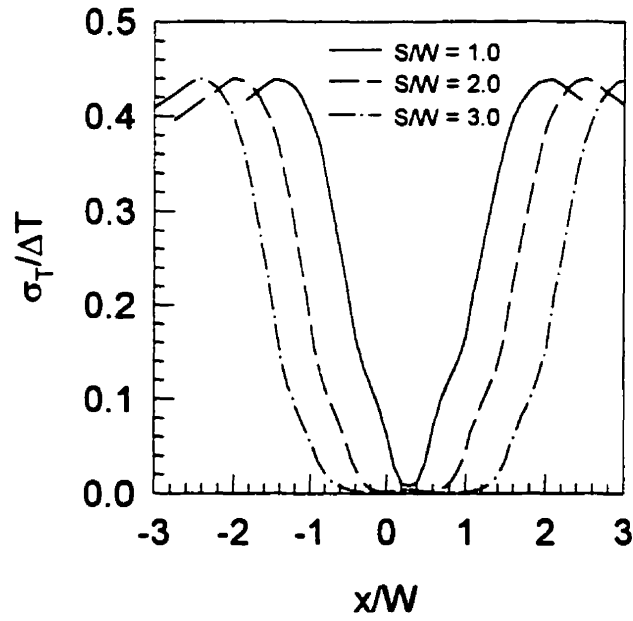
Figure 3.12. Mixing index (cont'd)
 (g) $H/W = 3.0$; $S/W = 1.0$ (h) $H/W = 3.0$; $S/W = 2.0$
 (i) $H/W = 3.0$; $S/W = 3.0$



(a)



(b)

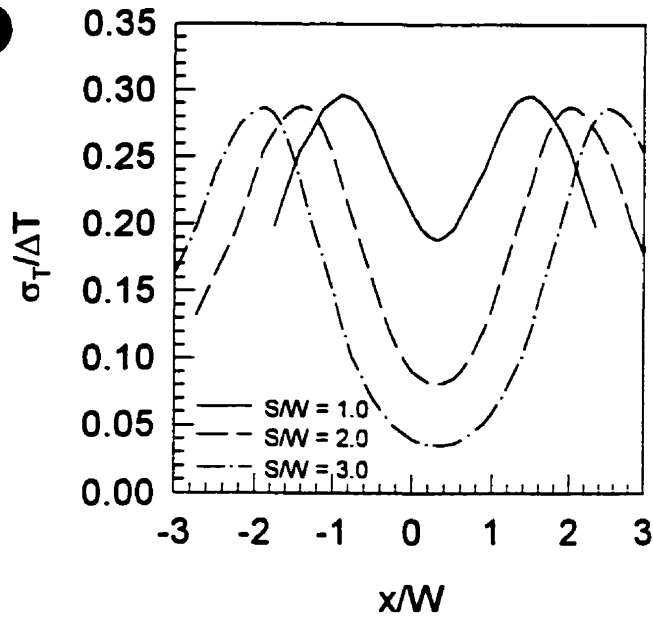


(c)

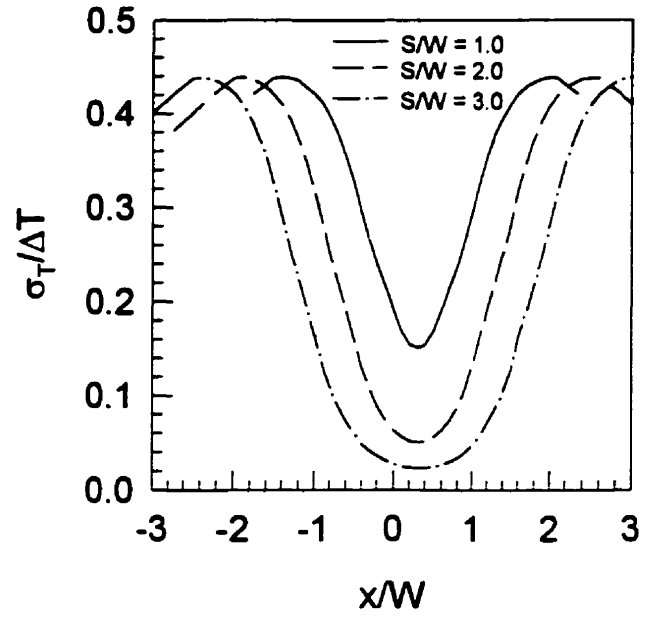
Figure 3.13. Mixing index.

(a) $H/W = 1.0$; $Re_j = 10$ (b) $H/W = 1.0$; $Re_j = 50$

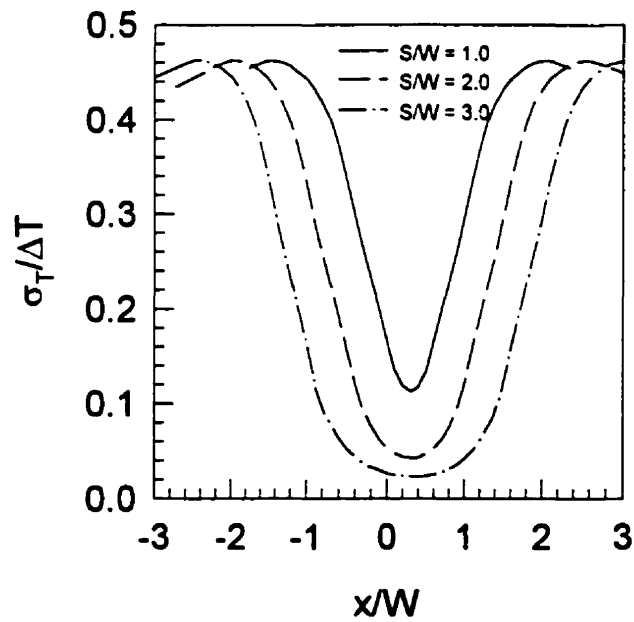
(c) $H/W = 1.0$; $Re_j = 100$



(d)

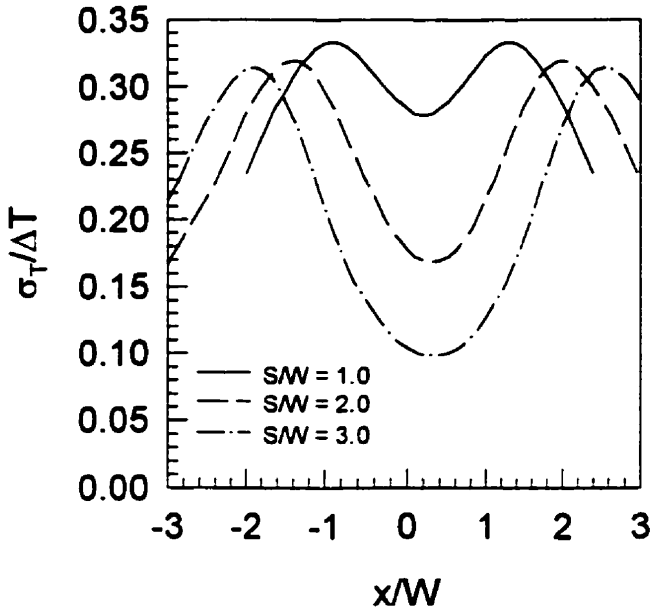


(e)

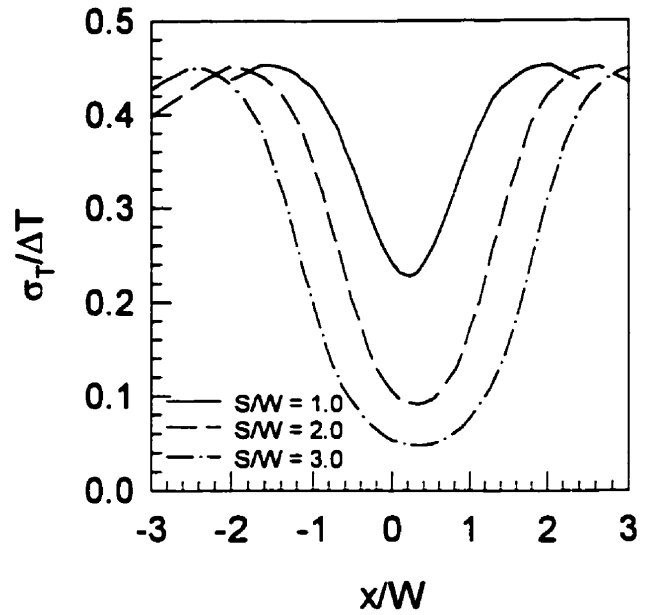


(f)

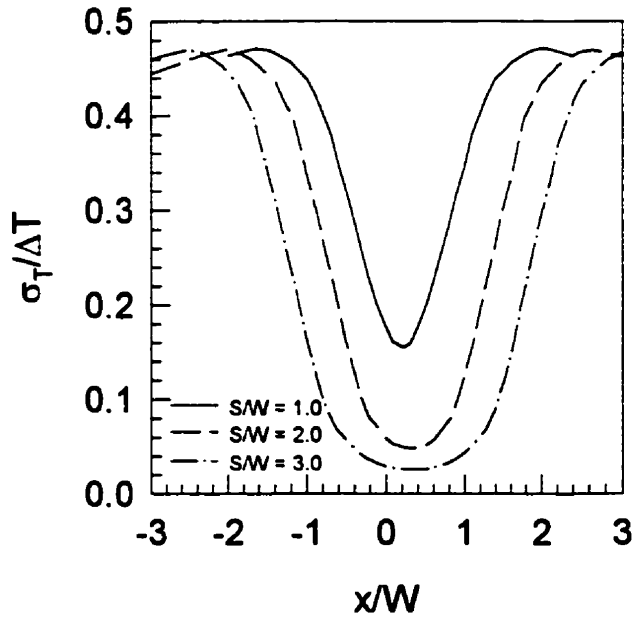
Figure 3.13. Mixing index (cont'd)
 (d) $H/W = 2.0$; $Re_j = 10$ (e) $H/W = 2.0$; $Re_j = 50$
 (f) $H/W = 2.0$; $Re_j = 100$



(g)

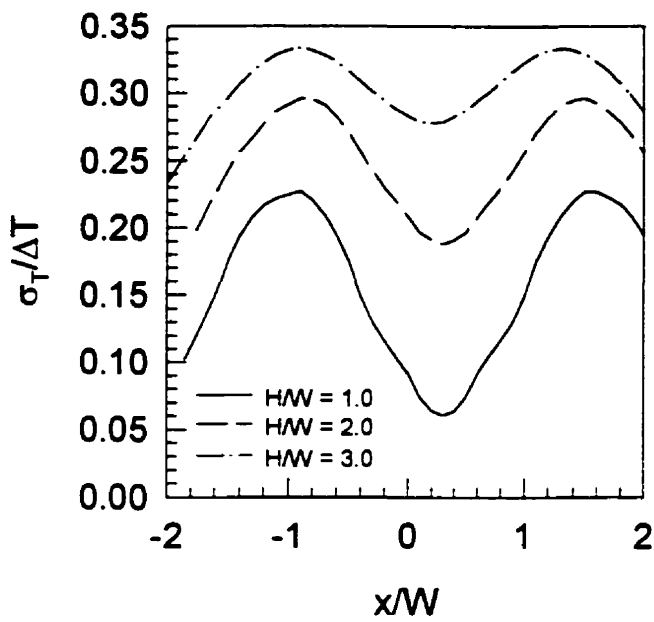


(h)

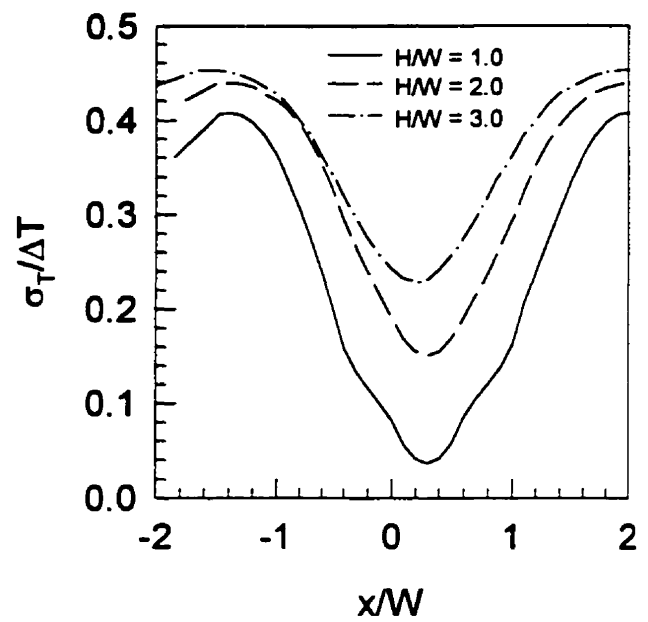


(i)

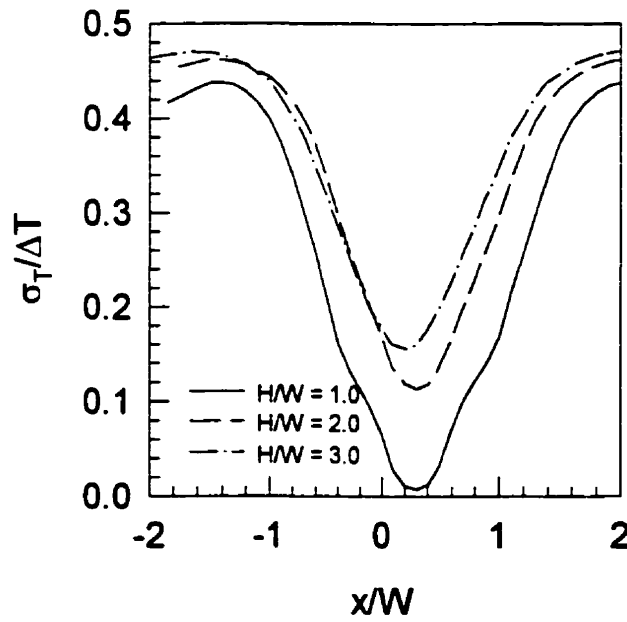
Figure 3.13. Mixing index (cont'd)
 (g) $H/W = 3.0$; $Re_j = 10$ (h) $H/W = 3.0$; $Re_j = 50$
 (i) $H/W = 3.0$; $Re_j = 100$



(a)

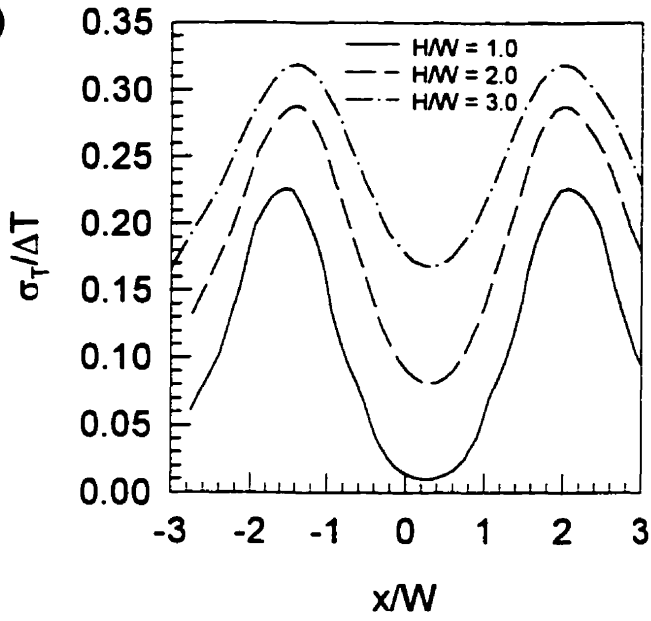


(b)

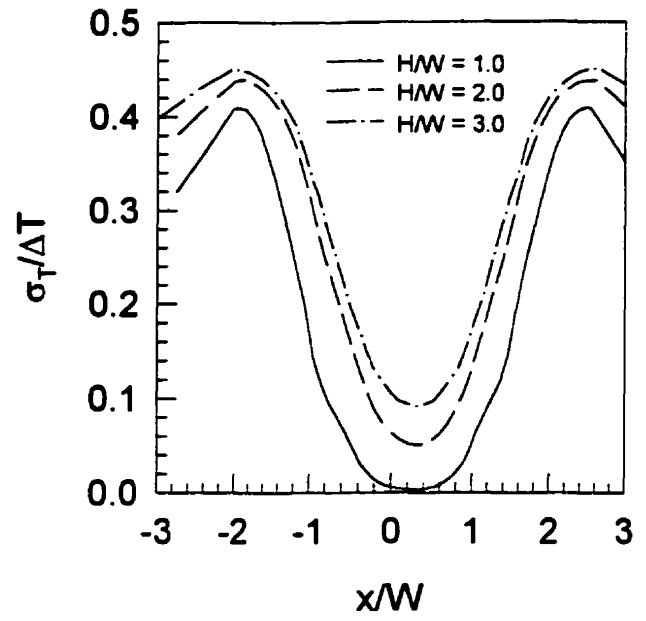


(c)

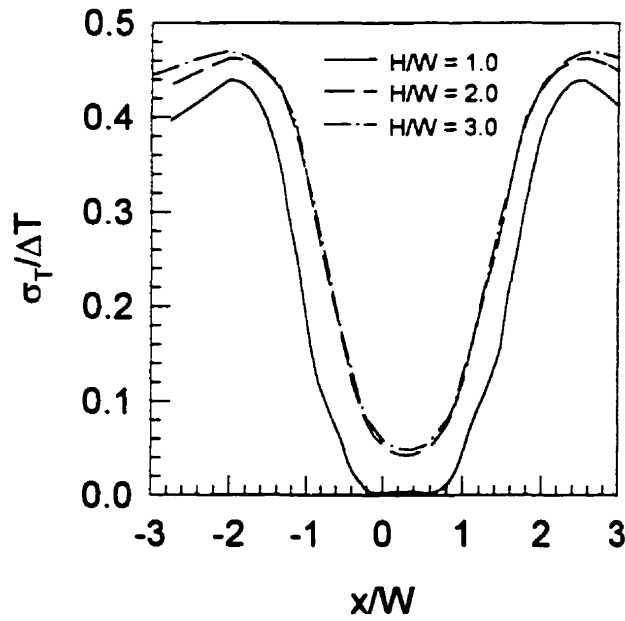
Figure 3.14. Mixing index.
 (a) $S/W = 1.0$; $Re_j = 10$ (b) $S/W = 1.0$; $Re_j = 50$
 (c) $S/W = 1.0$; $Re_j = 100$



(d)

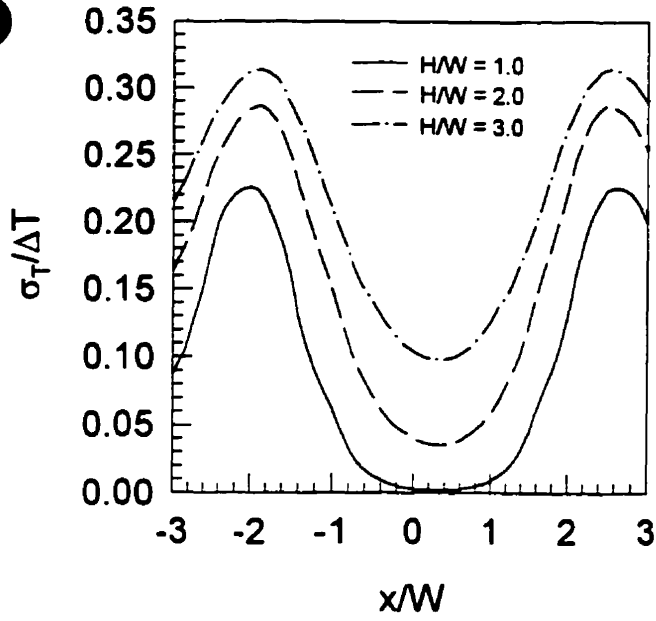


(e)

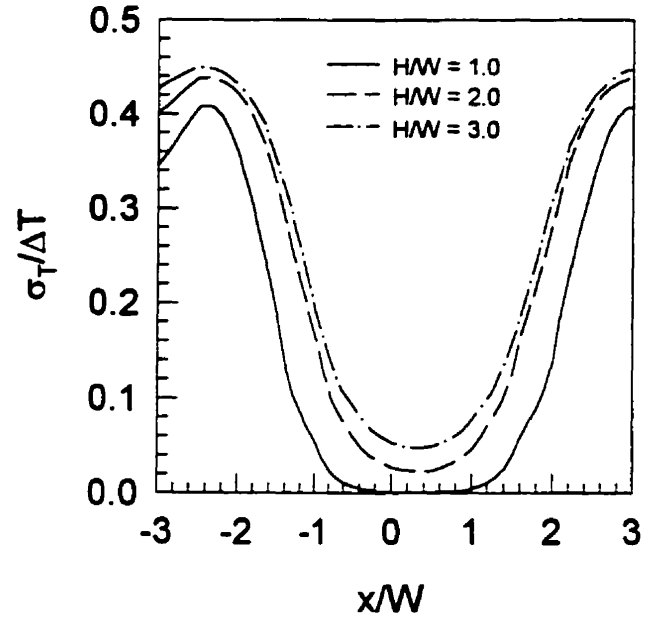


(f)

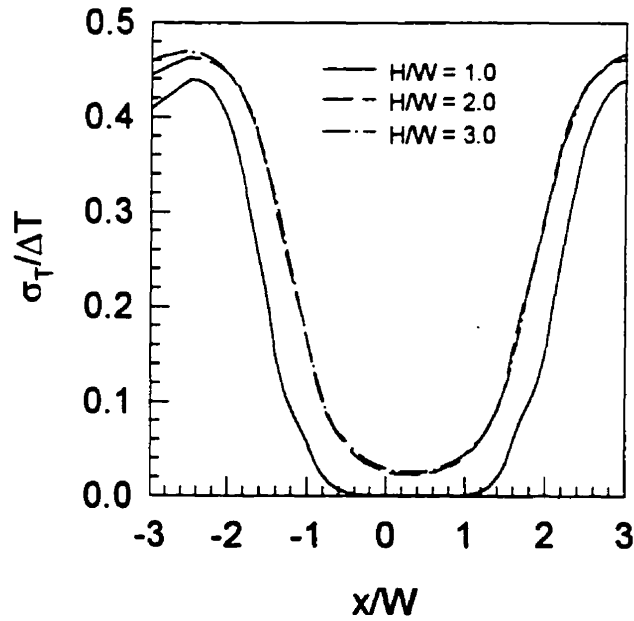
Figure 3.14. Mixing index (cont'd)
 (d) $S/W = 2.0$; $Re_j = 10$ (e) $S/W = 2.0$; $Re_j = 50$
 (f) $S/W = 2.0$; $Re_j = 100$



(g)



(h)



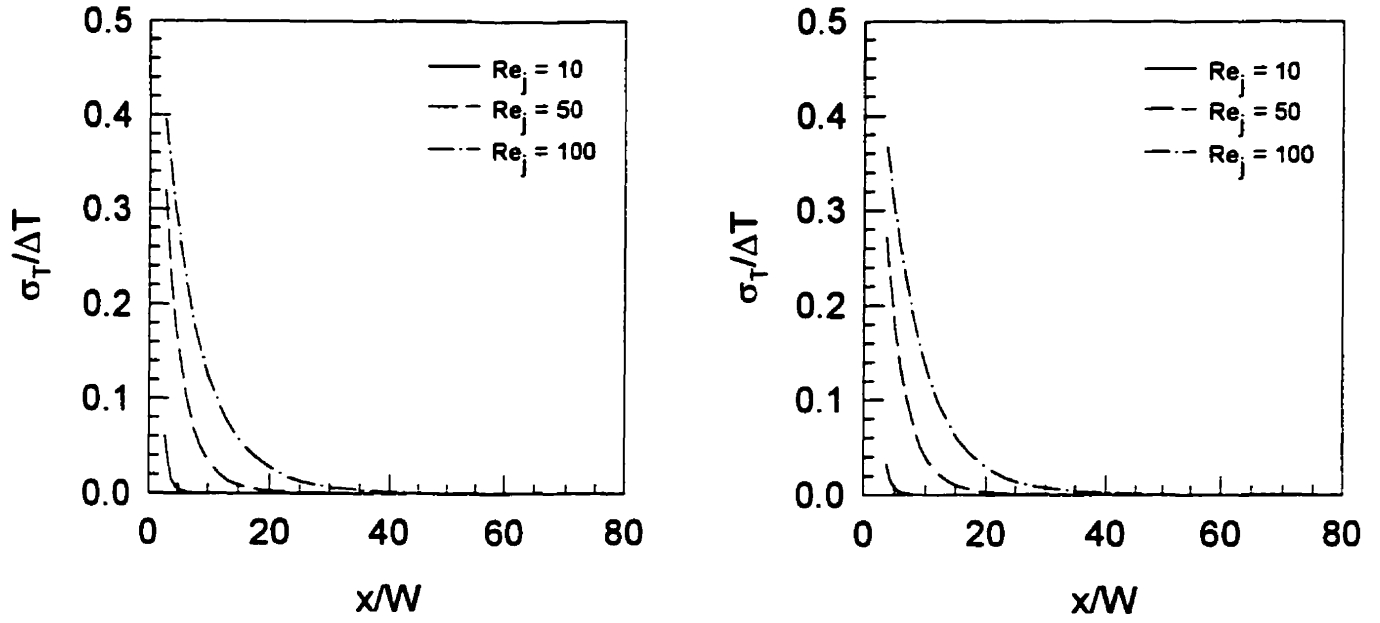
(i)

Figure 3.14. Mixing index (cont'd)
 (g) $S/W = 3.0$; $Re_j = 10$ (h) $S/W = 3.0$; $Re_j = 50$
 (i) $S/W = 3.0$; $Re_j = 100$

For design purposes the required length of the mixer to obtain a fully mixed condition at the outlets is shown in Figure 3.15 for various operating conditions and geometric configurations. The coordinates used are as shown in Figure 3.2. The general trend observed is that the required dimensionless length for good mixing increases with both Re_j and H/W but remains almost unchanged with S/W . As Re_j increases the fluid has a shorter residence time in the system due to the increased mean flowrate and hence poorer mixing. Similar behavior was also observed by Hosseinalipour and Mujumdar (1997a) who studied mixing of fluids in two-dimensional opposing jets. It is interesting to note that, dimensionally, the required length of the mixer may decrease with an increase in H/W ; the conclusions based on non-dimensional results should therefore be interpreted with care.

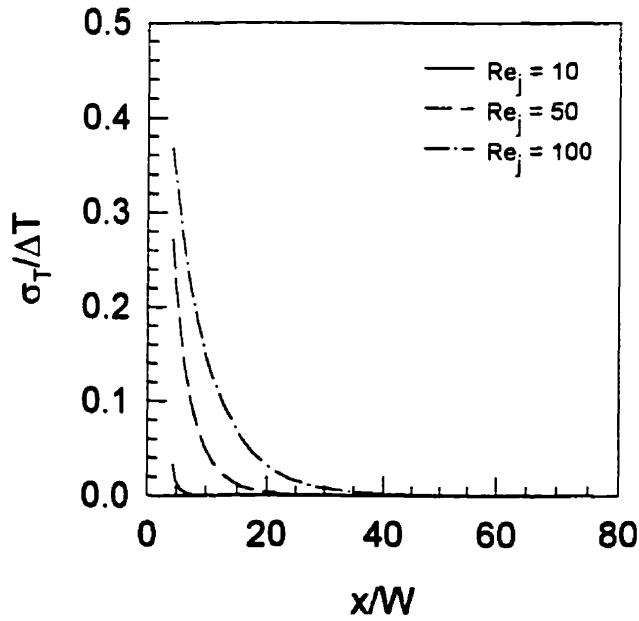
CLOSING REMARKS

In this chapter numerical simulations are reported on the flow and mixing characteristics of two-dimensional laminar confined impinging streams. In the first part time-dependent conservation equations for mass, momentum and energy were solved to determine the condition when the flow starts to shift from laminar to transitional and to random oscillatory flow regimes for various geometric configurations. Once the flow regime diagram has been established simulations were performed for cases in which steady-state solutions are obtainable to study the mixing characteristics of impinging streams. It is found that, for each geometric configuration, a longer exit channel is required to obtain the well-mixed condition as the inlet jet Reynolds number increases. For the same inlet jet Reynolds number, it is found that the distance to attain the well-mixed condition increases dimensionlessly but decreases dimensionally with H/W . Very good mixing is obtained over a rather short distance for all cases examined, however.



(a)

(b)



(c)

Figure 3.15. Mixing index in the exit channel.
 (a) $H/W = 1.0$; $S/W = 1.0$ (b) $H/W = 1.0$; $S/W = 2.0$
 (c) $H/W = 1.0$; $S/W = 3.0$

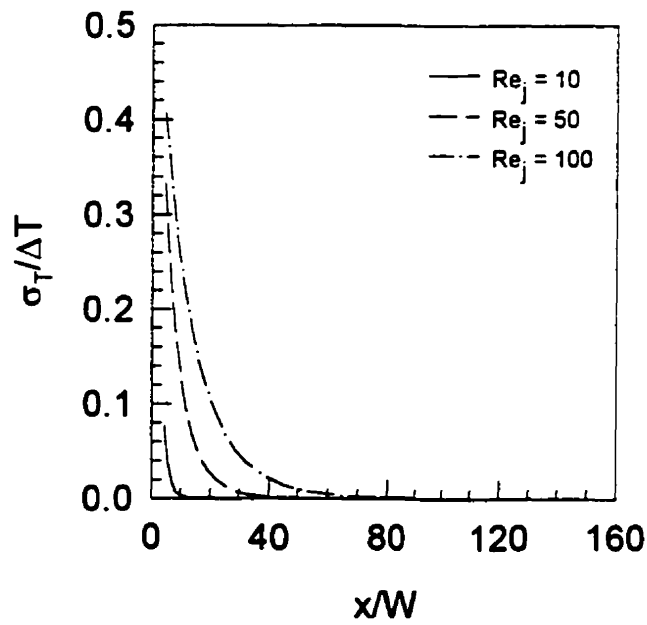
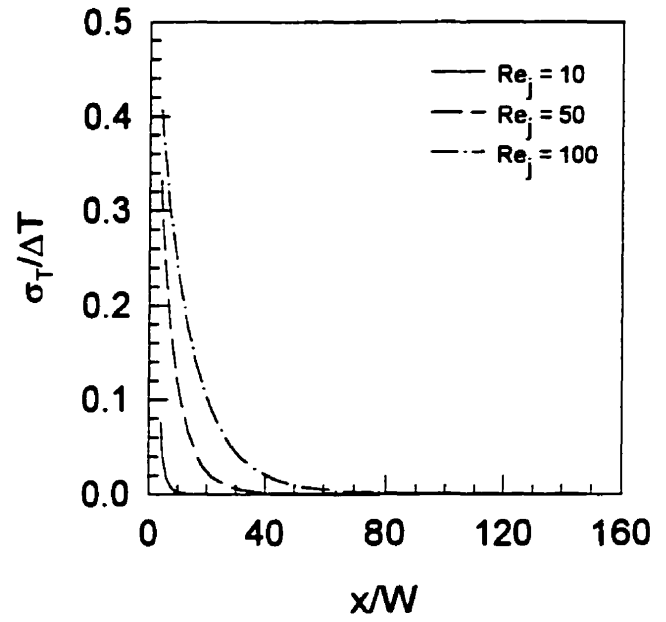
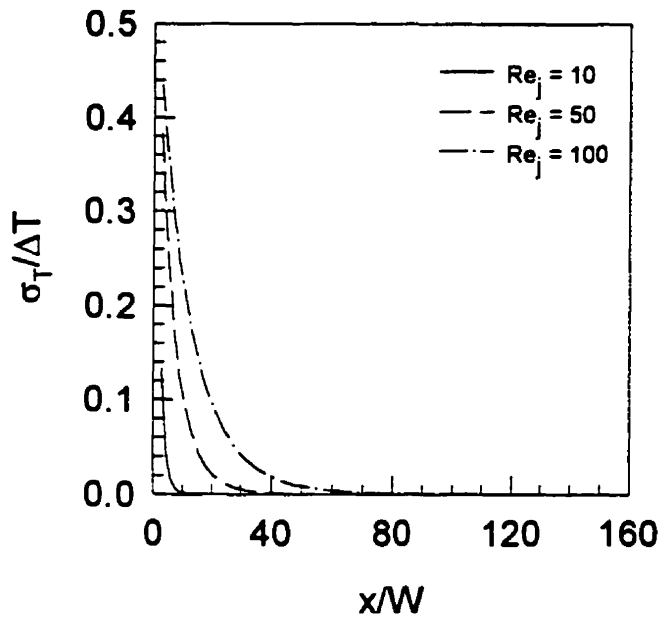
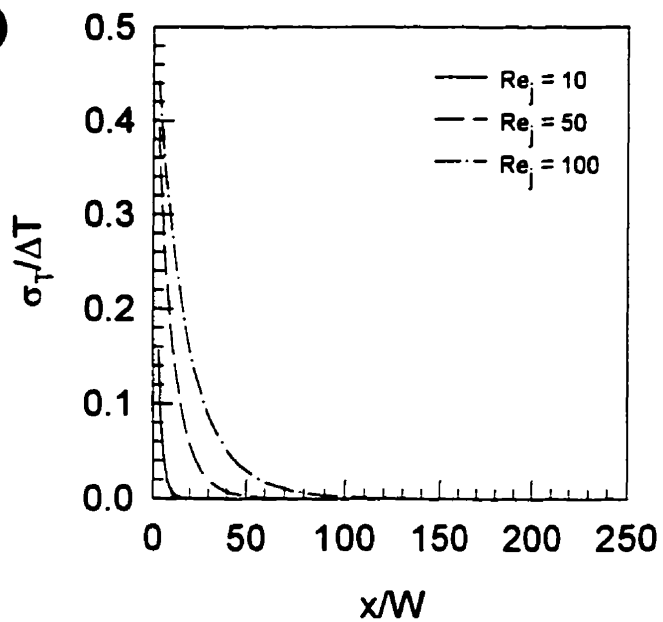


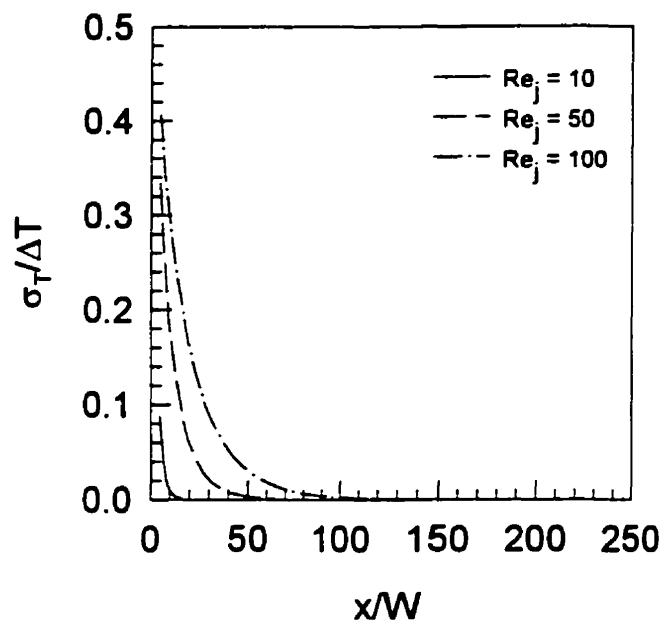
Figure 3.15. Mixing index in the exit channel (cont'd)

(d) $H/W = 2.0$; $S/W = 1.0$ (e) $H/W = 2.0$; $S/W = 2.0$

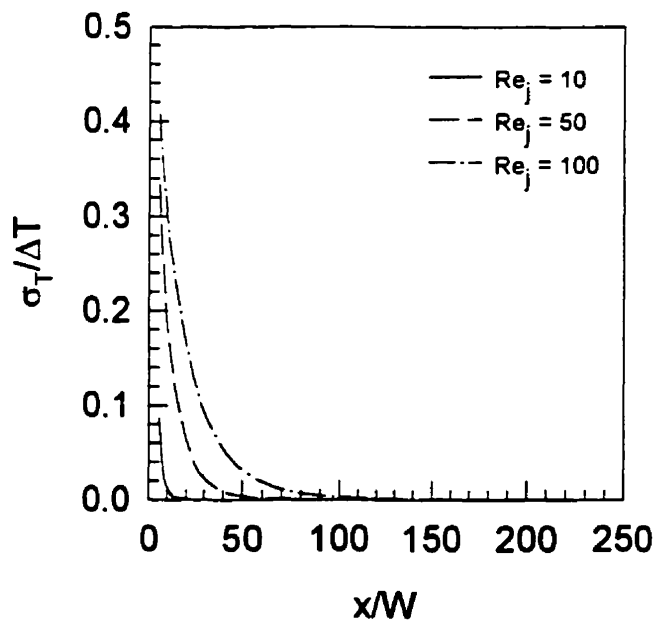
(f) $H/W = 2.0$; $S/W = 3.0$



(g)



(h)



(i)

Figure 3.15. Mixing index in the exit channel (cont'd)

(g) $H/W = 3.0$; $S/W = 1.0$ (h) $H/W = 3.0$; $S/W = 2.0$ (i) $H/W = 3.0$; $S/W = 3.0$

In the second part a numerical study was made of the mixing performance of a novel in-line fluid mixer utilizing multiple opposing jets in a two-dimensional channel. A simple technique to improve mixing viz. offsetting the top and bottom inlet jets, was proposed. It is found that this simple concept yields good mixing over a rather short distance in the channel mixer. Recirculation zones are observed only on one side (either near the top or bottom wall) of each pair of top and bottom jets due to the offset; each jet prevents formation of the recirculation bubble on the opposite wall. The absence of these recirculating zones is beneficial as it results in a more uniform mixing in the channel. Larger spacing between the inlet jets (higher S/W) results in better mixing in the region between these jets but yields no differences in the required channel length (between the last inlet and the exit port) to obtain a well-mixed condition at the exit. Higher Re_j also leads to a better mixing in the region between the inlet jets but to a poorer mixing in any other regions. This effect is, however, less clear at higher S/W due to the longer time available for fluid to mix in the region between the inlets. Increasing H/W leads to more uniform but poorer mixing. Again, a very good mixing is obtained over a rather short distance for all cases examined. This confirms the benefits of using impinging streams in conducting various unit operations including mixing.

In the next chapter heat transfer and mixing characteristics of turbulent confined impinging streams are reported. Different mixing behavior from the one reported in this chapter is observed for two-dimensional turbulent confined impinging streams. An explanation on the difference in the mixing behavior is given.

NOMENCLATURE

c_p	heat capacity, $J\ kg^{-1}\ K^{-1}$
D_h	inlet channel hydraulic diameter, m
g_i	gravitational force vector, $m\ s^{-2}$
H	height of the exit channel, fixed at 0.01 m
k	thermal conductivity, $W\ m^{-1}\ K^{-1}$
L	length of the exit channel, m
p	pressure, Pa

S	spacing between two inlet jets, m
t	time, s
T	temperature, °C
ΔT	temperature difference of the two inlet streams, °C
u	velocity component in x-direction, m s ⁻¹
u_i, u_j	velocity component, m s ⁻¹
u_{jet}	jet velocity, m s ⁻¹
V	dimensionless velocity component in y-direction, $V = u_z/u_{jet}$
W	width of the inlet channel, m
x_i, x_j	coordinate, m

Greek letters

μ	dynamic viscosity, kg m ⁻¹ s ⁻¹
ρ	density, kg m ⁻³
σ_T	standard deviation of temperature, °C
Θ	dimensionless time, $\Theta = t \cdot W / u_{jet}$

Dimensionless group

Re _j	jet Reynolds number, $\frac{D_h u_{jet} \rho}{\mu}$
-----------------	---

REFERENCES

- Baydar, E., 1999, Confined impinging air jet at low Reynolds numbers, *Experimental Thermal and Fluid Science*, 19, pp. 27-33.
- Berman, Y., Tamir, A., 1996, Experimental investigation of phosphate dust collection in impinging streams, *Canadian Journal of Chemical Engineering*, 74, pp. 817-821.
- Berman, Y., Tamir, A., 2000, Extraction in thin liquid films generated by impinging streams, *AIChE Journal*, 46, pp. 769-778.
- Berman, Y., Tanklevsky, A., Oren, Y., Tamir, A., 2000a, Modeling and experimental studies of SO₂ absorption in coaxial cylinders with impinging streams: part I, *Chemical Engineering Science*, 55, pp. 1009-1021.

- Berman, Y., Tanklevsky, A., Oren, Y., Tamir, A., 2000b, Modeling and experimental studies of SO₂ absorption in coaxial cylinders with impinging streams: part II, *Chemical Engineering Science*, 55, pp. 1023-1028.
- Bird, R.B., Stewart, W.E., Lightfoot, E.N., 1960, *Transport Phenomena*, Wiley, New York.
- Concentration, Heat and Momentum Limited (CHAM), 1997, *POLIS: Phoenix On-line Information System*, London, UK. <http://www.cham.co.uk>
- Hosseinalipour, S.M., Mujumdar, A.S., 1995, Flow, heat transfer and particle drying characteristics in confined opposing jets: a numerical study, *Drying Technology – An International Journal*, 13, pp. 753-781.
- Hosseinalipour, S.M., Mujumdar, A.S., 1997a, Flow and thermal characteristics of steady two-dimensional confined laminar opposing jets: part I. equal jets, *International Communications in Heat and Mass Transfer*, 24, pp. 27-38.
- Hosseinalipour, S.M., Mujumdar, A.S., 1997b, Flow and thermal characteristics of steady two-dimensional confined laminar opposing jets: part II. unequal jets, *International Communications in Heat and Mass Transfer*, 24, pp. 39-50.
- Johnson, D.A., Wood, P.E., 2000, Self-sustaining oscillations in opposed impinging jets in an enclosure, *Canadian Journal of Chemical Engineering*, 78, pp. 867-875.
- Kudra, T., Mujumdar, A.S., 1989, Impinging stream dryers for particles and pastes, *Drying Technology – An International Journal*, 7, pp. 219-266.
- Patankar, S.V., 1980, *Numerical Heat Transfer and Fluid Flow*, Hemisphere, Washington.
- Roy, J.C., Bertrand, C., Le Palec, G., 1994, Numerical and experimental study of mixed and forced convection in a junction, *International Journal of Heat and Mass Transfer*, 37, pp. 1985-2006.
- Tamir, A., 1989, Processes and phenomena in impinging-stream reactors, *Chemical Engineering Progress*, 85, pp. 53-61.
- Tamir, A., 1994, *Impinging-Stream Reactors: Fundamentals and Applications*, Elsevier, Amsterdam.

- Unger, D.R., Muzzio, F.J., Brodkey, R.S., 1998, Experimental and numerical characterization of viscous flow and mixing in an impinging jet contactor, *Canadian Journal of Chemical Engineering*, 76, pp. 546-555.
- Wood, P., Hrymak, A., Yeo, R., Johnson, D., Tyagi, A., 1991, Experimental and computational studies of the fluid mechanics in an opposed jet mixing head, *Physics of Fluids A*, 3, pp. 1362-1368.
- Yao, B., Berman, Y., Tamir, A., 1995, Evaporative cooling of air in impinging streams, *AIChE Journal*, 41, pp. 1667-1675.

**HEAT TRANSFER AND MIXING CHARACTERISTICS OF
TWO-DIMENSIONAL TURBULENT CONFINED IMPINGING STREAMS**

*A mathematician knows how to solve a
problem – but he can't do it*

W.E. Milne

4.1. INTRODUCTION

As mentioned in the previous chapters impinging streams (IS) provide a relatively new flow configuration that has proved useful in conducting a wide range of chemical engineering unit operations. A number of publications, as partially reviewed in Chapter 2, have reported applications of this flow configuration in such operations as absorption (Berman et al., 2000a,b), catalytic reactions (Sohrabi and Marvast, 2000), drying (Kitron and Tamir, 1988; Kudra and Mujumdar, 1989; Kudra and Mujumdar, 1995), dust collection (Berman and Tamir, 1996), liquid-liquid extraction (Berman and Tamir, 2000) as well as mixing (Tamir, 1994; Hosseinalipour and Mujumdar, 1997a,b; Unger et al., 1998). These papers, however, are based exclusively upon experimental results or else are limited to processes conducted in the laminar flow regime. Very few papers (e.g., Hosseinalipour and Mujumdar, 1995) have attempted modeling of turbulent transport processes in this flow configuration.

A number of papers have recently been published on modeling of turbulent flow and heat transfer behavior of impinging jets (IJ), which display characteristics somewhat similar to those of impinging streams. Seyedein et al. (1994) used both low-Reynolds

and high-Reynolds number versions of k - ε turbulence model to predict the flow field and heat transfer impingement due to a turbulent single headed slot jet discharging normally into a confined two-dimensional channel. Better agreement between numerical results obtained using low-Reynolds number models and the available experimental data is noted compared to those results obtained using high-Reynolds number model. Hosseinalipour and Mujumdar (1995) used five different versions of the low-Reynolds number k - ε models and the standard high-Reynolds number model to study the fluid flow and heat transfer characteristics of two-dimensional turbulent confined impinging and opposing jets flows. A so-called "Yap correction" was also tested with low-Reynolds number models to investigate its effect on the heat transfer predictions for the impinging jet case. Experimental data and numerical predictions by different turbulence models were compared for the turbulent impinging jet. Due to lack of experimental data, however, only the numerical results of the opposing jet case were presented. Morris et al. (1996) modified the converged solution obtained from commercial finite-volume code via the application of different turbulent Prandtl number functions in their post-processing program. Their predicted heat transfer results were then compared with selected experimental data; the predicted stagnation and average heat transfer coefficients agree with experiments to within a maximum deviation of 16-20 percent. To avoid using a full second moment closure, which may be a solution to modeling the flow with recirculation and streamline curvature, some investigators have recently employed simplified models which combine computational robustness and efficiency of the linear eddy viscosity models (e.g., k - ε models) with the improved model accuracy of second moment closures (e.g., Behnia et al., 1999; Bauer et al., 2000).

In this chapter a new composite turbulence model is proposed and applied to study thermal mixing of turbulent confined impinging streams. The model consists of a low-Reynolds number k - ε model, Yap correction as well as a formula for the turbulent (eddy) viscosity, which is incorporated directly into the computational fluid dynamic code. Experiments were conducted to verify the numerical results obtained using this model. The numerical results were also compared with experimental impingement heat transfer data available in the literature. Good agreement between the numerical and experimental data is noted for both impinging streams and impingement flows. The

model was then used to study the effects of various operating as well as geometric parameters on thermal mixing of two-dimensional turbulent confined impinging streams. It is found that the mixing behavior of turbulent confined impinging streams is quite different from that of laminar IS reported in Chapter 3. An explanation of the difference, based on results presented in this chapter and the previous one, is given.

4.2. EXPERIMENTAL SET-UP AND PROCEDURE

A schematic diagram of the overall heat transfer experimental set-up is shown in Figure 4.1a. Air was supplied by a blower (model no. 6350B-2, Wainbee Ltd., Pointe Claire, QC) and the flowrate in each flow branch was controlled by means of gate valves. One of the air streams was heated to pre-selected temperatures (either 10° or 20° C above the ambient) by an electric heater rated at 2.5 kW (model no. KSEF-30/120, Omega Engineering, Inc., Stamford, CT), which was controlled by a PID controller (model no. CN76000, Omega Engineering, Inc., Stamford, CT). The other air stream was left at ambient conditions. The air flowrate in each flow branch was measured using a pre-calibrated pitot tube (model no. FPT-6130, Omega Engineering, Inc., Stamford, CT). Differential pressure drop across the pitot tube was measured using a manometer filled with a manometric fluid (Red Gage Oil 0.826 SG, Dwyer Instruments, Inc., Michigan City, IN).

The air streams were then fed into the IS through two inlets (see Figure 4.1b). The two streams impinged normally against each other and left the IS through the exits situated symmetrically on either side of the impingement region. Temperature distributions in the IS were measured using 32 type K thermocouples (model no. EXFF-K-20-SLE, Omega Engineering, Inc., Stamford, CT; AWG no. 20), which were permanently mounted across the exit channel (see Figure 4.1c) and connected to an expansion board (model no. EXP-32, Omega Engineering, Inc., Stamford, CT). Thermocouple signals were multiplexed to a data acquisition card (model no. CIO-DAS16Jr, Omega Engineering, Inc., Stamford, CT) installed in a PC. LABTECH NOTEBOOK software (version 10.0.2, Laboratory Technologies Corp., Wilmington, MA) was used to read and record the temperature data for subsequent analyses. To test

whether these thermocouples had any effect on mixing of impinging streams two sets of experiments were conducted. In the first set of experiment only one thermocouple was used at a time while 32 thermocouples were used simultaneously in the second set of experiment. The maximum difference in temperature values at the same measuring locations obtained from these two sets of experiments was less than 5%. This indicates that the presence of thermocouples does not have significant effect on mixing of impinging streams. Experiments were also conducted to determine the effect of the third dimension (z dimension, which equals to 2.5 cm) on the thermal characteristics of the system. A maximum difference of 4.5% was noted between the temperature values measured at the middle plane (50% of 2.5 cm) and at the quarter (25% of 2.5 cm) of the z dimension. This justifies the two-dimensionality assumption used in the present study.

Photographs of the overall heat transfer experimental set-up and of the IS used in the heat transfer experiments are shown in Figures 4.1d and 4.1e, respectively.

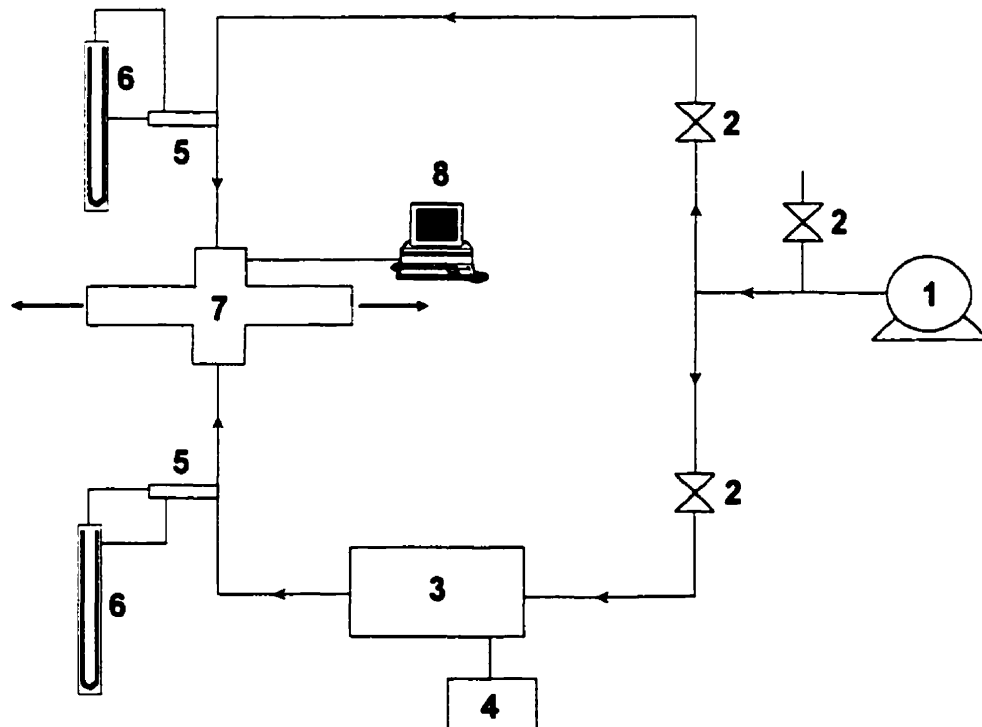


Figure 4.1a. A schematic diagram of the overall heat transfer experimental set-up
 1: air blower; 2: gate valves; 3: heater; 4: controller; 5: pitot tubes; 6: manometers; 7: IS;
 8: computer and data acquisition system

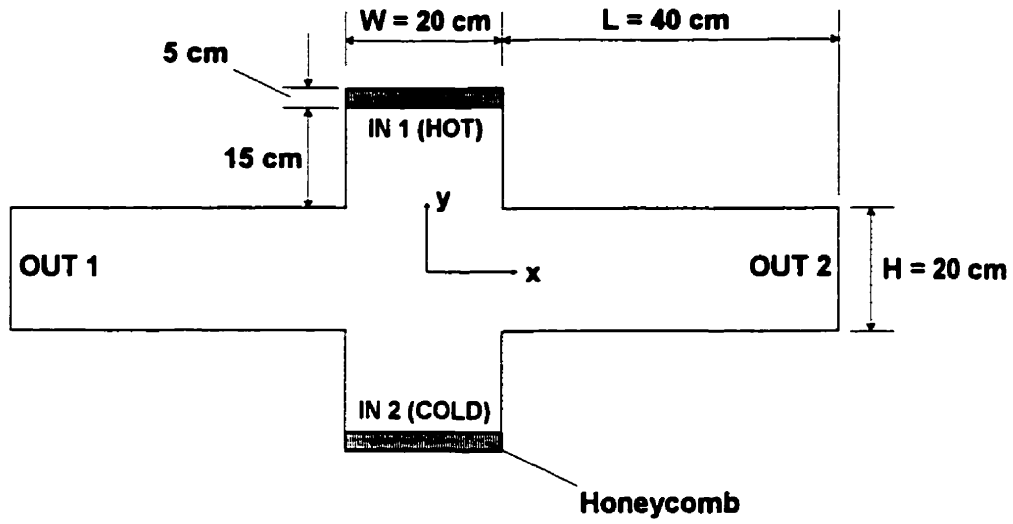


Figure 4.1b. Detailed diagram of the IS used in the heat transfer experiments

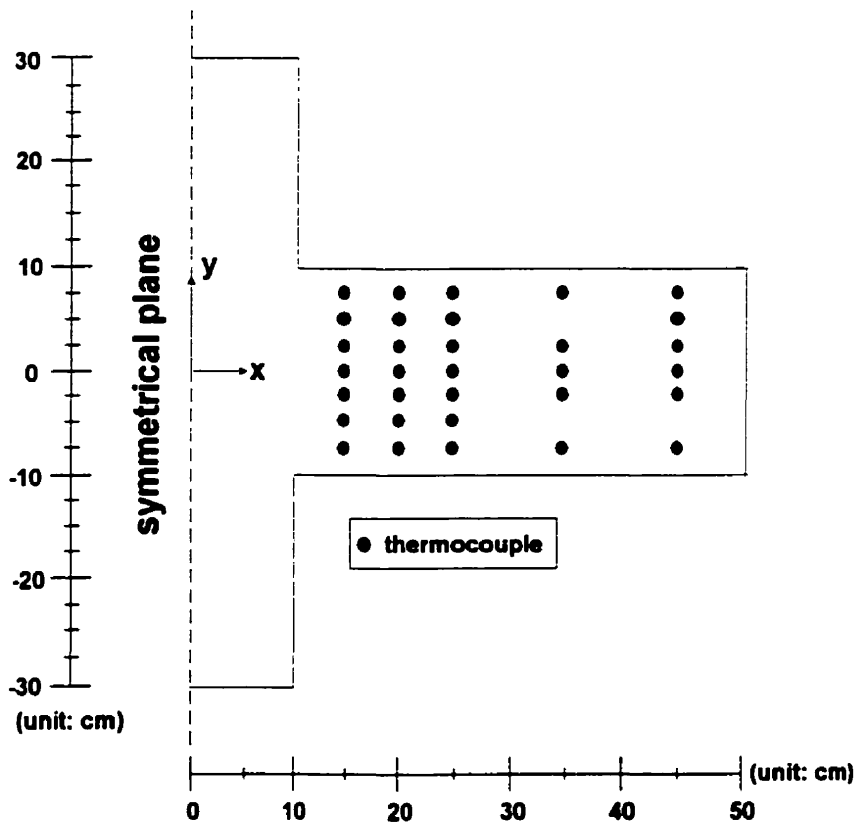


Figure 4.1c. Locations of thermocouples used in the heat transfer experiments

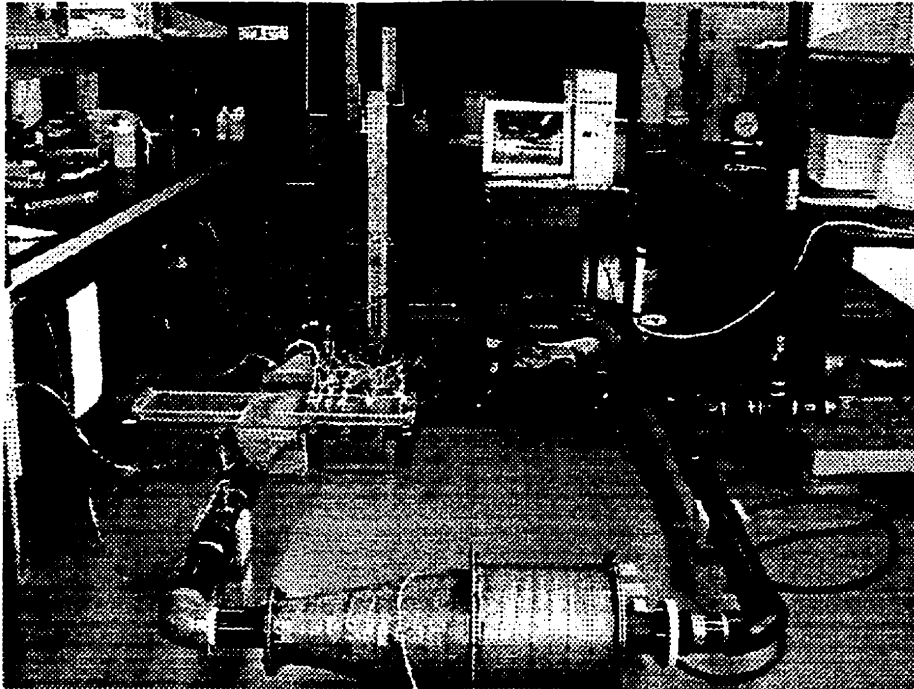


Figure 4.1d. A photograph of the overall heat transfer experimental set-up

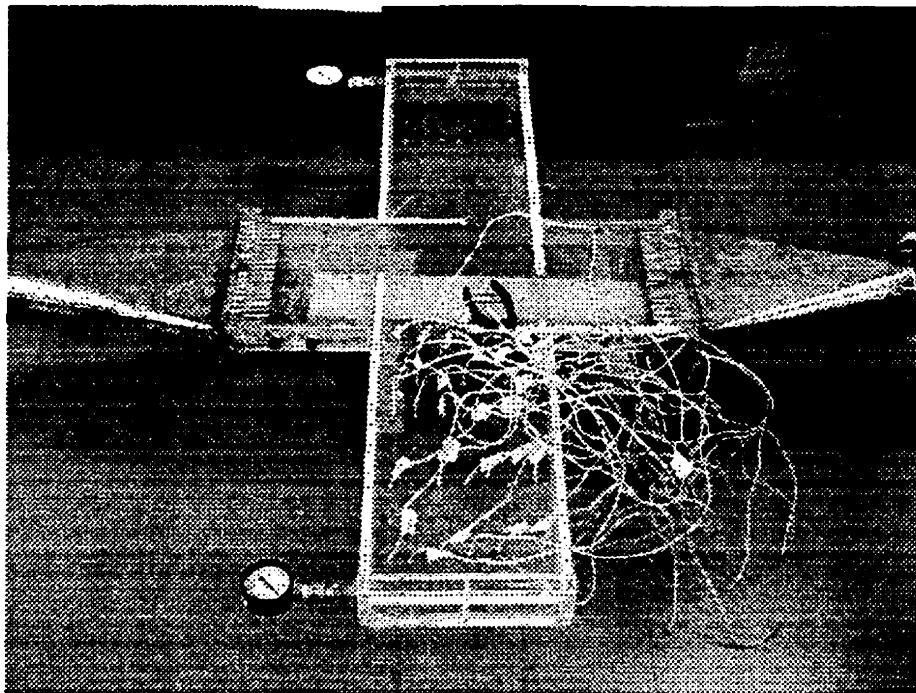


Figure 4.1e. A photograph of the IS used in the heat transfer experiments

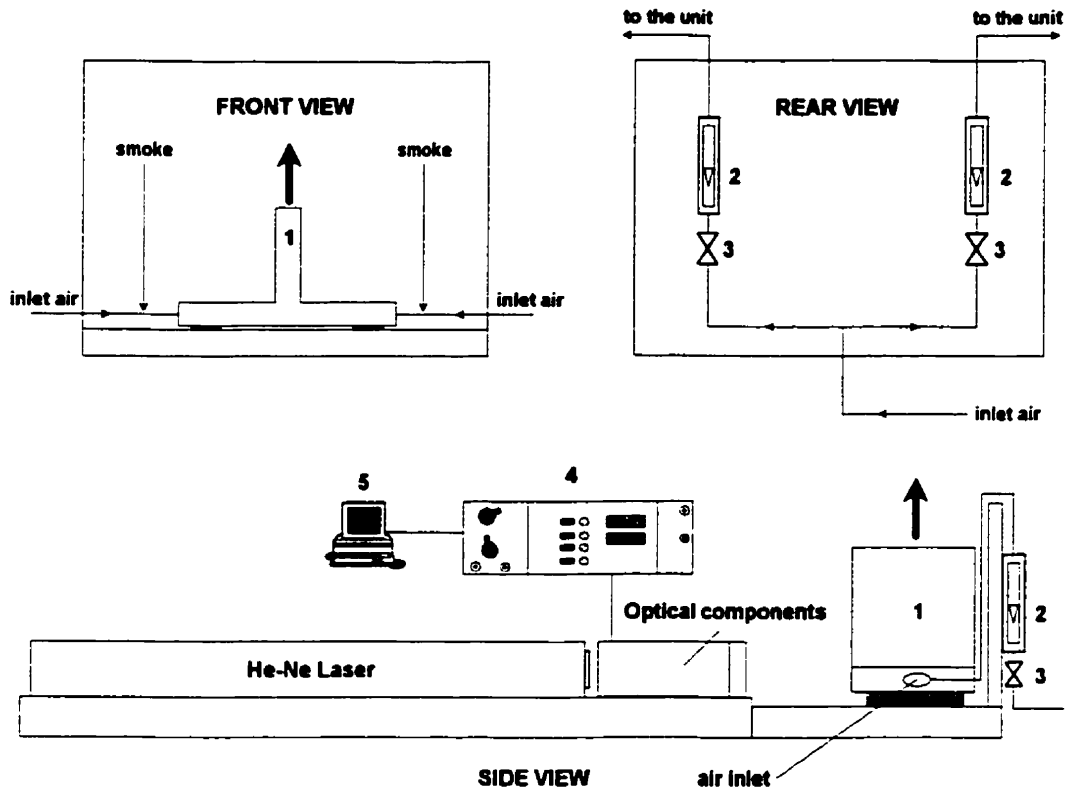


Figure 4.2a. A schematic diagram of the overall flow experimental set-up
 1: one-way exit IS; 2: in-line rotameters; 3: gate valves; 4: signal processor; 5: computer

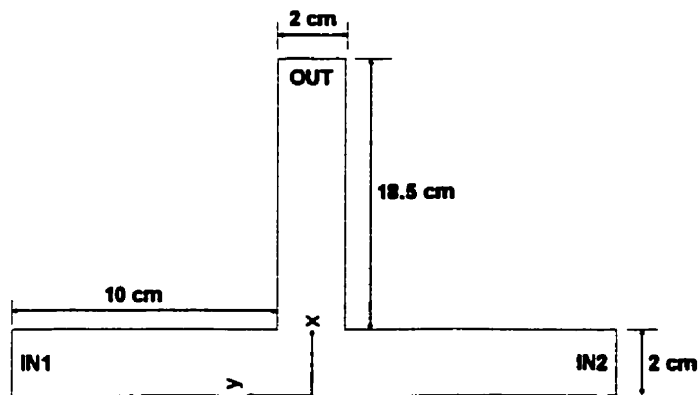


Figure 4.2b. Detailed diagram of the IS used in the flow experiments

A schematic diagram of the flow experimental set-up is shown in Figure 4.2a. Air was supplied to the IS through a compressed air line and the flowrate in each flow branch was controlled by a gate valve. The air flowrate in each flow branch was measured using an in-line rotameter (model no. FL-515, Omega Engineering, Inc., Stamford, CT).

The air streams were fed into a one-way exit IS through the two inlets (see Figure 4.2b). The two streams impinged normally against each other and left the IS through the exit. Velocity and turbulence intensity distributions in the IS were measured using a laser Doppler velocimeter (LDV) operated in the back-scattering mode. The system consisted of a 60 mW He-Ne laser (model no. 127, Spectra-Physics, Mountain View, CA), transmission optics with a beam splitter (model no. 9115-2, TSI, Inc., St. Paul, MN), a receiving assembly (model no. 9140, TSI, Inc., St. Paul, MN) with photomultiplier (model no. 9162, TSI, Inc., St. Paul, MN), which its power was supplied by a power supply (model no. 9165, TSI, Inc., St. Paul, MN). The focusing lens (model no. 9167-250, TSI, Inc., St. Paul, MN) used has a nominal focal length of 250 mm. An IS unit was mounted on a table with a traversing mechanism allowing measurements to be taken in the x and y directions. Smoke was introduced to the inlet air streams to provide seeding for the LDV. The signal obtained as particles suspended in the flow traversed the measuring field was processed by a signal processor (model no. 1990, TSI, Inc., St. Paul, MN). The processed signal was then transmitted to the computer for the final velocity and turbulence intensity computation using the software LDA Acquisition, version 1.0 (Plasma Technology Research Centre, Montreal, QC). At each measuring location the velocity and turbulence intensity were calculated by averaging the measurements of 2000 particles.

Photographs of the overall flow experimental set-up are shown in Figures 4.2c and 4.2d. A photograph of electronic components (signal processor, computer) of an LDV is shown in Figure 4.2e.

Since the fluid was confined, the laser beams must pass through a window of an IS before focusing. This window caused a deflection of the beams and a change in both the measuring volume location and the intersection angle of the two beams (TSI, 1980).

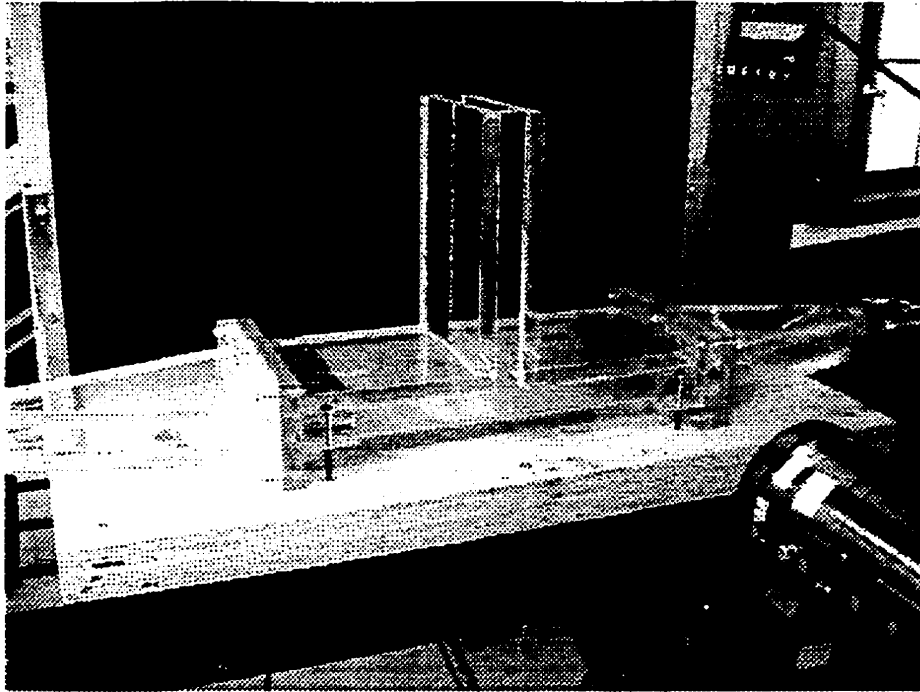


Figure 4.2c. A photograph of the overall flow experimental set-up (front view)

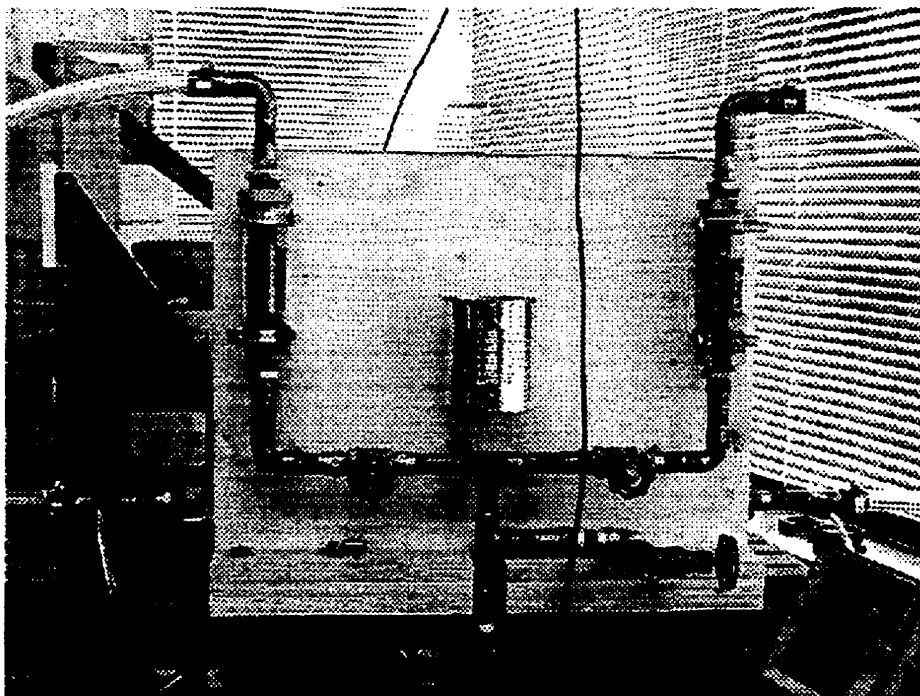


Figure 4.2d. A photograph of the overall flow experimental set-up (rear view)



Figure 4.2e. A photograph of electronic components of an LDV

A new focal distance, F , is calculated from the following equation:

$$F = F_D + t \left(1 - \frac{\tan \kappa_w}{\tan \kappa_f} \right) \quad (4.1)$$

where F is the actual focal distance, F_D is a given focal distance of lens, t is the thickness of the window. κ_w , the angle the beam within the window makes with the optical axis, is calculated from:

$$\kappa_w = \sin^{-1} \left(\frac{N_A \sin \kappa_A}{N_w} \right) \quad (4.2)$$

where N_A is the refractive index of the medium between the transmitting lens and the window, which equals to unity in the case of air. N_w is the refractive index of the window, which equals to 1.49 for Plexiglas used in the present study. For the case of air $\kappa_f = \kappa_A$, where κ_A is half angle of lens.

In addition to the above correction a lens mask (Figure 4.2f) was used to reduce beam reflections from the measuring window to enter the receiving optics.

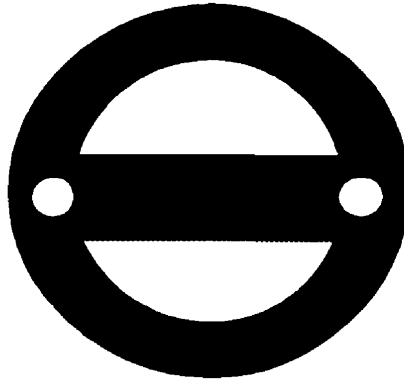


Figure 4.2f. A lens mask used in the flow experiments

To test the reproducibility of the data, replicates were made of randomly selected experiments. From these tests the reproducibility values for the temperature and velocity (as well as turbulence intensity) were within ± 4.7 and 3.3%, respectively.

4.3. MATHEMATICAL FORMULATION

To formulate the mathematical description of the transport processes in impinging streams the following assumptions are made: the mean flow is steady, incompressible and the fluid is Newtonian with constant physical properties. Viscous dissipation is neglected. The flow is assumed to be fully developed (both hydrodynamically and thermally) at the exit of the IS.

Based on the aforementioned assumptions the time-averaged conservation equations for mass, momentum and energy (in tensor form) can be written as follows:

Continuity equation:

$$\frac{\partial U_i}{\partial x_i} \quad (4.3)$$

Momentum equation:

$$\rho \left(U_i \frac{\partial U_j}{\partial x_i} \right) = -\frac{\partial P}{\partial x_j} + \frac{\partial}{\partial x_i} \left[\mu \left(\frac{\partial U_i}{\partial x_j} + \frac{\partial U_j}{\partial x_i} \right) - \overline{\rho u_i u_j} \right] \quad (4.4)$$

Energy equation:

$$\rho c_p \left(U_i \frac{\partial T}{\partial x_i} \right) = \frac{\partial}{\partial x_i} \left[k \frac{\partial T}{\partial x_i} - \overline{\rho u_i T} \right] \quad (4.5)$$

Reynolds stresses and turbulent heat flux are expressed as follows:

$$-\overline{\rho u_i u_j} = \mu_t \left(\frac{\partial U_i}{\partial x_j} + \frac{\partial U_j}{\partial x_i} \right) - \frac{2}{3} \rho k \delta_{ij} \quad (4.6)$$

$$-\overline{\rho u_i T} = \frac{\mu_t}{\sigma_T} \frac{\partial T}{\partial x_i} \quad (4.7)$$

The first ingredient of the composite turbulence model is a low-Reynolds number version of the k - ε model proposed by Lam and Bremhorst (1981). This model has been chosen based on the study of impingement heat transfer of Seyedein et al. (1994). In their work the Lam-Bremhorst (hereafter denoted by LB) model was shown to predict the heat transfer coefficient distributions very satisfactorily compared to other turbulence models tested.

In the LB model the turbulence kinetic energy and the isotropic component of the turbulence energy dissipation rate are determined from the following transport equations (Lam and Bremhorst, 1981):

$$\frac{\partial(\rho k)}{\partial t} + \frac{\partial(\rho U_i k)}{\partial x_i} = \frac{\partial}{\partial x_i} \left[\left(\frac{\mu_t}{\sigma_k} + \mu \right) \frac{\partial k}{\partial x_i} \right] + \mu_t \left(\frac{\partial U_i}{\partial x_j} + \frac{\partial U_j}{\partial x_i} \right) \frac{\partial U_i}{\partial x_j} - \rho \varepsilon \quad (4.8)$$

$$\frac{\partial(\rho \varepsilon)}{\partial t} + \frac{\partial(\rho U_i \varepsilon)}{\partial x_i} = \frac{\partial}{\partial x_i} \left[\left(\frac{\mu_t}{\sigma_\varepsilon} + \mu \right) \frac{\partial \varepsilon}{\partial x_i} \right] + C_1 f_1 \mu_t \frac{\varepsilon}{k} \left(\frac{\partial U_i}{\partial x_j} + \frac{\partial U_j}{\partial x_i} \right) \frac{\partial U_i}{\partial x_j} - C_2 f_2 \frac{\varepsilon^2}{k} \quad (4.9)$$

where $C_\mu = 0.09$; $\sigma_k = 1.00$; $\sigma_\varepsilon = 1.314$; $C_1 = 1.44$ and $C_2 = 1.92$.

The wall-damping functions f_1 , f_2 and f_μ are defined as follows:

$$f_1 = \left(1 + \frac{0.05}{f_\mu} \right)^3 \quad (4.10)$$

$$f_2 = 1 - \exp(-R_t^2) \quad (4.11)$$

$$f_{\mu} = \left[1 - \exp(-0.0165R_y)\right]^2 \left(1 + \frac{20.5}{R_t}\right) \quad (4.12)$$

where $R_t = \frac{\rho k^2}{\mu \varepsilon}$ and $R_y = \frac{\rho y k^{1/2}}{\mu}$.

As quoted by Hosseinalipour and Mujumdar (1995) there exists a secondary source/sink term in the ε equation that is taken as zero in most studies. This leads to an underestimation of near-wall ε values, which can cause an overestimation of the predicted heat transfer rate in separated flows. An example of this overestimation of heat transfer will be given in the subsequent section. Yap (1987) proposed the use of the following secondary source term:

$$S_{\varepsilon} = \max \left[0.83 \left(\frac{l}{l_e} - 1 \right) \left(\frac{l}{l_e} \right)^2 \frac{\varepsilon^2}{k}, 0 \right] \quad (4.13)$$

where l_e denotes near-wall equilibrium length scale taken as 2.5 times the distance from the wall, while l , turbulence length scale, is defined as:

$$l \equiv \frac{k^{3/2}}{\varepsilon} \quad (4.14)$$

Finally, the time-averaged flow field can be determined using the turbulent viscosity modified by multiplication by a factor, which is a function of the local Reynolds number of turbulence (CHAM, 1997):

$$\mu_{\text{mod}} = \mu_t \cdot \min \left[1.0, (A \cdot R_t)^B \right] \quad (4.15)$$

$$\mu_t = \rho C_{\mu} f_{\mu} \frac{k^2}{\varepsilon} \quad (4.16)$$

where μ_{mod} is the turbulent viscosity to be used and μ_t is the nominal (high-Reynolds-number) value of μ_{mod} . A , B are constants in which the values, obtained in the present study by fitting numerical results to experimental impingement heat transfer data, equal to 0.05 and 2.40, respectively.

To ensure adequate concentration of grid cells near the wall the values of dimensionless distance of the first grid points normal to the wall, y^+ , were always kept lower than unity.

Boundary conditions

To save computer time only half of the IS was simulated in all cases. In the following paragraphs W is the width of the inlet channels; H and L are the height and the length of the exit (or main flow) channels, respectively. The coordinates used are shown in Figure 4.1b. For parametric study H is fixed at $H = 1$ cm.

Inlet 1

$$(0 < x < W/2; y = W+H/2) \quad U_1 = 0; U_2 = -U_{2,jet} \text{ and } T = T_{inlet 1} \quad (4.17)$$

Inlet 2

$$(0 < x < W/2; y = -(W+H/2)) \quad U_1 = 0; U_2 = U_{2,jet} \text{ and } T = T_{inlet 2} \quad (4.18)$$

and $k = (U_{jet} I)^2$; $\varepsilon = C_\mu^{3/4} \frac{k^{3/2}}{l}$ where $l = 0.1L$ and L is the characteristic length of the

system; I represents the turbulence intensity.

Top and bottom walls

$$(W/2 < x < L+W/2) \quad u_i = 0 \text{ and } \frac{\partial T}{\partial y} = 0; k = 0 \text{ and } \frac{\partial \varepsilon}{\partial y} = 0 \quad (4.19)$$

Outlet

$$(x = L+W/2) \quad \frac{\partial \phi}{\partial x} = 0 \quad (4.20)$$

where ϕ represents all solved variables.

The conservation equations, along with the boundary conditions, were solved numerically using the control-volume-based computational fluid dynamic software PHOENICS version 2.2.2 (CHAM, 1997). In this code the convection terms in the conservation equations were discretized using the hybrid scheme (Patankar, 1980). The discretized equations were solved using the well-known SIMPLEST algorithm (CHAM, 1997). The solution was considered converged when the following criterion is met for all the dependent variables:

$$\max \left| \frac{\phi^{n+1} - \phi^n}{\phi_r} \right| \leq 10^{-3} \quad (4.21)$$

between sweeps n and $n+1$; ϕ_r represents the reference value for the dependent variable ϕ . To improve convergence underrelaxation of the false transient type was used for the two velocity components and temperature. Linear relaxation was used for the pressure as

well as the turbulence kinetic energy and its dissipation rate. Whole-field residuals were checked to ensure that the converged solution set satisfies the governing equations within a prescribed error.

Due to the large number of cases studied it was not possible to check the grid independence for each individual case. To overcome this problem, as suggested by Hosseinalipour and Mujumdar (1997a), the appropriate number of grids were found through a grid doubling procedure for the “worst” case with the highest Reynolds number for each geometry and applied to all other cases for that particular geometry. This procedure results in longer running times for the lower Reynolds number cases but it was compensated for by the time saving in not running grid doubling runs for each individual case. For details regarding the discretization of the governing equations and various schemes used to solve the discretized equations the reader may refer to Patankar (1980).

4.4. RESULTS AND DISCUSSION

The composite model was first verified by comparing the predicted results with experimental impingement heat transfer data of van Heiningen (1982). The system configuration is shown in Figure 4.3. Flat velocity profile was used at the nozzle exit. The temperature of the confinement surface was kept equal to the temperature of the incoming jet while the temperature of the impingement surface was kept at some higher value. Local Nusselt number is calculated as:

$$Nu_x = \frac{(T_{imp} - T_{px})}{(T_{imp} - T_j)} \cdot \frac{W}{y_{px}} \quad (4.22)$$

The comparison between experimental results and numerical results obtained with the LB, LB with Yap correction (hereafter denoted by LBY) and composite models is shown in Figure 4.4. Grids of 80×70 nodes were used in all computations.

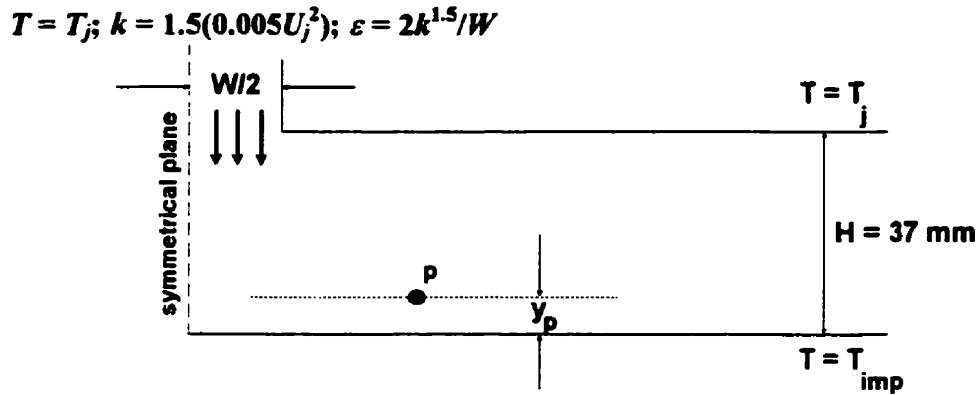


Figure 4.3. Impinging jet configuration used in model verification. P = near-wall node

It can be seen in Figure 4.4a that the LB model overestimates the values of Nusselt numbers at both stagnation point and points located downstream. This model predicts the shape of the Nusselt number profiles quite adequately, however. By applying Yap correction to the LB model, the overestimation of the stagnation Nusselt number decreases. However, the LBY model fails to capture the variation of local Nusselt numbers in the range $5 < x/W < 20$. By using the composite model, the stagnation Nusselt number is predicted well and the variation of the local heat transfer coefficients is also described well. Numerical results are also compared with experimental results in Figure 4.4b for another set of operating and geometric parameters. In this figure the LBY model performs similarly to the composite model since the profiles vary smoother along the impingement surface in this case than the one presented in Figure 4.4a.

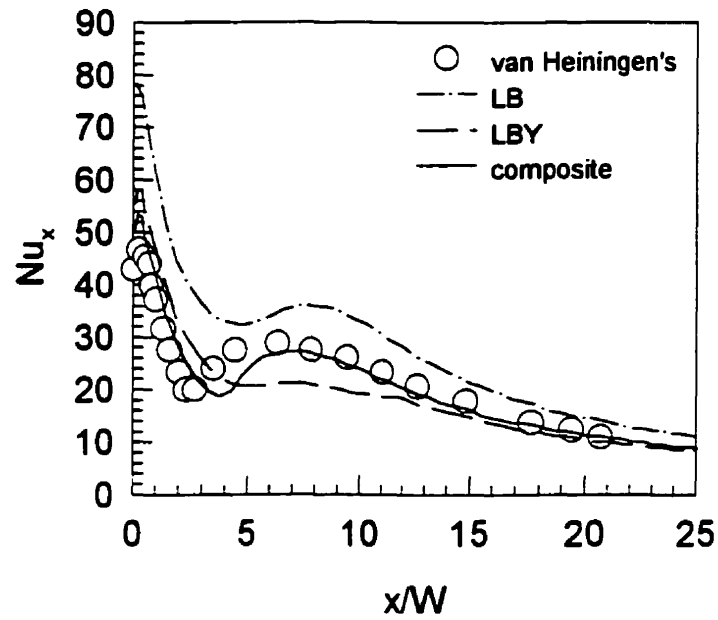


Figure 4.4a. Comparison between predicted and experimental local Nusselt number profiles along the impingement surface. $Re_j = 10400$; $H/W = 2.6$

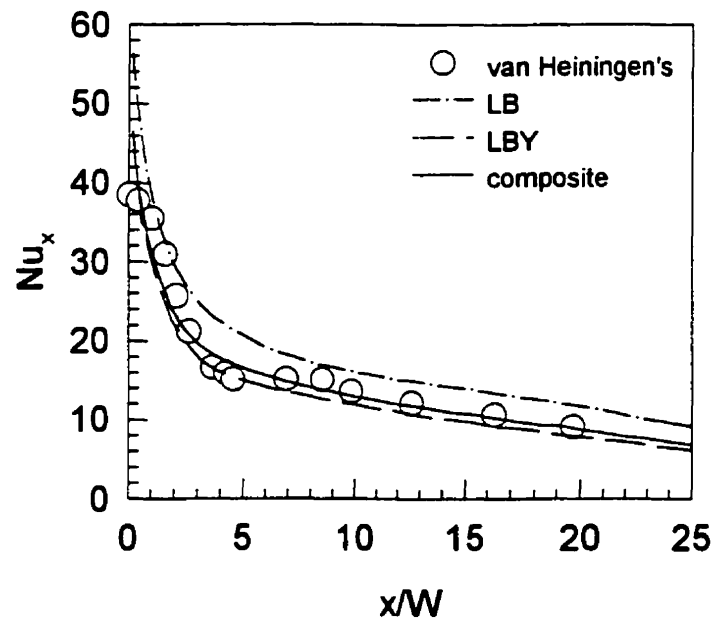
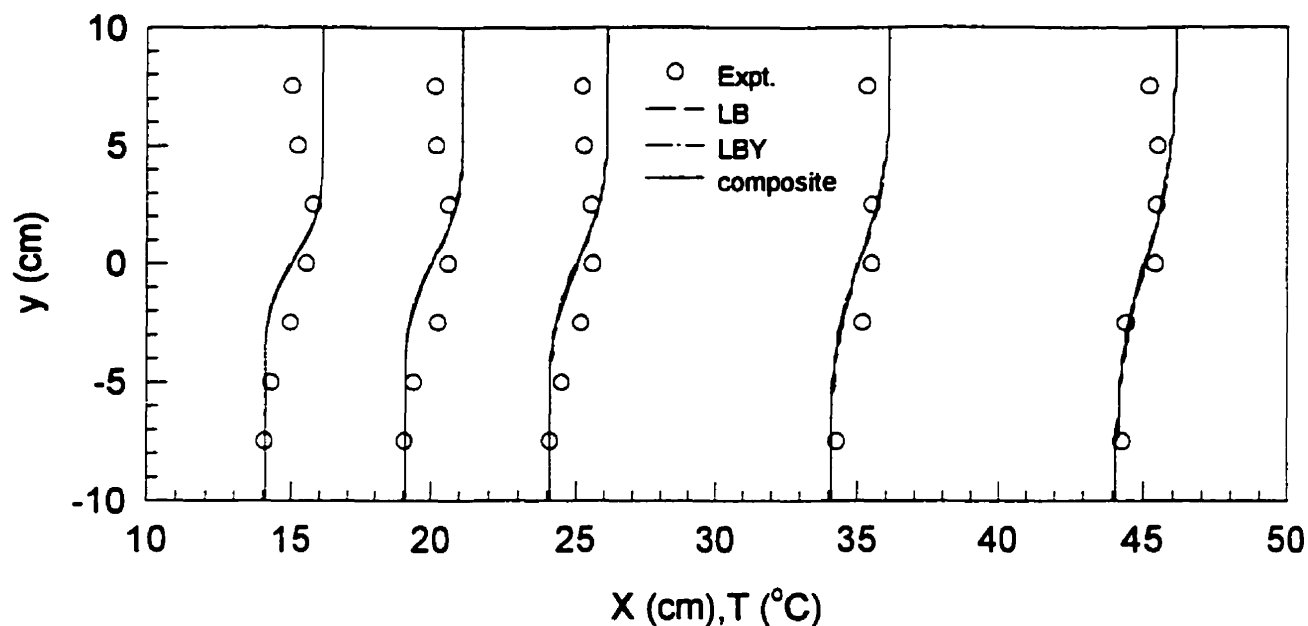


Figure 4.4b. Comparison between predicted and experimental local Nusselt number profiles along the impingement surface. $Re_j = 5200$; $H/W = 6.0$

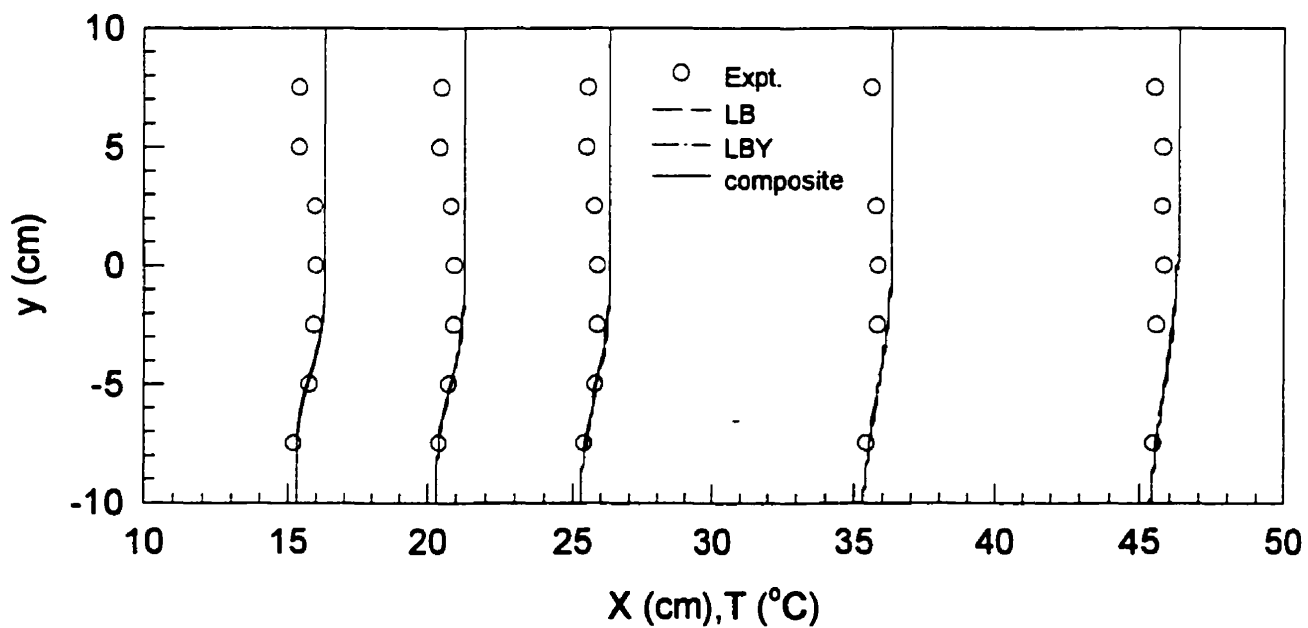
The comparison between normalized numerical and experimental temperature profiles in IS is shown in Figure 4.5. Grids of 100×80 nodes provide adequate resolution in these cases. The computational domain was extended long enough in the downstream direction to satisfy the fully developed flow assumption at the exits of the IS. Temperatures were measured at 5 different x -locations, i.e., at $x = 15, 20, 25, 35$ and 45 cm from the origin of the x -coordinate (see Figure 4.1c). Temperature values are normalized with the reference temperatures of 30° and 40° C when the temperature difference between the hot and cold streams is 10° and 20° C, respectively. Inlet jet turbulence intensity was assumed to be $I = 2\%$.

At each measuring location the value of the reference temperature is taken as zero in terms of the modified x -coordinate (X); the difference between the actual and reference temperatures is then plotted with the scale of 0.1 cm per 1° C. For example, in Figure 4.5a, at $x = 15$ cm and $y = 5$ cm, the actual temperature is 42.3° C and the reference temperature is 40° C. The modified x -coordinate of this point on the graph is then $X = 15 + ((42.3 - 40) \times 0.1) = 15.23$ cm.

It can be seen from Figures 4.5a and 4.5b that the composite model predicts the temperature profiles very similarly to those predicted by LB and LBY models. This is not unexpected since the mean flow properties (e.g., temperature profiles) are normally not as much affected by the choice of the turbulence model as the near-wall quantities and their gradients (e.g., heat flux) are. Also, turbulent viscosity (and hence turbulent Prandtl number) variations cannot explain the 100% error of the standard k - ϵ model (Behnia et al., 1999). The maximum deviation of about 25% between numerical and experimental results observed in the upper left corner of Figure 4.5a may be attributed also to the simplifying assumption of constant physical fluid properties as well as the implicit assumption of adiabatic wall condition in the simulation; the model predicts the results well within $\pm 5\%$ in the lower left region where the inlet temperature was lower (and hence less heat loss through the wall). The model performs better as the fluid approaches the outlet, as expected. It is important to note, however, that the composite model gives much faster convergence than do the LB and LBY models. The model also captures well the location of impingement planes as it is pushed towards the weaker jet in Figure 4.5b (compared to being more or less at the middle of the channel in Figure 4.5a).



(a) $Re_j = 18000$ (top)-18000 (bottom); $I = 2\%$; $\Delta T = 20^\circ\text{C}$ ($51^\circ\text{C}/31^\circ\text{C}$); normalized $T = 40^\circ\text{C}$



(b) $Re_j = 20000$ (top - hot stream) - 10000 (bottom - cold stream); $I = 2\%$; $\Delta T = 10^\circ\text{C}$ ($43^\circ\text{C}/33^\circ\text{C}$); normalized $T = 30^\circ\text{C}$

Figure 4.5. Comparison between predicted and experimental normalized temperature profiles in IS

The comparison between normalized numerical and experimental velocity profiles in a one-way exit IS is shown in Figure 4.6a. Grids of 110×60 nodes provide adequate resolution in these cases. The computational domain was again extended long enough in the downstream direction to satisfy the fully developed flow assumption at the exit of the IS. Velocities were measured at 5 different x -locations, i.e., at $x = 3.5, 7.5, 11.5, 15.5$ and 19.5 cm from the origin of the x -coordinate in Figure 4.2b. The velocity values are normalized with the zero reference velocity. The same calculation procedure as used in the temperature case applies; the difference between the actual and reference velocities is plotted, in this case, with the scale of 0.3 cm per 1 m s^{-1} .

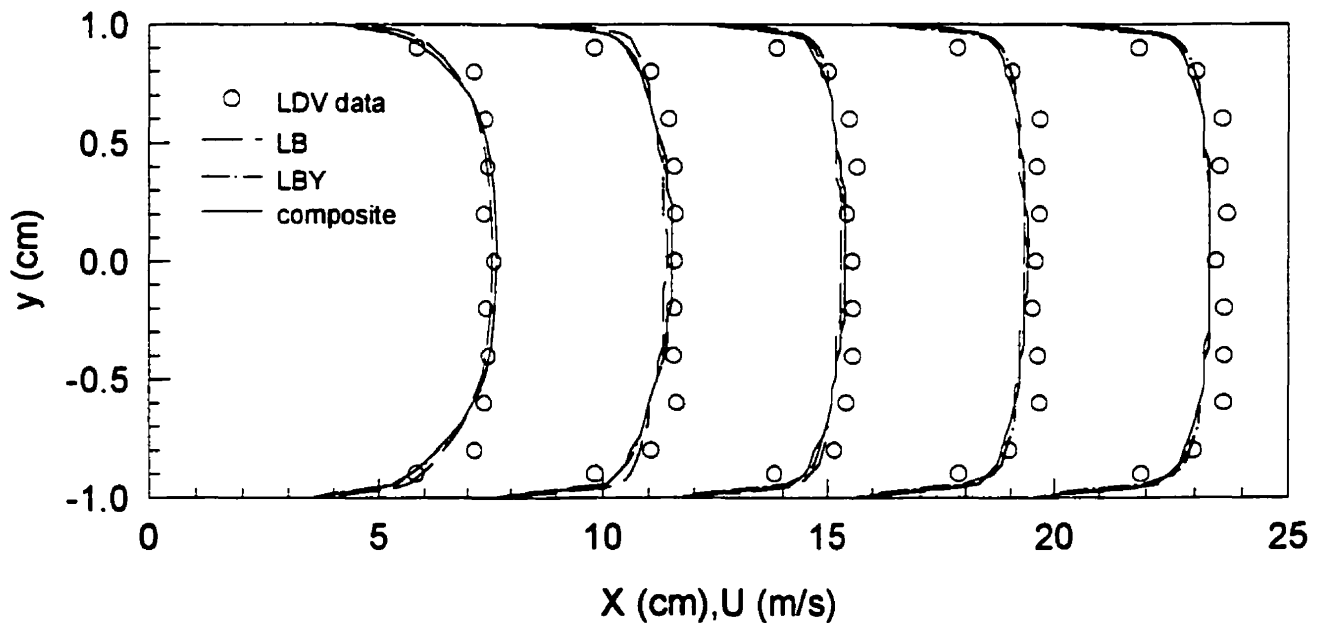


Figure 4.6a. Comparison between predicted and experimental normalized velocity profiles in IS. $Re_j = 12600$; $I = 15\%$; normalized $U = 0 \text{ m s}^{-1}$

Figure 4.6a compares the LDV measurements of the axial mean velocity with the numerical results predicted by the LB, LBY and composite models. It can be seen from this figure that the composite model performs slightly better than the LB model but gives no appreciably different results from the LBY model. The model overestimates the velocity in the near-wall region (up to about 20%) but slightly underestimates

(approximately 7%) it in the region far away from the wall. It should be noted, however, that the near-wall measurements are also subjected to higher errors due to the reflection of the laser light from the edge of the model IS used in the experiments. Nevertheless, this confirms the usability of the composite model, especially when taking into account the fact that convergence is much faster with this model than the other two models tested here.

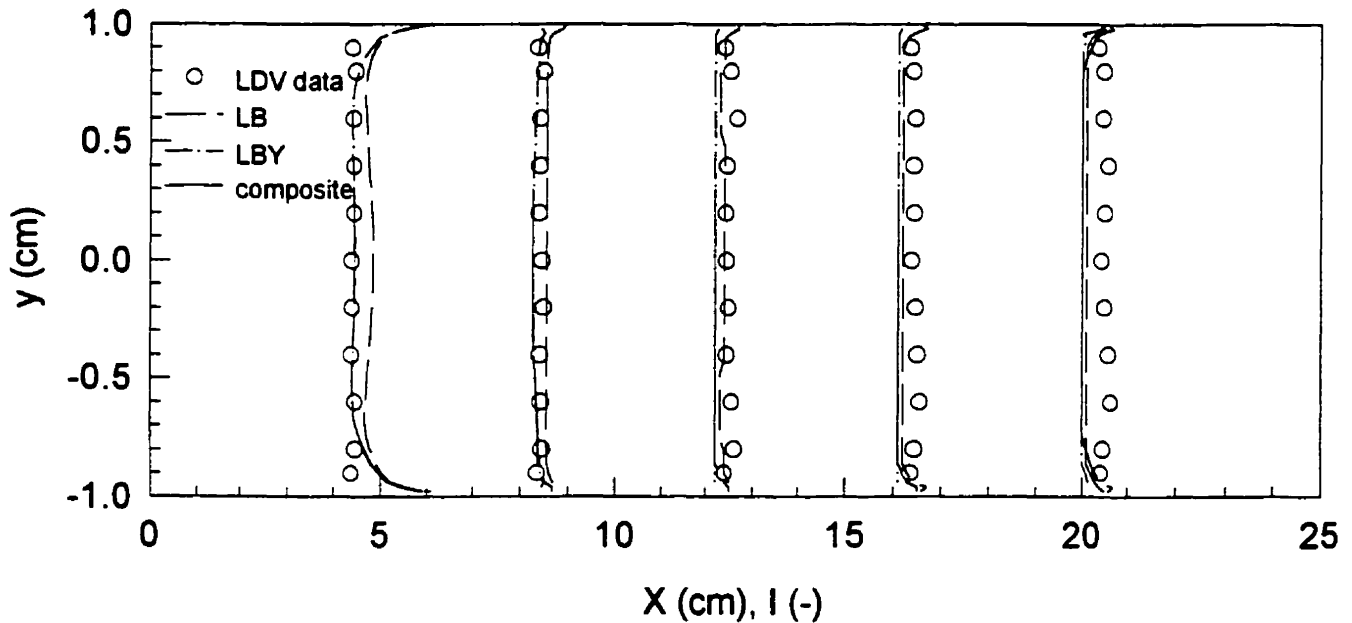


Figure 4.6b. Comparison between predicted and experimental normalized turbulence intensity profiles in IS. $Re_j = 12600$; $I = 15\%$; normalized $I = 0\%$

The comparison between normalized numerical and experimental turbulence intensity profiles in a one-way exit IS is shown in Figure 4.6b. The measuring locations and computational grid density are the same as the one used for the velocity measurements and calculation. The turbulence intensity values are normalized with the zero reference intensity. The difference between the actual and reference intensities is plotted, in this case, with the scale of 5 cm per I .

It can be seen from this figure that the composite model predicts the distribution of I better than does the LB model, especially in the area not so far downstream of the impingement region. The overestimation of I (hence the turbulence kinetic energy) by the LB model is due to the omission of the secondary source/sink term in the ε equation mentioned earlier. Further downstream, however, the two models seem to give no appreciably different results. The composite model predicts the intensity profiles very similarly to the LBY but convergence is again much faster. Again, the model overestimates the intensity in the near-wall region but underestimates it in the region far away from the wall. The implicit assumption of isotropy in the model also will affect the results. Unfortunately, it was not possible with the instrumentation available to measure the three components of the turbulence intensity.

Temperature was used as a passive tracer to monitor mixing of the two fluid streams. As the two streams mix and approach the exit ports the temperature profiles across the exit channel height are flattened; the well-mixed condition is satisfied when no temperature gradient exists across the channel height, i.e., the temperature profile is flat. To quantify the mixing performance of the system at different operating conditions and geometric configurations a mixing index was defined as follows:

$$\text{Mixing index} = \frac{\sigma_T}{\Delta T} \quad (4.23)$$

where σ_T is the standard deviation of the fluid temperature across the channel height at a specific axial location and ΔT is the temperature difference between the two inlet streams. $\sigma_T = 0$ thus implies well-mixed condition. Note that different criteria for mixing (e.g., the one proposed by Hosseinalipour and Mujumdar (1997a)) may be used but the above criterion is conceptually easier to visualize. Nonetheless, either index should equally predict the channel length required to well mix the two streams. The ranges of parameters studied are: inlet jet Reynolds number (Re_j) from 10000 to 30000; inlet jet turbulence intensity (I) from 1 to 2%; the ratio of the height of the exit channel to the width of the inlet jet (H/W) was varied from 1.0 to 2.0. Inlet jet hydraulic diameter is calculated assuming the aspect ratio of 5 between the width and the height of the exit channel.

The plots of the mixing index versus dimensionless axial distance with the inlet jet Reynolds number as a parameter are shown in Figures 4.7a-4.7d. Both dimensional

and dimensionless coordinates are shown in these figures for easy comparison. Grids of 155×62 nodes were used in all computations.

It can be seen from these figures that as the jet Reynolds number increases mixing is improved until some specific values of x/W are reached. These critical values depend on both the operating conditions as well as the geometry of the system. This behavior is quite different from what is observed in laminar IS of similar geometries (see Chapter 3). For the same H/W laminar IS mixing is always poorer as Re_j increases due to the increase in mean flow rate of the fluid in the system (and hence shorter residence time of the fluid in the system). For turbulent IS increasing Re_j leads to higher levels of the turbulence kinetic energy, especially in the impingement zone. The values of the turbulent viscosity are also higher at higher Re_j ; this increase leads to a stronger eddy mixing. Once the critical value of x/W is reached, however, the mixing behavior is reversed. This may be ascribed to the already mentioned increased mean flow rate; the effect of higher turbulence kinetic energy at higher Re_j is overshadowed by the effectively shorter transit time.

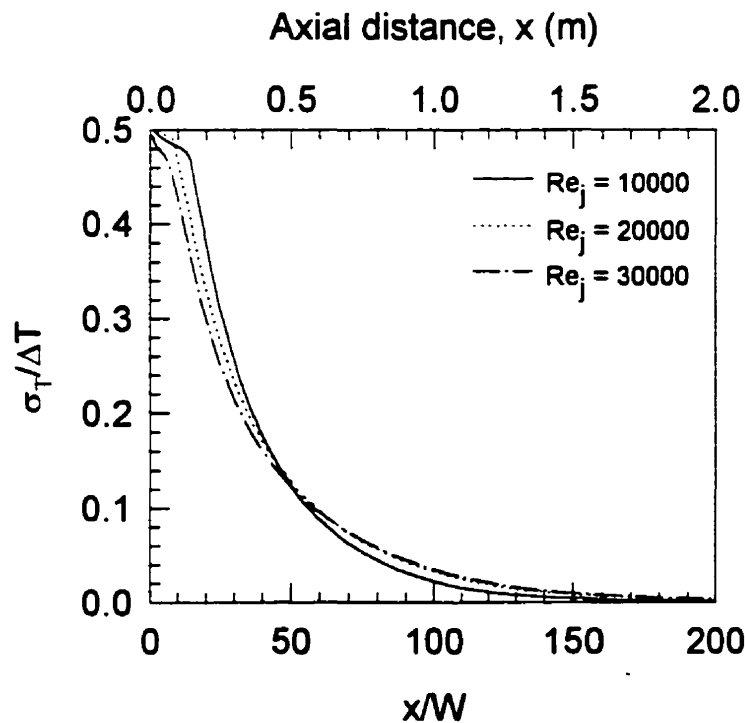


Figure 4.7a. Mixing index for $H/W = 1.0$; $I = 1\%$

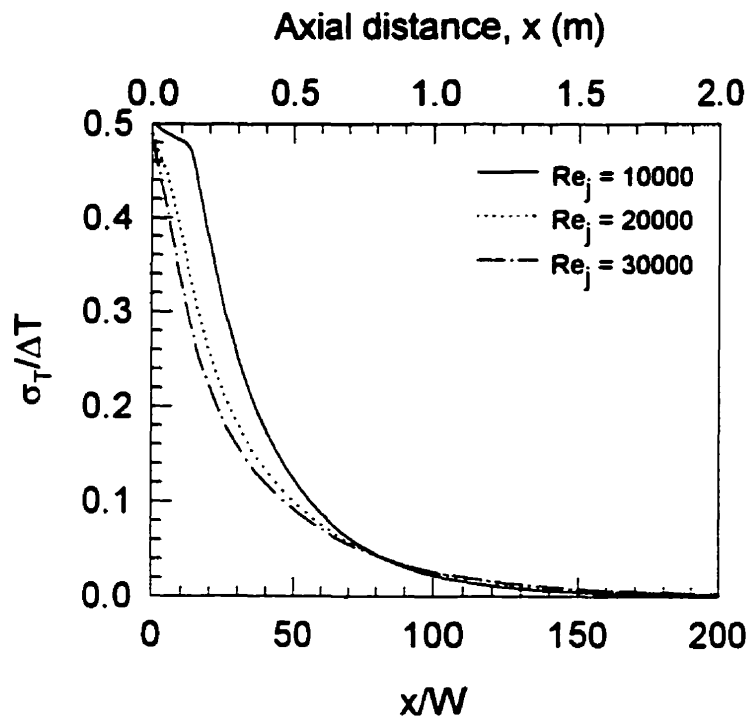


Figure 4.7b. Mixing index for $H/W = 1.0$; $I = 2\%$

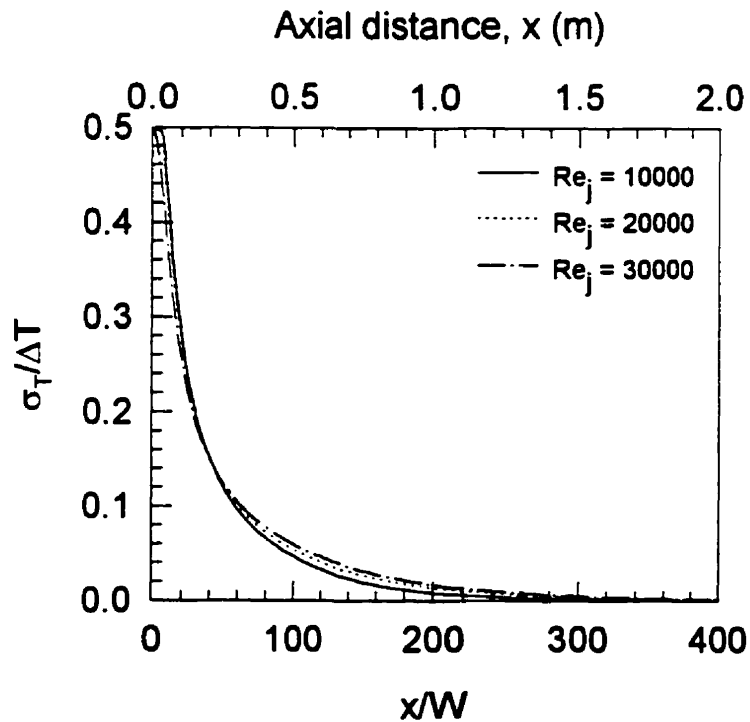


Figure 4.7c. Mixing index for $H/W = 2.0$; $I = 1\%$

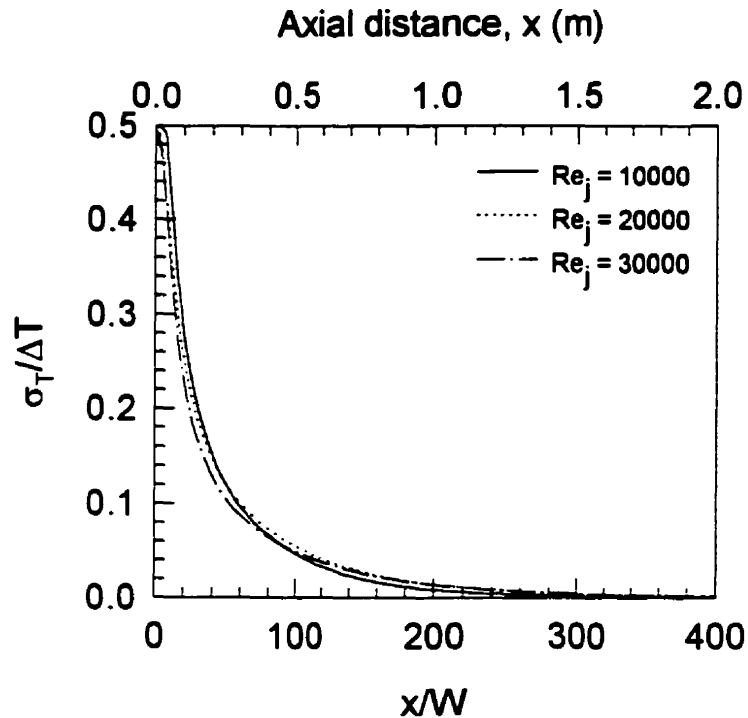


Figure 4.7d. Mixing index for $H/W = 2.0$; $I = 2\%$

Increasing H/W results in smaller effect of Re_j on the mixing in IS at low x/W values (i.e., before the critical x/W is reached). The effect is more pronounced at higher inlet jet turbulence intensities. This again is due to the increased eddy mixing as mentioned earlier. Increasing the turbulence intensity also increases the critical value of x/W where the mixing behavior is reversed as more turbulence energy is generated resulting in better mixing.

Figure 4.8 gives an example of the effect of the system geometry on mixing in IS. For each Re_j and turbulence intensity increasing H/W leads to better mixing at low x/W values but poorer mixing at x/W values beyond the critical value. For the same Re_j the jet velocity is higher in the case of IS with higher H/W due to the smaller jet opening (H is fixed at a constant value). This leads to higher turbulent viscosity and hence better eddy mixing. However, as the jet velocity increases the lateral component of momentum tends to push the fluid out of the system faster. The fluids thus have lesser time in the system to mix.

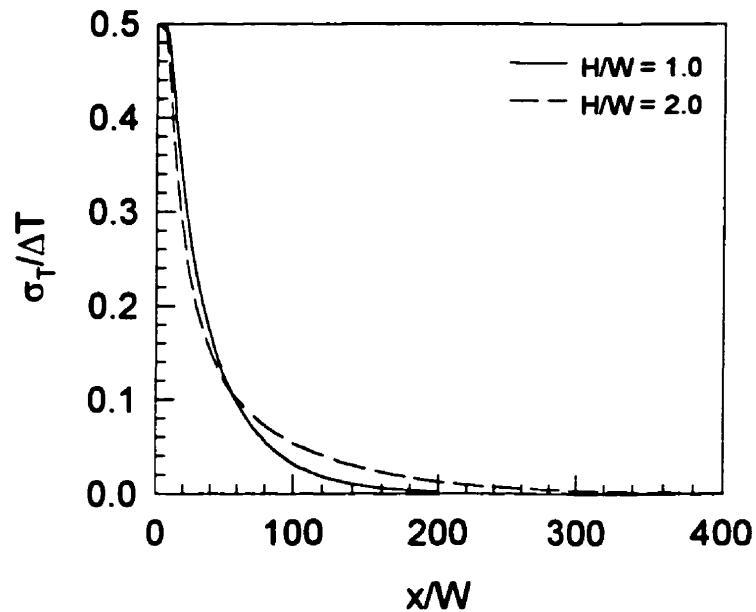


Figure 4.8. Mixing index for $Re_j = 20000$; $I = 1\%$

The effect of inlet jet turbulence intensity is shown in Figure 4.9 for $Re_j = 20000$. For the case with $Re_j = 10000$ there is no difference between $I = 1$ or 2% . The inlet jet velocity (in combination with the turbulence intensity) may not be high enough to yield any difference in the turbulence energy and turbulent viscosity to make any difference in the mixing. The characteristics of the mixing curves for the cases with $Re_j = 20000$ and 30000 are very similar. It can be seen in this figure that increased turbulence intensity leads to better mixing despite the small increase in the absolute turbulence kinetic energy.

The reason is as mentioned earlier. The difference in terms of the distance to attain well-mixed condition is not significant, however.

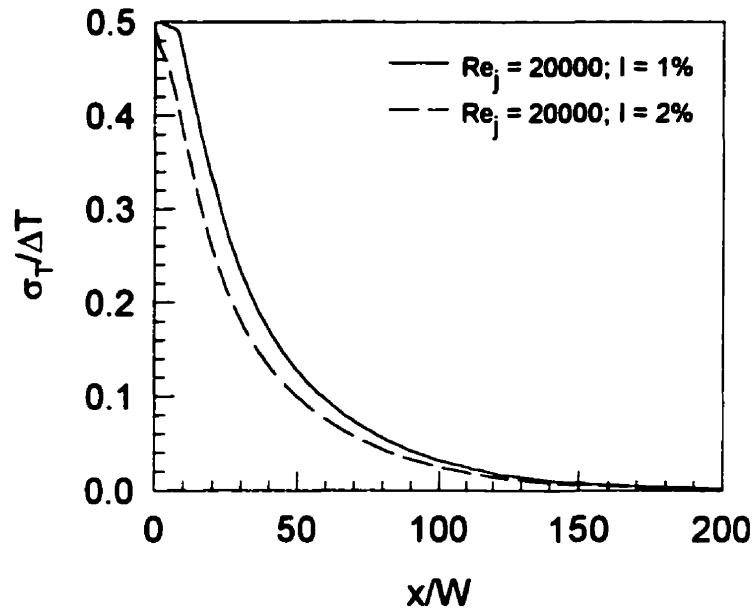


Figure 4.9. Mixing index for $H/W = 1.0$; $Re_j = 20000$

CLOSING REMARKS

A study was performed of the mixing characteristics of turbulent confined impinging streams. A new composite turbulence model is proposed and verified by comparing its predictions with available experimental impingement heat transfer data as well as the experimental temperature and velocity distributions in impinging streams obtained in the present work. The model is found to give better agreement between experimental and numerical impingement heat transfer results than two other low-Reynolds number $k-\varepsilon$ turbulence models tested. The model was then used to perform a parametric study of mixing in a two-dimensional turbulent confined IS. It is found that, for each H/W , as the jet Reynolds number increases mixing is better until a critical value of x/W is reached beyond which the mixing behavior is reversed. This behavior is quite

different from that of two-dimensional laminar confined impinging streams reported in Chapter 3. Increasing H/W results in reduced effect of Re_j on mixing at low x/W values. The effect is more pronounced at higher inlet jet turbulence intensity particularly at high Re_j . For each Re_j and turbulence intensity increasing H/W leads to better mixing at low x/W values but poorer mixing at x/W values beyond the critical value. Good mixing is obtained over a rather short distance for all cases examined. To improve mixing even further two-stage IS may be used. Fluid can be drawn from the first stage at a selected location and fed into the second stage for additional mixing.

NOMENCLATURE

A, B, C_1	
C_2, C_μ	turbulence model constants, -
c_p	heat capacity, $J\ kg^{-1}\ K^{-1}$
D_h	inlet channel hydraulic diameter, m
f_1, f_2, f_μ	turbulence model functions, -
F	actual focal distance of lens, mm
F_D	given focal distance of lens, mm
H	height of the exit channel, m
I	turbulence intensity, %
k	thermal conductivity, $W\ m^{-1}\ K^{-1}$ (equation (4.5))
k	turbulence kinetic energy, $m^2\ s^{-2}$
l	turbulence length scale, m
l_e	near-wall equilibrium length scale, m
L	length of the exit channel, m
N_A	refractive index of the medium (between transmitting lens and window), -
N_w	refractive index of the window, -
P	time-averaged pressure, Pa
Re_t	turbulence Reynolds number, $\frac{\rho k^2}{\mu \epsilon}$, -

R_y	turbulence Reynolds number, $\frac{\rho y k^{1/2}}{\mu}$, -
t	time, s
t	thickness of the measuring window, mm
T	time-averaged temperature, °C
T'	fluctuating component of temperature, °C
ΔT	temperature difference of the two inlet streams, °C
u'_i, u'_j	fluctuating velocity components, m s ⁻¹
u_τ	friction velocity, $\sqrt{\tau_w / \rho}$, m s ⁻¹
U_i, U_j	time-averaged velocity components, m s ⁻¹
W	width of the inlet channel, m
x_i, x_j	coordinates, m
y^+	dimensionless distance from the wall, $\frac{u_\tau y \rho}{\mu}$, -

Greek letters

δ_{ij}	Kronecker delta, -
ε	isotropic turbulence dissipation rate, m ² s ⁻³
κ_A	angle the incident beam makes with the optical axis (half angle of lens), °
κ_f	angle the beam within the fluid makes with the optical axis, °
κ_w	angle the beam within the window makes with the optical axis, °
μ	dynamic viscosity, kg m ⁻¹ s ⁻¹
μ_t	turbulent viscosity, kg m ⁻¹ s ⁻¹
ρ	density, kg m ⁻³
σ_T	standard deviation of temperature, °C
σ_k	diffusion Prandtl number for turbulence kinetic energy, -
σ_ε	diffusion Prandtl number for dissipation rate, -
σ_T	turbulent Prandtl number, -
τ_w	shear stress at the wall, kg m ⁻¹ s ⁻²

Subscripts

<i>imp</i>	impingement surface
------------	---------------------

j jet

p near-wall grid point

Dimensionless group

Re_j jet Reynolds number, $\frac{D_h U_{jet} \rho}{\mu}$

REFERENCES

- Bauer, W., Haag, O., Hennecke, D.K., 2000, Accuracy and robustness of nonlinear eddy viscosity models, *International Journal of Heat and Fluid Flow*, 21, pp. 312-319.
- Behnia, M., Parneix, S., Shabany, Y., Durbin, P.A., 1999, Numerical study of turbulent heat transfer in confined and unconfined impinging jets, *International Journal of Heat and Fluid Flow*, 20, pp. 1-9.
- Berman, Y., Tamir, A., 1996, Experimental investigation of phosphate dust collection in impinging streams, *Canadian Journal of Chemical Engineering*, 74, pp. 817-821.
- Berman, Y., Tamir, A., 2000, Extraction in thin liquid films generated by impinging streams, *AIChE Journal*, 46, pp. 769-778.
- Berman, Y., Tanklevsky, A., Oren Y., Tamir, A., 2000a, Modeling and experimental studies of SO₂ absorption in coaxial cylinders with impinging streams, part I, *Chemical Engineering Science*, 55, pp. 1009-1021.
- Berman, Y., Tanklevsky, A., Oren Y., Tamir, A., 2000b, Modeling and experimental studies of SO₂ absorption in coaxial cylinders with impinging streams, part II, *Chemical Engineering Science*, 55, pp. 1023-1028.
- Concentration, Heat and Momentum Limited (CHAM), 1997, *POLIS: Phoenix On-Line Information System*, London, UK.
- Hosseinalipour, S.M., Mujumdar, A.S., 1995, Comparative evaluation of different turbulence models for confined impinging and opposing jet flows, *Numerical Heat Transfer, Part A*, 28, pp. 647-666.
- Hosseinalipour, S.M., Mujumdar, A.S., 1997a, Flow and thermal characteristics of steady two-dimensional confined laminar opposing jets: part I. equal jets, *International Communications in Heat and Mass Transfer*, 24, pp. 27-38.

- Hosseinalipour, S.M., Mujumdar, A.S., 1997b, Flow and thermal characteristics of steady two-dimensional confined laminar opposing jets: part II. unequal jets, *International Communications in Heat and Mass Transfer*, 24, pp. 39-50.
- Kitron, Y., Tamir, A., 1988, Performance of a coaxial gas-solid two-impinging-streams reactor: hydrodynamics, residence time distribution, and drying heat transfer, *Industrial & Engineering Chemistry Research*, 27, pp. 1760-1767.
- Kudra, T., Mujumdar, A.S., 1989, Impinging stream dryers for particles and pastes, *Drying Technology – An International Journal*, 7, pp. 219-266.
- Kudra, T., Mujumdar, A.S., 1995, Impinging stream dryers, pp. 539-566, in A.S. Mujumdar (Ed.) *Handbook of Industrial Drying, 2nd Edition*, Marcel Dekker, New York.
- Lam, C.K.G., Bremhorst, K., 1981, A modified form of the k- ϵ model for predicting wall turbulence, *ASME Journal of Fluids Engineering*, 103, pp. 456-460.
- Morris, G.K., Garimella, S.V., Amano, R.S., 1996, Prediction of jet impingement heat transfer using a hybrid wall treatment with different turbulent Prandtl number functions, *ASME Journal of Heat Transfer*, 118, pp. 562-569.
- Patankar, S.V., 1980, *Numerical Heat Transfer and Fluid Flow*, Hemisphere, Washington.
- Seyedein, S.H., Hasan, M., Mujumdar, A.S., 1994, Modelling of a single confined turbulent slot jet impingement using various k- ϵ turbulence models, *Applied Mathematical Modelling*, 18, pp. 526-537.
- Sohrabi, M., Marvast, M.A., 2000, Application of a continuous two impinging streams reactor in solid-liquid enzyme reactions, *Industrial & Engineering Chemistry Research*, 39, pp. 1903-1910.
- Tamir, A., 1994, *Impinging-Stream Reactors: Fundamentals and Applications*, Elsevier, Amsterdam.
- TSI Incorporated, 1980, *Systems 9100-4 and 9100-5 Laser Doppler Velocimeters Instruction Manual*, St. Paul, MN.
- Unger, D.R., Muzzio, F.J., Brodkey, R.S., 1998, Experimental and numerical characterization of viscous flow and mixing in an impinging jet contactor, *Canadian Journal of Chemical Engineering*, 76, pp. 546-555.

- van Heiningen, A.R.P., 1982, Heat transfer under an impinging slot jet, Ph.D. Thesis, Department of Chemical Engineering, McGill University, Canada.
- Yap, C.R., 1987, Turbulent heat and momentum transfer in recirculating and impinging flows, Ph.D. Thesis, Faculty of Technology, University of Manchester, UK (Quoted by Hosseinalipour and Mujumdar, 1995).

**FLOW AND DRYING CHARACTERISTICS OF
TWO-DIMENSIONAL GAS-PARTICLE IMPINGING STREAMS**

The game is not over until it is over

Yogi Berra

5.1. INTRODUCTION

In the previous chapters flow, heat transfer and mixing characteristics of both laminar and turbulent single-phase confined impinging streams have been examined. As mentioned in Chapter 1 impinging stream flow configuration was first suggested as a method for intensifying transfer processes in heterogeneous system (Tamir, 1994). Through this objective that the model, which allows accurate prediction of transport processes in gas-particle impinging streams, is needed. The development and verification of the aforementioned model along with the illustration of its use is the subject of the present chapter.

Although a number of papers have been published on gas-particle and gas-droplet contacting operations in impinging streams (e.g., Tamir et al., 1984; Kitron and Tamir, 1988; Kudra and Mujumdar, 1989; Kudra and Mujumdar, 1995; Hu and Liu, 1999), very few papers have attempted modeling of these operations from first principles. A large pool of literature on gas-particle flows in other configurations is available, however. Only closely related publications are reviewed here.

Yoshida et al. (1990) conducted experiments to study the flow and heat transfer mechanisms of a two-dimensional gas-solid impinging jet via the use of an LDV. They reported the presence of particles rebounding from the impingement plate and the gas-phase reverse flow caused by those particles. This leads to significant heat transfer enhancement near the stagnation point due to the production of turbulence in the viscous sublayer by particles. However, the turbulence structure undergoes only a slight change in the wall jet region where the gas-solid interaction is smaller.

Bar and Tamir (1990) studied the behavior of the particles and their residence time distribution in two tangentially fed impinging streams reactor using a stochastic Markov chain model. The true residence time distribution (RTD) curve and the nature of particles circulating on the walls of the reactor were determined using the model.

Hosseinalipour (1996) and Hosseinalipour and Mujumdar (1997) studied numerically the flow, heat transfer and drying characteristics of particles in confined turbulent opposing jets using superheated steam as the drying medium. They computed particle trajectories as well as temperature and moisture content histories of particles (up to 2000 particles entering the contactor through one inlet nozzle). Effects of various operating and geometric parameters on various transport processes were investigated in detail. This is by far the most extensive study on mathematical modeling of gas-particle flow with heat and mass transfer in two-dimensional confined impinging streams. They developed a computer code to solve the coupled equations that included effects of the restitution coefficient and turbulence modulation by the presence of particles. They examined the effects of both flow and geometric parameters on the particle mean residence time as well as its distribution according to the particle size and its initial location at entry into the contactor. Extremely large computing times limited their parametric studies, unfortunately.

Berman and Tamir (1996) studied coalescence of particles in coaxial impinging streams and proposed a coalescence model, which is based on equation expressing the condition for inter-particle collision rate as well as the equation of motion of a single particle. The model assumes coalescence only between small and large particles. It also assumes that the probability of inter-particle collisions between large particles is negligible when comparing with the collisions between small and large particles.

Wu and Wu (1997) studied experimentally and theoretically the pressure drop across the impinging stream contactor (ISC) resulted from the acceleration of particles as well as the impingement of two inlet streams. It is found that a large proportion of the power (more than 80%) used for the operation of ISC is being consumed in the acceleration of particles while the pressure drop due to the impingement of inlet streams is independent of the presence of particles. The proposed model for the total pressure drop predicts the experimental results satisfactorily.

Kleingeld et al. (1999) developed a model for the prediction of the interfacial area production in their IS reactor based on a Monte Carlo simulation of bubble breakup in a turbulent environment. The model gives reasonable predictions of experimental results although certain areas have been identified where the model needs further improvement.

In this chapter numerical results of the study of gas-particle flow and drying in turbulent two-dimensional confined impinging streams are presented. Continuous-phase conservation equations are written in the Eulerian frame while the particle equations are written in the Lagrangian frame. Two-way physical coupling between the continuous and particulate phases is taken into account in the governing conservation equations. This technique is based on the particle-source-in cell (PSI-CELL) model of Crowe et al. (1977). Monte Carlo stochastic approach is used to model particle dispersion due to the turbulent fluctuations of the continuous-phase velocity. Effects of various operating parameters on the flow and drying behavior of the system are reported and discussed.

5.2. MATHEMATICAL FORMULATION

5.2.1. Continuous-phase equations

To formulate the mathematical description of the transport processes in the continuous phase the following assumptions are made: the flow is incompressible and the fluid is Newtonian. Viscous dissipation is neglected. The flow is assumed to be fully developed at the exit of the IS.

Based on the aforementioned assumptions the time-averaged conservation equations for mass, momentum and energy (in tensor form) can be written as follows.

Interactive source terms are added to these equations to take into account the interphase transport.

Continuity equation:

$$\frac{\partial(\rho U_i)}{\partial x_i} = S_m \quad (5.1)$$

Momentum equation:

$$\frac{\partial(\rho U_i U_j)}{\partial x_j} = -\frac{\partial P}{\partial x_j} + \frac{\partial}{\partial x_i} \left[\mu \left(\frac{\partial U_i}{\partial x_j} + \frac{\partial U_j}{\partial x_i} \right) - \overline{\rho u_i u_j} \right] + S_{v,i} \quad (5.2)$$

Energy equation:

$$\frac{\partial(\rho c_p U_i T)}{\partial x_i} = \frac{\partial}{\partial x_i} \left[k \frac{\partial T}{\partial x_i} - \overline{\rho u_i T} \right] + S_h \quad (5.3)$$

Species equation

$$\frac{\partial(\rho U_i Y)}{\partial x_i} = \frac{\partial}{\partial x_i} \left[D \frac{\partial Y}{\partial x_i} - \overline{\rho u_i Y} \right] + S_m \quad (5.4)$$

where S_m , $S_{v,i}$ and S_h are interactive source terms accounting for the interphase transport.

Reynolds stresses, turbulent heat and mass fluxes are expressed as follows:

$$-\overline{\rho u_i u_j} = \mu_t \left(\frac{\partial U_i}{\partial x_j} + \frac{\partial U_j}{\partial x_i} \right) - \frac{2}{3} \rho k \delta_{ij} \quad (5.5)$$

$$-\overline{\rho u_i T} = \frac{\mu_t}{\sigma_T} \frac{\partial T}{\partial x_i} \quad (5.6)$$

$$-\overline{\rho u_i Y} = \frac{\mu_t}{\sigma_Y} \frac{\partial Y}{\partial x_i} \quad (5.7)$$

The turbulence model used to close the system above is as described in Chapter 4. For the sake of completeness it is repeated here briefly. For additional details of it the reader is referred to Section 4.2 of Chapter 4.

The turbulence kinetic energy and the isotropic component of the turbulence energy dissipation rate are determined from the following transport equations:

$$\frac{\partial(\rho k)}{\partial t} + \frac{\partial(\rho U_i k)}{\partial x_i} = \frac{\partial}{\partial x_i} \left[\left(\frac{\mu_t}{\sigma_k} + \mu \right) \frac{\partial k}{\partial x_i} \right] + \mu_t \left(\frac{\partial U_i}{\partial x_j} + \frac{\partial U_j}{\partial x_i} \right) \frac{\partial U_i}{\partial x_j} - \rho \epsilon \quad (5.8)$$

$$\frac{\partial(\rho\varepsilon)}{\partial t} + \frac{\partial(\rho U_i \varepsilon)}{\partial x_i} = \frac{\partial}{\partial x_i} \left[\left(\frac{\mu_t}{\sigma_\varepsilon} + \mu \right) \frac{\partial \varepsilon}{\partial x_i} \right] + C_1 f_1 \mu_t \frac{\varepsilon}{k} \left(\frac{\partial U_i}{\partial x_j} + \frac{\partial U_j}{\partial x_i} \right) \frac{\partial U_i}{\partial x_j} - C_2 f_2 \frac{\varepsilon^2}{k} \quad (5.9)$$

where $C_\mu = 0.09$; $\sigma_k = 1.00$; $\sigma_\varepsilon = 1.314$; $C_1 = 1.44$ and $C_2 = 1.92$.

The wall-damping functions f_1 , f_2 and f_μ are defined as follows:

$$f_1 = \left(1 + \frac{0.05}{f_\mu} \right)^3 \quad (5.10)$$

$$f_2 = 1 - \exp(-R_t^2) \quad (5.11)$$

$$f_\mu = \left[1 - \exp(-0.0165 R_y) \right]^2 \left(1 + \frac{20.5}{R_t} \right) \quad (5.12)$$

where $R_t = \frac{\rho k^2}{\mu \varepsilon}$ and $R_y = \frac{\rho y k^{1/2}}{\mu}$.

The following secondary source term is added to the ε equation:

$$S_\varepsilon = \max \left[0.83 \left(\frac{l}{l_e} - 1 \right) \left(\frac{l}{l_e} \right)^2 \frac{\varepsilon^2}{k}, 0 \right] \quad (5.13)$$

where l_e denotes near-wall equilibrium length scale taken as 2.5 times the distance from the wall, and l is the turbulence length scale.

The time-averaged flow field is determined using the turbulent viscosity modified by multiplication by a factor, which is a function of the local Reynolds number of turbulence:

$$\mu_{\text{mod}} = \mu_t \cdot \min \left[1.0, (A \cdot R_t)^B \right] \quad (5.14)$$

$$\mu_t = \rho C_\mu f_\mu \frac{k^2}{\varepsilon} \quad (5.15)$$

where μ_{mod} is the turbulent viscosity to be used and μ_t is the nominal (high-Reynolds-number) value of μ_{mod} . A , B are constants in which the values, obtained in the present study by fitting numerical results to experimental impingement heat transfer data, equal to 0.05 and 2.40, respectively. The values of dimensionless distance of the first grid points normal to the wall, y^+ , were again kept lower than unity to ensure adequate concentration of near-wall grids.

5.2.2. Disperse-phase equations

In order to describe the evolution of the particle position, velocity, temperature as well as mass, the Lagrangian equations are solved. In the following sub-sections each of the Lagrangian equations is described (Fueyo et al., 1997). It should be noted that particle-particle interactions are neglected since the particle concentration considered in this work is not high (initial particle loading ratio is fixed at only 0.1).

5.2.2.1. Particle position equation

The evolution of the particle position is determined from the following equation:

$$\frac{dx_{p,i}}{dt} = u_{p,i} \quad (5.16)$$

where $x_{p,i}$ is the particle position and $u_{p,i}$ is the particle velocity. The particle velocity is determined from the solution of the particle momentum equation discussed next.

5.2.2.2. Particle momentum equation

The velocity of the particle is calculated from the following equation of motion (Faeth, 1983; Hosseinalipour, 1996; Hosseinalipour and Mujumdar, 1997):

$$\begin{aligned} m_p \frac{du_{p,i}}{dt} = & f_D(u_i - u_{p,i}) + m_p g_i - V_p \frac{\partial P}{\partial x_i} + K_m V_p \frac{d}{dt}(u_i - u_{p,i}) + \\ & \frac{K_B D_p^2 (\pi \rho \mu)^{1/2}}{4} \int_{t_0}^t \frac{d}{dt}(u_i - u_{p,i}) \frac{dt}{(t-t_0)^{1/2}} + \frac{\pi}{8} \rho D_p^3 \omega_p \xi_{ijk} n_{j,1} (u_k - u_{p,k}) + \\ & 1.6(\rho \mu)^{1/2} D_p^2 \gamma_{ijk} (u_j - u_{p,j}) n_{k,2} \left(\frac{\partial u_l}{\partial x_l} \right) + F_e \end{aligned} \quad (5.17)$$

where f_D is a drag function defined below, V_p is the particle volume and $n_{j,1}$ and $n_{k,2}$ represent unit vectors. The ξ_{ijk} and γ_{ijk} are third-order tensors defined below:

$$\begin{aligned} & 1 \text{ for } ijk = 123, 231, 312 \\ \xi_{ijk} = & -1 \text{ for } ijk = 132, 213, 321 \\ & 0 \text{ otherwise} \end{aligned} \quad (5.18)$$

and

$$\begin{aligned} \gamma_{ijk} &= 1 \text{ for } ijk = 123, 213, 312, \dots \text{ (non-repeating indices)} \\ &= -1 \text{ for } ijk = 121, 322, 221, \dots \text{ (repeating indices)} \end{aligned} \quad (5.19)$$

The term on the left-hand side of equation (5.17) represents the inertial force of the particle. The first term on the right-hand side of equation (5.17) represents the drag force on the particle, which includes both skin friction and form drag. The second term represents the gravitational force while the third term accounts for the static pressure gradients in the flow. The fourth term accounts for the force on the particle due to the inertia of fluid displaced by its motion, which is often called the virtual (added) mass. The value of the empirically determined K_m is approximately 0.5. The fifth term, Basset force, allows for effects of the deviation of the flow from a steady flow pattern around the particle. The value of K_B is of the order of 6.0. The sixth and seventh terms are the Magnus force and the Saffman force, respectively. The Magnus effect appears when the particle is rotating. Rotation of the particle distorts the gas flow field in its neighborhood, giving rise to this force. This effect causes the particle to be deflected toward the side where the peripheral motion of the particle is in the same direction as relative gas flow. The Saffman term accounts for the force induced on the particle by the gradient in the local gas velocity; this induces a transverse force (lift) on the particle. The last term accounts for any other forces.

Since, in the present case, the particle density is much higher than the gas density, the virtual mass and the Basset force are neglected. At higher pressures their effects may not be negligible, however (Faeth, 1983). It is also shown that the lift force is normally at least an order of magnitude smaller than the drag force throughout the dilute spray region (Faeth, 1983). This term is thus neglected here. Although the Magnus force is generally small in the dilute spray region, its effect could still be comparable to processes such as turbulent particle dispersion. However, for simplicity, this effect is also neglected here. Recent laser holography studies have also shown that in most regions of the flow field the particle does not rotate. Therefore, except in the region adjacent to the wall, this force is not important (Lixing, 1993).

The drag function f_D is calculated from the following equation:

$$f_D = \frac{1}{2} \rho A_p C_D |u_i - u_{p,i}| \quad (5.20)$$

where A_p is the particle projected area. C_D is the drag coefficient, which is given by the following equation:

$$C_D = \frac{24}{\text{Re}} (1 + 0.15 \text{Re}^{0.687}) + \frac{0.42}{1 + 4.25 \times 10^4 \text{Re}^{-1.16}} \quad (5.21)$$

where Re is the particle Reynolds number defined as:

$$\text{Re} = \frac{\rho |u_i - u_{p,i}| D_p}{\mu} \quad (5.22)$$

The correlation for the drag coefficient is valid for rigid spherical particles and when $\text{Re} < 3 \times 10^5$ (Clift et al., 1978).

5.2.2.3. Particle mass equation

The evolution of the mass of the particle is described by the following equation:

$$\frac{dm_p}{dt} = -\pi D_p \frac{k_v}{c_{pv}} \text{Nu} \ln(1 + B_M) \quad (5.23)$$

where k_v is the thermal conductivity of the vapor produced by the evaporation of the particle and c_{pv} is the specific heat capacity of that vapor. Nu is the Nusselt number, determined from the following equation:

$$\text{Nu} = 2(1 + 0.3 \text{Re}^{0.5} \text{Pr}^{0.33}) F \quad (5.24)$$

Where Pr is the laminar Prandtl number for the continuous phase and F is the Frössling correction for mass transfer, which is given by:

$$F = \frac{1}{B_M} \ln(1 + B_M) \quad (5.25)$$

B_M is the mass transfer number, which represents the driving force in the mass transfer process and is defined by:

$$B_M = \frac{Y_{vs} - Y_{v\infty}}{1 - Y_{vs}} \quad (5.26)$$

where Y_{vs} is the mass fraction of vapor at the surface of the particle, $Y_{v\infty}$ is the mass fraction of vapor in the gas surrounding the particle. The mass fraction of vapor at the surface of the particle is calculated by:

$$Y_{vs} = \left[1 + \left(\frac{P}{P_{vs}} - 1 \right) \frac{W_c}{W_v} \right]^{-1} \quad (5.27)$$

where P is the total pressure of the fluid surrounding the particle, P_{vs} is the partial pressure of the vapor at the surface of the droplet at the saturation conditions defined by the droplet temperature, W_c and W_v are the molecular weight of the surrounding fluid and of the vapor, respectively.

5.2.2.4. Particle enthalpy equation

The temperature of the particle is determined from the solution of the particle enthalpy equation as follows:

$$m_p c_p \frac{dT_p}{dt} = \lambda_{fg} \frac{dm_p}{dt} + h(T_g - T_p) \quad (5.28)$$

where c_p is the specific heat capacity of the particle, λ_{fg} is the latent heat of vaporization and h is the convective heat transfer coefficient between the particle and the surrounding fluid.

5.2.3. Turbulent dispersion of particles

The effect of the turbulence on the droplet motion is simulated here by a Monte Carlo stochastic approach, in which the gas turbulence is randomly sampled during each particle flight and allowed to influence its motion. The gross particle behavior is then obtained by averaging over a statistically significant sample of particles (Gosman and Ioannides, 1981). The turbulence is assumed to be isotropic and to possess a Gaussian probability distribution in the fluctuating velocity. Among the stochastic models the Monte Carlo method has been tested in a broader range of theoretical and practical problems and has given satisfactory predictions (Hosseinalipour, 1996) and hence the choice of the model here.

The model uses a sum of the time-average velocity U_i and a fluctuating component u_i' as the continuous-phase velocity in the drag force term of the particle momentum equation, equation (5.17):

$$u_i = U_i + u_i' \quad (5.29)$$

where U_i is obtained from the Eulerian equations for the continuous phase and u_i' is calculated assuming that each component follows a normal distribution with a mean value of 0.0 and a standard deviation of:

$$\sigma = \sqrt{\frac{2k}{3}} \quad (5.30)$$

where k is the turbulence kinetic energy.

The interaction between the gas phase turbulence and the particle motion occurs over a time interval, which is the minimum of the two time scales, namely, a turbulent eddy lifetime and the residence time of the particle in the eddy:

$$t_{\text{int}} = \min(t_e, t_R) \quad (5.31)$$

where t_e , the lifetime of the local eddy, which the particle is assumed to be traversing, is given by:

$$t_e = \frac{l_e}{|u_i|} \quad (5.32)$$

where l_e is the eddy size:

$$l_e = \frac{C_\mu^{3/4} k^{3/2}}{\varepsilon} \quad (5.33)$$

where ε is the rate of dissipation of the turbulence kinetic energy and C_μ is a constant in the turbulence model.

The particle transit time, which is the time for the particle to cross the eddy, is given by:

$$t_R = \frac{l_e}{|u_i - u_{p,i}|} \quad (5.34)$$

The numerical integration of the particle equations takes place according to the following sequence: the Lagrangian time-step is calculated, the particle is moved, the

particle properties at the new position are calculated and the interactive source terms are calculated. For more detail the reader is referred to Crowe et al. (1998).

5.2.4. Calculation of interactive source terms

As the particles traverse each cell, exchange of momentum, energy and mass between phases occurs. The source terms, which must be added to the continuous-phase transport equations to represent these transport effects, are calculated as follows.

5.2.4.1. Mass transfer source

An interactive source term for mass transfer is calculated by:

$$S_m = \frac{\pi}{6} \sum \eta [\rho_p^0 (D_p^0)^3 - \rho_p^n (D_p^n)^3] \quad (5.35)$$

where n denotes values at the end of the Lagrangian time step, 0 denotes the values at the start of the Lagrangian time step, η is the mass flowrate of a particular parcel of particles divided by the mass of an individual particle and Σ is the summation over all of the Lagrangian time steps required for the particle to traverse the cell and for all particles.

5.2.4.2. Momentum transfer source

The source of momentum, which appears in the continuous-phase momentum equations, is equal to the rate of change of particle momentum as each particle parcel traverses a cell and is calculated by:

$$S_{v,i} = \frac{\pi}{6} \sum \eta [\rho_p^0 u_{p,i}^0 (D_p^0)^3 - \rho_p^n u_{p,i}^n (D_p^n)^3] \quad (5.36)$$

5.2.4.3. Enthalpy transfer source

The source of enthalpy, which appears in the continuous-phase energy equation, is calculated by:

$$S_h = \frac{\pi}{6} \sum \eta [\rho_p^0 h_p^0 (D_p^0)^3 - \rho_p^n h_p^n (D_p^n)^3] \quad (5.37)$$

where h_p is the enthalpy of the particle relative to a value of zero at 0.0 K.

5.2.5. Particle-wall interaction

When a particle tries to cross into a wall or obstacle during a time-step the time-step is reduced so that the particle is placed on the wall or obstacle surface. The velocity component parallel to the wall after the bounce is set to the same component before the bounce while the velocity component perpendicular to the wall after the bounce is set to the negative of the same component before the bounce (Fueyo et al., 1997). This corresponds to the use of the unity restitution coefficient, which is adopted in this work.

5.2.6. Boundary conditions

In the following paragraphs W is the width of the inlet channels; H and L are the height and the length of the exit (or main flow) channels, respectively. The coordinates used are shown in Figure 5.1. Boundary conditions for the continuous-phase equations are as follows:

Inlet 1

$$(0 < x < W; y = W + H/2) \quad U_1 = 0; U_2 = -U_{2,jet}; T = T_{inlet 1} \text{ and } Y = Y_{inlet 1} \quad (5.38)$$

Inlet 2

$$(0 < x < W; y = -(W + H/2)) \quad U_1 = 0; U_2 = U_{2,jet}; T = T_{inlet 2} \text{ and } Y = Y_{inlet 2} \quad (5.39)$$

and $k = (U_{jet} I)^2$; $\varepsilon = C_\mu^{3/4} \frac{k^{3/2}}{l}$ where $l = 0.1L$ and L is the characteristic length of the system; I represents the turbulence intensity.

Top and bottom walls

$$(W < x < L + W) \quad u_x = 0 \text{ and } \frac{\partial T}{\partial y} = 0; \frac{\partial Y}{\partial y} = 0; k = 0 \text{ and } \frac{\partial \varepsilon}{\partial y} = 0 \quad (5.40)$$

Outlet

$$(x = L + W) \quad \frac{\partial \phi}{\partial x} = 0 \quad (5.41)$$

where ϕ represents all solved variables.

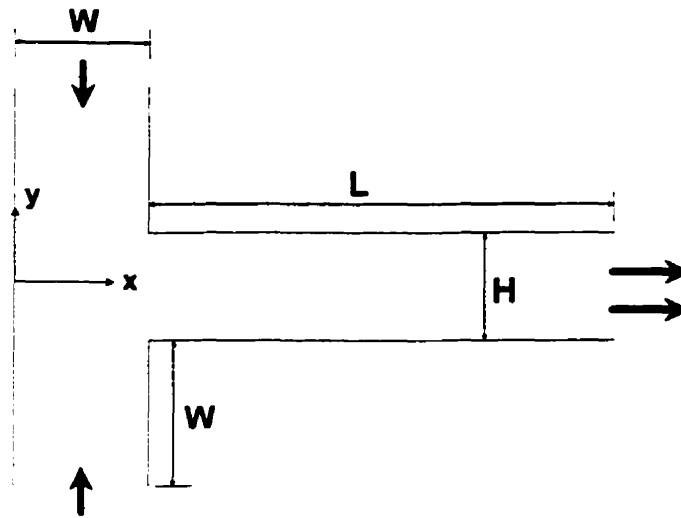


Figure 5.1. Schematic diagram of a one-way exit IS used in the present study

For the particle equations the following particle inlet conditions must be specified for each parcel of particles: inlet position, inlet velocity (which, in the present study, is assumed to be equal to the inlet jet velocity), particle diameter, particle density, particle mass flowrate and particle inlet temperature.

The continuous-phase equations, along with the boundary conditions, were solved numerically using the control-volume-based computational fluid dynamic software PHOENICS version 2.2.2 (CHAM, 1997). In this code the convection terms in the conservation equations were discretized using the hybrid scheme (Patankar, 1980). The discretized equations were solved using the well-known SIMPLEST algorithm (CHAM, 1997). The solution was considered converged when the following criterion is met for all the dependent variables:

$$\max \left| \frac{\phi^{n+1} - \phi^n}{\phi_r} \right| \leq 10^{-3} \quad (5.42)$$

between sweeps n and $n+1$; ϕ_r represents the reference value for the dependent variable ϕ . To improve convergence underrelaxation of the false transient type was used for the

two velocity components and temperature. Linear relaxation was used for the pressure as well as the turbulence kinetic energy and its dissipation rate. Whole-field residuals were checked to ensure that the converged solution set satisfies the governing equations within a prescribed error. The Lagrangian equations were solved numerically using a PHOENICS software option GENTRA version 2.2 (Fueyo et al., 1997).

5.3. RESULTS AND DISCUSSION

The above-mentioned model was first verified by comparing its predicted results with experimental gas-particle impinging jet data of Yoshida et al. (1990). The system configuration is shown in Figure 5.2.

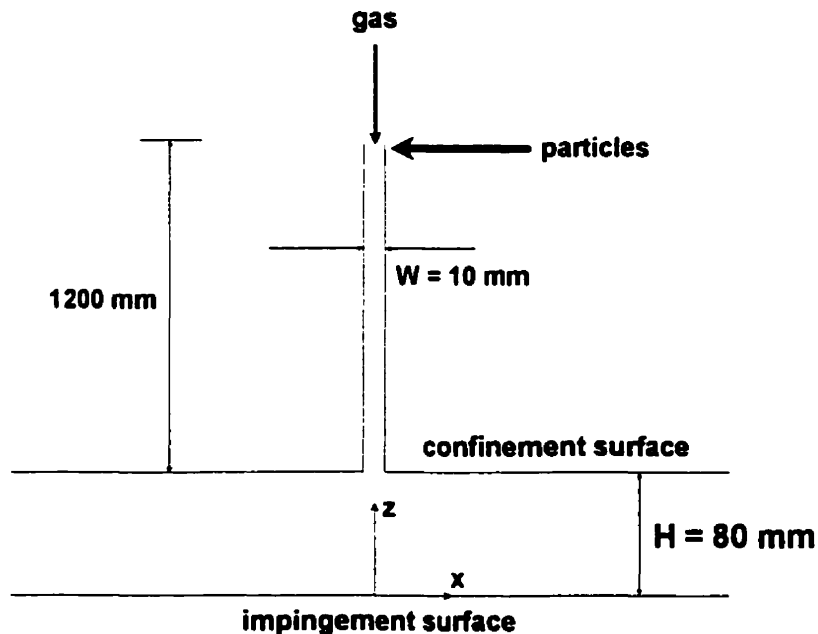


Figure 5.2. Impinging jet configuration used in model validation

The mean diameter of the spherical glass beads used in the experiments was $48.9 \mu\text{m}$ and its standard deviation was $8.7 \mu\text{m}$. The dimensionless nozzle-to-plate spacing was held constant at $H/W = 8$. The jet Reynolds number, based on the bulk mean gas velocity at the nozzle exit and the nozzle width, was fixed at 10000. The initial particle

loading ratio used in the experiments was 0.1. As noted by Yoshida et al. (1990), highly dense suspensions exist in the vicinity of the stagnation point even if the initial loading ratio is rather small.

The comparison between experimental and numerical profiles of gas-phase mean velocity upstream of the stagnation point is shown in Figure 5.3. Grids of 95×130 were used in the computation. The profiles to the left of the centerline are for the single-phase flow while the profiles to the right belong to the gas-particle flow. Two thousand isothermal particles were tracked in the computational run. Since the detailed experimental particle size distribution is not known, no attempt has been made to represent it with multiple discrete particle sizes. The mean particle diameter was used in the simulation.

It can be seen from this figure that the model predicts the experimental data reasonably well considering the fact that the complete boundary conditions, i.e., turbulence intensity at the nozzle exit, necessary for the numerical computation were not available; the value of $I = 5\%$ was assumed here. Far from the impingement surface the spreading rate of the gas-particle jet is slightly lower than that of the single-phase flow. The gas velocities of the two-phase jet along the stagnation streamline are also slightly lower than those of the single-phase jet. This is due to the momentum transfer from the gas to the particles. Very close to the impingement surface, i.e., at $z/W = 1$, where the impingement plate has a considerable influence on the flow field, the profiles of the two phases are appreciably different from each other. The model does not perform well in the vicinity of the impingement surface due probably to the absence of the turbulence modulation effect in the model. The presence of particles rebounding from the impingement plate and of the gas-phase reverse flow caused by those particles leads to an increase in the turbulence intensity near the stagnation point. Nevertheless, the computational profiles of the two phases are still quite different due to the particle rebounding and the momentum transfer between phases, which are captured by the model.

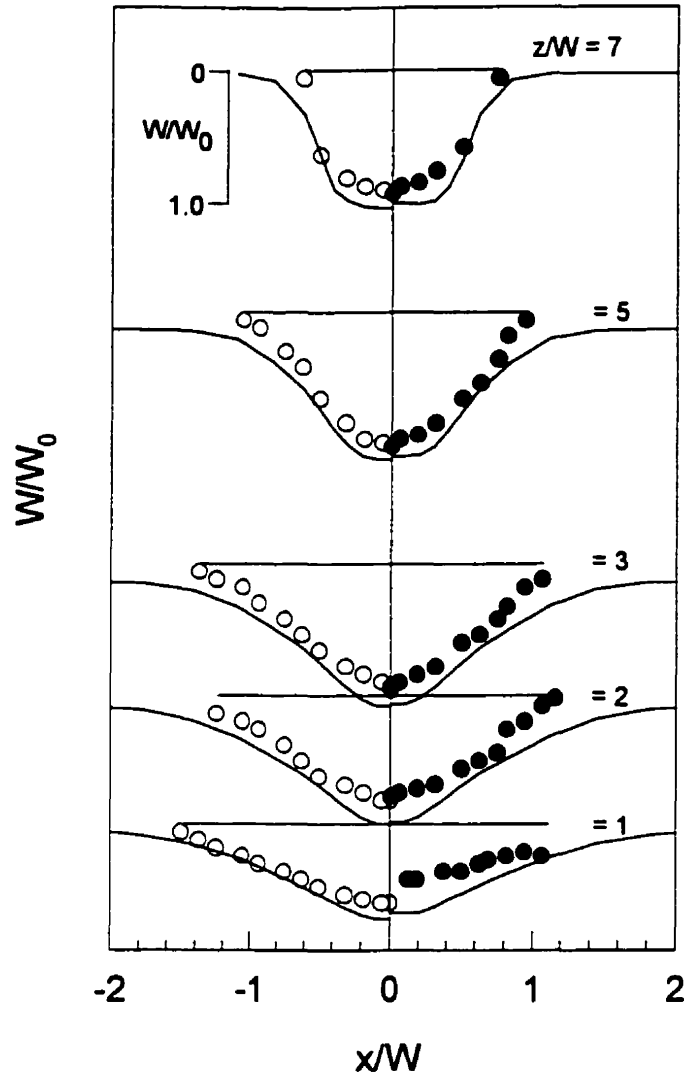


Figure 5.3. Comparison of gas-phase mean velocity profiles
 ◦ experimental single-phase profiles; • experimental two-phase profiles;
 — corresponding computational profiles

Figure 5.4 shows the profiles of the lateral mean velocities in the downstream region of the stagnation point. It can be seen that the peak velocity for the gas phase is smaller than that of the single-phase flow. This is, again, due to the momentum transfer between phases. Particles initially do not have momentum in the x -direction so they become a load for the gas phase and hence the drop in the gas phase velocity. The large discrepancy between the numerical and experimental results may be again attributed to

the absence of the turbulence modulation term in the model as well as an uncertainty in the boundary conditions at the nozzle inlet mentioned earlier.

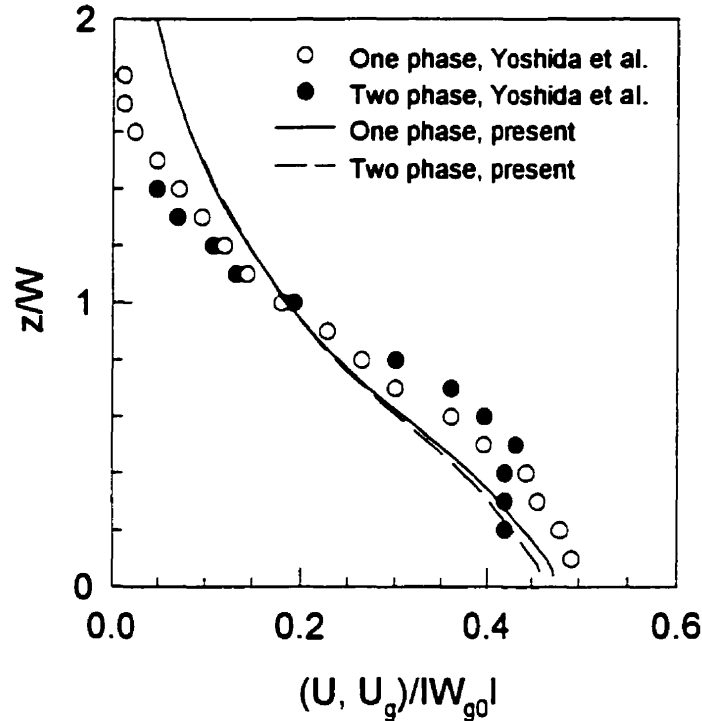


Figure 5.4. Profiles of mean gas-phase velocities at $x/W = 1$

The gas-particle transport model is next used to illustrate the flow and drying behavior of a two-dimensional flash dryer based on an IS flow configuration. Thermodynamic and transport properties of air-water system used in the present study are listed in Table 5.1. Grids of 110×60 were used in all computations. The ranges of operating parameters investigated are: inlet gas temperature from 100 to 300° C and initial particle diameter from 200 to 800 μm (the minimum particle diameter below which the particle is assumed to be completely evaporated was fixed at 100 μm). The initial particle loading ratio (Γ_0) was fixed at 0.1 and the inlet particle temperature was held constant at 50° C. Inlet jet hydraulic diameter is calculated assuming the aspect ratio of 5 between the width and the height of the exit channel. One thousand particles were tracked in each computation. As noted by Chang and Wu (1994) the use of no less than

1000 computational particles for each representative size in the stochastic separated flow (SSF) model yields a nearly invariant solution. Particles were entrained into the top jet at $x/W = 0.5$.

Table 5.1. Thermodynamic and transport properties of air-water system used in the present study

Property	Expression (Fueyo et al., 1997)
c_{pv}	$c_{pv} = 1.2745 \times 10^{-7} T^5 - 1.2475 \times 10^{-4} T^4 + 4.7457 \times 10^{-2} T^3 - 8.711 T^2 + 773.98 T - 2.45 \times 10^4$
k_v	$k_v = 10^{9.1 \times 10^{-4} (T - 373.0) + 1.39} / 1000$; T in Kelvin
P_s	$P_s = 6894.76 \exp(G)$ For $T_R \leq 672^\circ \text{R}$, $G = 73.326 - 8.2 \log(T_R) + 0.003 T_R - \frac{13023.8}{T_R}$ For $672^\circ \text{R} < T_R < T_{cr}$, $G = 15.183 - \frac{8310.453}{T_R} + J + K$ $J = \frac{0.00017Z[\exp(A_1) - 1]}{T_R}$; $K = -0.01 \exp(A_2)$; $A_1 = 2.624 \times 10^{-12} Z^2$; $A_2 = -0.0063 H^{1.25}$; $Z = T_R^2 - 951588$; $H = 1165.09 - T_R$; $T_R = 1.8T + 492.0$
T_s	$T_s = 0.319 P_x^3 + 3.103 P_x^2 + 27.287 P_x + 370.8$; $P_x = \log(P) - 5.0$
ρ	$\rho = (P + 1 \times 10^5) / RT$; T in Kelvin
λ_l	$\lambda_l = -1.802 \times 10^6 - 2.658 \times 10^5 T_x^4 + 1.356 \times 10^6 T_x^3 - 2.565 \times 10^6 T_x^2 + 3.276 \times 10^6 T_x$; $T_x = T(\text{K}) / 273.15$
λ_{fg}	$\lambda_{fg} = 6.291 \times 10^6 - 2.746 \times 10^4 T + 65.991 T^2 - 5.765 \times 10^{-2} T^3$; T in Kelvin

Figure 5.5a compares the dimensionless axial mean velocity profiles of the single-phase flow and gas-particle flow cases at 4 dimensionless axial locations, i.e., $x/W = 1, 5, 10$ and 20 . The plotting procedure used is the same as the one described in Chapter 4. Velocity values were normalized with the inlet gas velocity with the scale of one x/W per U/U_{jet} .

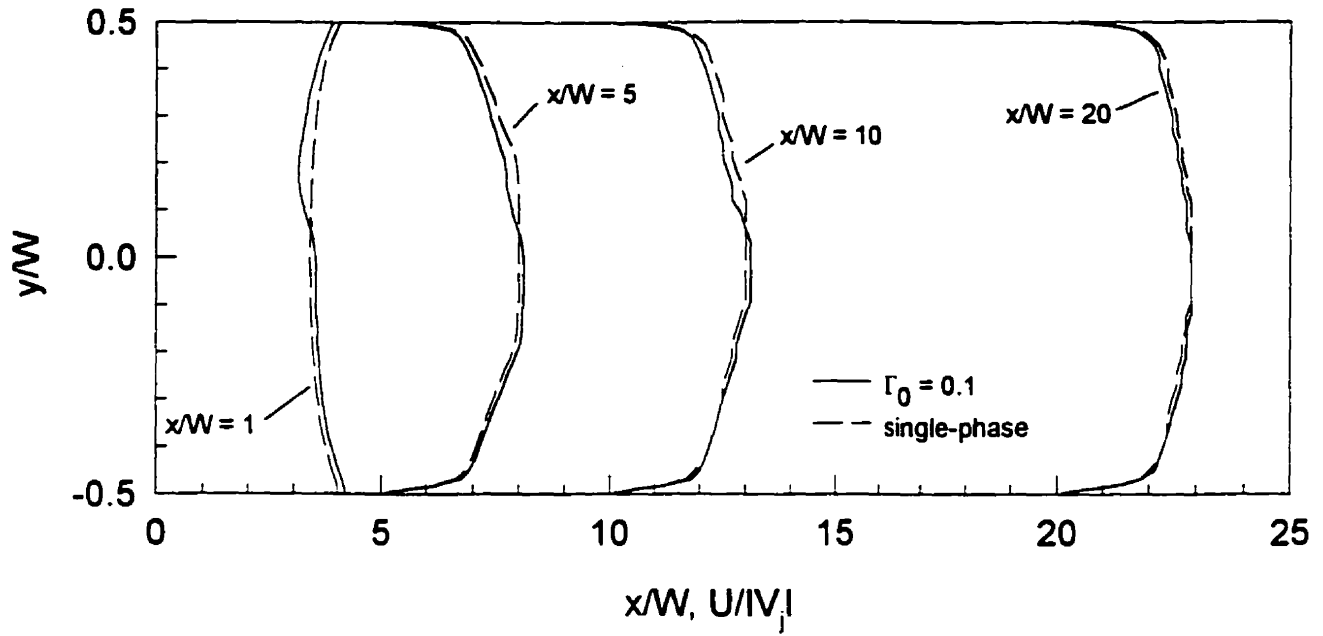


Figure 5.5a. Comparison of gas-phase mean velocity profiles

$Re_j = 10000; I = 1\%; T_0 = 100^\circ\text{C}; D_p = 500 \mu\text{m}; \Gamma_0 = 0.1$

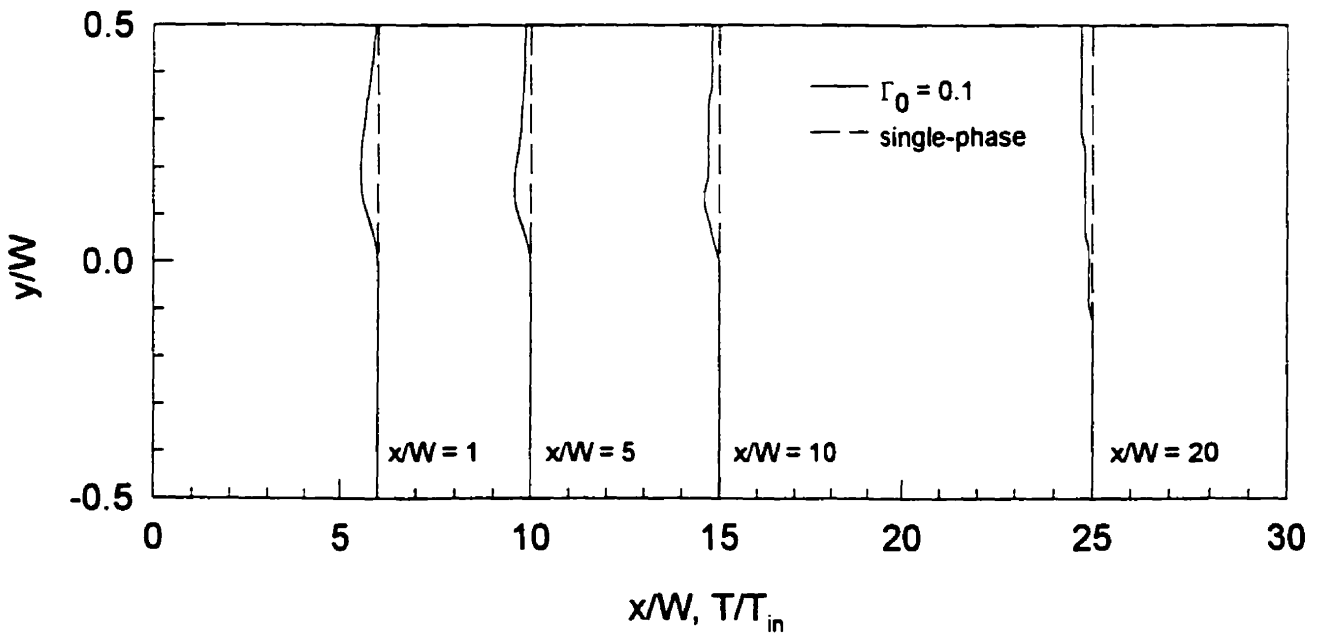


Figure 5.5b. Comparison of gas-phase mean temperature profiles

$Re_j = 10000; I = 1\%; T_0 = 100^\circ\text{C}; D_p = 500 \mu\text{m}; \Gamma_0 = 0.1$

It can be seen that, initially, the gas phase velocity in the upper part of the exit channel is smaller than that of the single-phase flow. This is due to the momentum transfer between phases; particles initially having no momentum in the axial direction and they become a burden to the gas phase. As the distance from the impingement region increases the difference between the two phases decreases indicating the equalization of the momentum of both phases.

Time-averaged temperature profiles of the single-phase flow and gas-particle flow cases at the same 4 dimensionless axial locations are compared in Figure 5.5b. Temperature values were normalized with the inlet gas temperature. The scale used in this case is $5 \times W$'s per one unit normalized temperature.

The temperature drops seen in this figure are due to the enthalpy transfer between phases; the particle inlet temperature was lower than the inlet gas temperature. Again as the distance from the impingement region increases the difference in temperature decreases. The spreading of particles across the exit channel can also be seen in this figure, especially at the distance rather far downstream of the impingement region, e.g., at $x/W = 20$.

The plots of the dimensionless moisture content versus dimensionless axial distance with the initial particle diameter as a parameter are shown in Figure 5.6. It is seen from this figure that drying occurs mainly in the impingement region and its vicinity; once particles leave this region very little drying takes place.

Since smaller particles, $D_p = 200 \mu\text{m}$ in this case, have smaller inertia, the penetration of particles into the opposite jet as mentioned in Chapter 1 does not occur and hence the absence of the oscillatory motion, which increases the residence time of particles in the highly turbulent region. Drying for smaller particles is thus achieved to a smaller extent than for larger particles, e.g., particles with $D_p = 500$ and $800 \mu\text{m}$. Similar behavior has been reported by Hosseinalipour and Mujumdar (1997) who studied superheated steam drying of particles in an IS dryer. Once the particles leave the impingement region they move rapidly through the exit channel and little drying occurs in this downstream region as can be seen in Figure 5.6. Negligible difference in moisture loss can be observed among those larger particles as they have larger inertia to penetrate into the opposite jet and hence have higher residence time in this region.

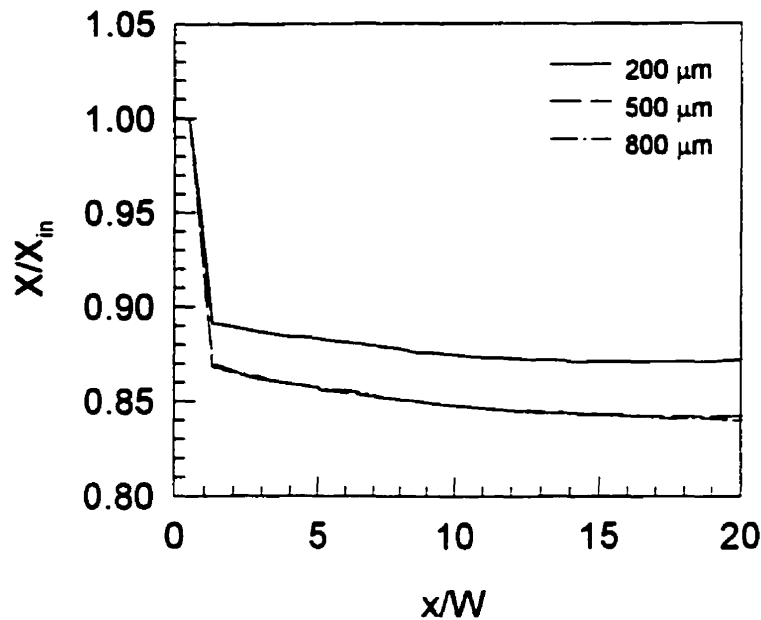


Figure 5.6. Moisture content profiles in an IS flash dryer

$$Re_j = 10000; I = 1\%; T_0 = 100^\circ\text{C}; \Gamma_0 = 0.1$$

Since drying takes place only in the constant rate period, particle surface temperature attains and remains at the wet-bulb temperature throughout the whole drying process (Mujumdar and Devahastin, 2000).

The effect of the inlet gas temperature on the dimensionless moisture content profile is shown in Figure 5.7. Again drying occurs mostly in the impingement region. Increasing the gas inlet temperature from 100°C to 200°C does not promote drying as much as one might expect in this case. The reason for this behavior is ascribed to the variable fluid properties used in the present study. As the gas temperature increases the gas kinematic viscosity increases. Since the inlet jet Reynolds number was fixed in this case, the inlet gas mass flowrate increases with increased inlet gas temperature. The particle mean residence time in the dryer therefore decreases and hence less drying. At the inlet gas temperature of 300°C the gas mass flowrate was rather high that the unfavorable behavior due to an increase in the inlet gas temperature is observed. In practical, however, gas mass flowrate (and hence the particle mass flowrate, if Γ_0 is kept constant) is normally held constant and the effect of increased inlet temperature will be

different from what is shown here. Drying rate is normally higher at higher inlet gas temperature.

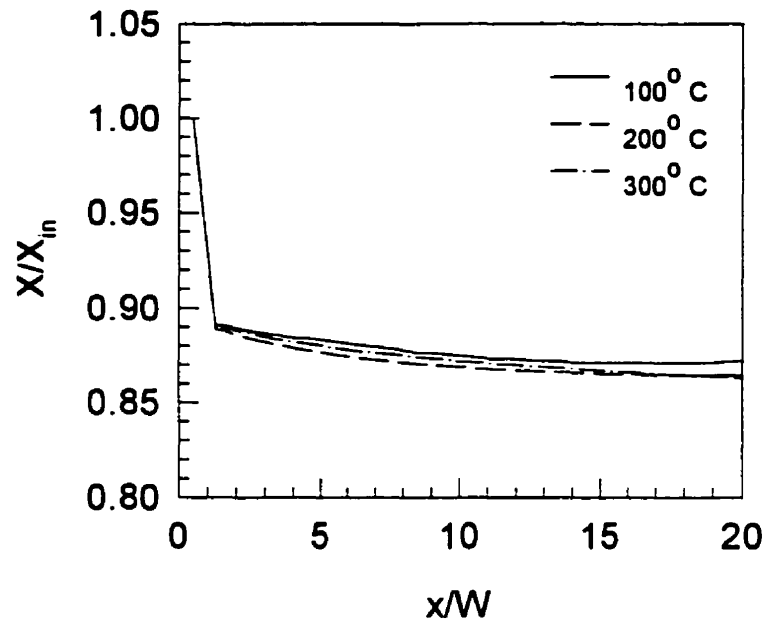


Figure 5.7. Moisture content profiles in an IS flash dryer

$$Re_j = 10000; I = 1\%; D_p = 500 \mu\text{m}; \Gamma_0 = 0.1$$

CLOSING REMARKS

Numerical results based on a study of the gas-particle flow and drying in turbulent two-dimensional confined impinging streams are reported in this chapter. Continuous-phase turbulence behavior is modeled using the composite model proposed in Chapter 4. The gas-particle transport model was first verified by comparing its predictions with experimental gas-particle impinging jet flow data available in the literature. Reasonable agreement is obtained despite the simplifying model assumptions and the lack of complete boundary conditions for the simulation. The model was then used to illustrate the use of an IS flow configuration as a flash dryer. It is found that drying occurs mainly

in the impingement region and its vicinity; once particles leave this region very little drying takes place. This result suggests the use of a multi-stage IS operation to improve drying. It is also observed that drying for smaller particles is achieved to a lesser extent than for larger particles due to their smaller inertia and hence smaller mean residence time in the impingement region. Increasing inlet gas temperature does not yield expected results in this case due to the use of the variable fluid properties assumption and fixed inlet dimensionless boundary conditions.

NOMENCLATURE

A, B, C_l	
C_2, C_μ	turbulence model constants, -
A_p	particle projected area, m^2
B_M	mass transfer number, -
c_p	heat capacity, $J\ kg^{-1}\ K^{-1}$
c_{pv}	specific heat of the vapor, $J\ kg^{-1}\ K^{-1}$
C_D	drag coefficient, -
D	mass diffusivity, $m^2\ s^{-1}$
D_h	inlet channel hydraulic diameter, m
D_p	particle diameter, m
f_1, f_2, f_μ	turbulence model functions, -
f_D	drag function, $kg\ s^{-1}$
F	Frössling number, -
g_i	gravitational force vector, $m\ s^{-2}$
h	convective heat transfer coefficient, $W\ m^{-2}\ K^{-1}$
H	height of the exit channel, m
I	turbulence intensity, %
k	thermal conductivity, $W\ m^{-1}\ K^{-1}$ (equation (5.3))
k	turbulence kinetic energy, $m^2\ s^{-2}$
k_v	thermal conductivity of the vapor, $W\ m^{-1}\ K^{-1}$
l	turbulence length scale, m

K_B	empirical constant, -
K_m	empirical constant, kg m^{-3}
l_e	near-wall equilibrium length scale, m
L	length of the exit channel, m
m_p	mass of the particle, kg
$n_{j,1}, n_{k,2}$	unit vectors, -
P	time-averaged pressure, Pa
P_s	saturation pressure, Pa
P_{vs}	saturated vapor partial pressure at the particle surface, Pa
R	gas constant, $2.871 \times 10^2 \text{ J kg}^{-1} \text{ K}^{-1}$
R_t	turbulence Reynolds number, $\frac{\rho k^2}{\mu \varepsilon}$, -
R_y	turbulence Reynolds number, $\frac{\rho y k^{1/2}}{\mu}$, -
S_h	interactive source term for enthalpy transfer, $\text{J m}^{-3} \text{ s}^{-1}$
S_m	interactive source term for mass transfer, $\text{kg m}^{-3} \text{ s}^{-1}$
$S_{v,i}$	interactive source term for momentum transfer, $\text{kg m}^{-2} \text{ s}^{-2}$
t	time, s
t_e	eddy lifetime, s
t_R	particle transit time, s
T	time-averaged temperature, $^{\circ} \text{C}$
T_{cr}	critical temperature, $^{\circ} \text{C}$ (or $^{\circ} \text{R}$)
T_s	saturation temperature, $^{\circ} \text{C}$
T'	fluctuating component of temperature, $^{\circ} \text{C}$
u_i	instantaneous gas-phase velocity, m s^{-1}
u'_i, u'_j	fluctuating gas-phase velocity components, m s^{-1}
$u_{p,i}$	particle velocity, m s^{-1}
u_{τ}	friction velocity, $\sqrt{\tau_w / \rho}$, m s^{-1}
U_i, U_j	time-averaged velocity components, m s^{-1}
V_p	particle volume, m^3

W	width of the inlet channel, m
W_c	molecular weight of the surrounding fluid, kg/kg mol
W_v	molecular weight of the vapor, kg/kg mol
x_i, x_j	coordinates, m
$x_{p,i}$	particle position, m
y^+	dimensionless distance from the wall, $\frac{u_\tau y \rho}{\mu}$, -
Y	mass fraction of vapor, kg water/kg dry air
Y'	fluctuating component of mass fraction of vapor, kg water/kg dry air
Y_{vs}	mass fraction of vapor at the particle surface, kg water/kg dry air
$Y_{v\infty}$	mass fraction of vapor in the surrounding fluid, kg water/kg dry air

Greek letters

δ_{ij}	Kronecker delta, -
ε	isotropic turbulence dissipation rate, $m^2 s^{-3}$
γ_{ijk}, ξ_{ijk}	third-order tensors, -
Γ	particle loading ratio, -
λ_{fg}	latent heat of vaporization, $J kg^{-1}$
λ_l	liquid saturation enthalpy of the particle, $J kg^{-1}$
μ	dynamic viscosity, $kg m^{-1} s^{-1}$
μ_t	turbulent viscosity, $kg m^{-1} s^{-1}$
ρ	density, $kg m^{-3}$
σ_k	diffusion Prandtl number for turbulence kinetic energy, -
σ_ε	diffusion Prandtl number for dissipation rate, -
σ_T	turbulent Prandtl number, -
σ_Y	turbulent Schmidt number, -
τ_w	shear stress at the wall, $kg m^{-1} s^{-2}$
ω_p	angular velocity, $rad s^{-1}$

Superscripts

0	value at the start of the Lagrangian time step
n	value at the end of the Lagrangian time step

Subscripts

0	inlet
<i>g</i>	gas-phase
<i>p</i>	particle
<i>v</i>	vapor

Dimensionless group

Nu	Nusselt number, $\frac{hD_p}{k}$
Pr	Prandtl number, $\frac{c_p\mu}{k}$
Re _j	jet Reynolds number, $\frac{D_h U_{jet} \rho}{\mu}$

REFERENCES

- Berman, Y., Tamir, A., 1996, Coalescence model of particles in coaxial impinging streams, *Canadian Journal of Chemical Engineering*, 74, pp. 822-833.
- Bar, T., Tamir, A., 1990, An impinging-streams reactor with two pairs of tangential air feeds, *Canadian Journal of Chemical Engineering*, 68, pp. 541-552.
- Chang, K.-C., Wu, W.-J., 1994, Sensitivity study of Monte Carlo solution procedure of two-phase turbulent flow, *Numerical Heat Transfer, Part B*, 25, pp. 223-244.
- Clift, R., Grace, J.R., Weber, M.E., 1978, *Bubbles, Drops and Particles*, Academic Press, New York.
- Concentration, Heat and Momentum Limited (CHAM), 1997, *POLIS: Phoenix On-Line Information System*, London, UK.
- Crowe, C.T., Sharma, M.P., Stock, D.E., 1977, The particle-source-in cell (PSI-CELL) model for gas-droplet flows, *ASME Journal of Fluids Engineering*, 99, pp. 325-332.
- Crowe, C., Sommerfeld, M., Tsuji, Y., 1998, *Multiphase Flows with Droplets and Particles*, CRC Press, Boca Raton.
- Faeth, G.M., 1983, Evaporation and combustion of sprays, *Progress in Energy and Combustion Science*, 9, pp. 1-76.

- Fueyo, N., Hamill, I., Zhang, Q., Adair, D., 1997, *The GENTRA User's Guide*, Concentration, Heat and Mass Limited (CHAM), London, UK.
- Gosman, A.D., Ioannides, E., 1981, Aspects of computer simulation of liquid-fuelled combustors, AIAA Paper 81-0323, *Proceedings of the 19th AIAA Aerospace Sciences Meeting*, St. Louis, MO.
- Hosseinipour, S.M., 1996, Transport processes in laminar and turbulent opposing jet contactors, Ph.D. Thesis, Department of Chemical Engineering, McGill University, Canada.
- Hosseinipour, S.M., Mujumdar, A.S., 1997, A model for superheated steam drying of particles in an impinging streams dryer, pp. 537-574, in I. Turner and A.S. Mujumdar (Eds.) *Mathematical Modeling and Numerical Techniques in Drying Technology*, Marcel Dekker, New York.
- Hu, X., Liu, D., 1999, Experimental investigation on flow and drying characteristics of a vertical and semi-cyclic combined impinging streams dryer, *Drying Technology – An International Journal*, 17, pp. 1879-1892.
- Kitron, Y., Tamir, A., 1988, Performance of a coaxial gas-solid two-impinging streams reactor: hydrodynamics, residence time distribution, and drying heat transfer, *Industrial & Engineering Chemistry Research*, 27, pp. 1760-1767.
- Kleingeld, A.W., Lorenzen, L., Botes, F.G., 1999, The development and modelling of high-intensity impinging stream jet reactors for effective mass transfer in heterogeneous systems, *Chemical Engineering Science*, 54, pp. 4991-4995.
- Kudra, T., Mujumdar, A.S., 1989, Impinging stream dryers for particles and pastes, *Drying Technology – An International Journal*, 7, pp. 219-266.
- Kudra, T., Mujumdar, A.S., 1995, Impinging stream dryers, pp. 539-566, in A.S. Mujumdar (Ed.) *Handbook of Industrial Drying*, 2nd Edition, Marcel Dekker, New York.
- Lixing, Z., 1993, *Theory and Numerical Modeling of Turbulent Gas-Particle Flows and Combustion*, CRC Press, Boca Raton.
- Mujumdar, A.S., Devahastin, S., 2000, Fundamental principles of drying, pp. 1-22, in S. Devahastin (Ed.) *Mujumdar's Practical Guide to Industrial Drying*, Exergex, Montreal, Canada.

-
- Patankar, S.V., 1980, *Numerical Heat Transfer and Fluid Flow*, Hemisphere, Washington.
- Tamir, A., Elperin, I., Luzzatto, K., 1984, Drying in a new two impinging streams reactor, *Chemical Engineering Science*, 39, pp. 139-146.
- Tamir, A., 1994, *Impinging-Stream Reactors: Fundamentals and Applications*, Elsevier, Amsterdam.
- Wu, G., Wu, Y., 1997, Resistance of impinging stream contactor to solid-air suspensionflow, *Chinese Journal of Chemical Engineering*, 5, pp. 270-279.
- Yoshida, H., Suenaga, K., Echigo, R., 1990, Turbulence structure and heat transfer of a two-dimensional impinging jet with gas-solid suspensions, *International Journal of Heat and Mass Transfer*, 33, pp. 859-867.

**CONCLUSIONS, CONTRIBUTIONS TO KNOWLEDGE
AND RECOMMENDATIONS**

*This is not the end.
It is not even the beginning of the end.
But it is the end of the beginning
Winston Churchill*

6.1. CONCLUSIONS

This thesis has examined the fluid mechanics, heat transfer as well as mixing characteristics of two-dimensional confined impinging streams (IS) operated in both laminar and turbulent flow regimes. Drying characteristics of a novel two-dimensional flash dryer based on this flow configuration has also been investigated. The following conclusions are made based on these studies:

I. Laminar impinging streams

- The Reynolds numbers beyond which the flow displays periodicity and in some cases random fluctuations were identified for different geometric configurations of the IS. It is found that this transition Reynolds number depends strongly on the geometric parameter viz. the ratio of the height of the exit channel (H) to the width of the inlet jets (W), especially at lower values of this ratio.
- For each geometric configuration of the laminar IS, a longer exit channel is required to obtain the well-mixed condition as the inlet jet Reynolds number increases. For

the same inlet jet Reynolds number, it is found that the distance to attain the well-mixed condition increases dimensionlessly but decreases dimensionally with H/W . Very good mixing is obtained over a rather short distance for all cases examined, however.

- A simple technique to improve mixing viz. offsetting the top and bottom inlet jets with respect to their centerlines, is proposed. It is found that this simple concept yields good mixing over a rather short distance in the channel mixer. Recirculation zones are observed only on one side (either near the top or bottom wall) of each pair of top and bottom jets due to the offset; each jet prevents formation of the recirculation bubble on the opposite wall. The absence of these recirculating zones is beneficial as it results in a more uniform mixing in the channel. Larger spacing between the inlet jets (higher S/W) results in better mixing in the region between these jets but yields no differences in the required channel length (between the last inlet and the exit port) to obtain the well-mixed condition at the exit. Higher Re_j also leads to better mixing in the region between the inlet jets but to a poorer mixing in any other regions. This effect is, however, less clear at higher S/W due to the longer time available for fluid to mix in the region between the inlets. Increasing H/W leads to more uniform but poorer mixing.

II. Turbulent impinging streams

- A new composite turbulence model is proposed and verified by comparing its predictions with available experimental impingement heat transfer data as well as the experimental velocity, turbulence intensity and temperature distributions in impinging streams obtained in the present work. The model is found to give better agreement between experimental and numerical impingement heat transfer results than two other low-Reynolds number $k-\varepsilon$ models tested.
- The maximum deviation of about 25% between numerical and experimental temperature distributions was observed. However, this high level of deviation may be attributed to the simplifying assumption of constant physical fluid properties and the adiabatic wall boundary condition used in the simulation since the model predicts the

results well in the region where the flow condition was similar but with lower inlet temperature.

- The composite model overestimates the velocity in the near-wall region (up to about 20%) but slightly underestimates (approximately 7%) it in the region far away from the wall. Similar trend is observed when comparing numerical and experimental distributions of the turbulence intensity. The near-wall measurements, however, are subjected to higher errors due to the reflection of the laser light from the edge of the model IS used in the experiments. The use of an LDV operated in the front-scattering mode may alleviate this problem.
- It is found that, for each H/W , as the jet Reynolds number increases mixing is better until a critical value of x/W beyond which the mixing behavior is reversed is reached. Increasing H/W results in reduced effect of Re_j on mixing at low x/W values. The effect is more pronounced at higher inlet jet turbulence intensity particularly at high Re_j . For each Re_j and turbulence intensity increasing H/W leads to better mixing at low x/W values but poorer mixing at x/W values beyond the critical value.

III. Gas-particle impinging streams

- Continuous-phase turbulence behavior of the gas-particle flow in IS was modeled using the composite model proposed in Chapter 4. Reasonable agreement between numerical and available experimental gas-particle impinging jet flow data is obtained despite the simplifying model assumptions and the lack of complete boundary conditions for the simulation.
- Drying is found to occur mainly in the impingement region of IS and its vicinity; once particles leave this region very little drying takes place.
- Drying is achieved to a lesser extent for smaller particles than for larger particles due to their smaller inertia and hence smaller mean residence time in the impingement region.
- Increasing inlet gas temperature does not yield expected results in this case due to the use of the variable fluid properties assumption and fixed inlet dimensionless

boundary conditions. Different results may be obtained for fixed mass flowrate operation, however.

6.2. CONTRIBUTIONS TO KNOWLEDGE

As a result of the present study, the following contributions to knowledge are made:

- Fundamental transport processes in laminar IS have been studied in detail. The transition Reynolds numbers beyond which the flow displays periodicity and even randomly fluctuates have been identified for different geometric configurations of IS. The physical relationship between the flow and heat transfer behavior of the system has also been investigated and explained thoroughly.
- A novel conceptual design of an in-line fluid mixer has been proposed and verified numerically. The mixer has a potential of replacing a conventional in-line mixer for high-viscosity fluids due to the absence of any mechanical obstructions in the channel, which are potential sources for fouling and also high pressure drop. The problem of air entrapment in the fluids would also be alleviated in this design compared to the mixing in a conventional mixing vessel. Chemical reactions could also be conducted simultaneously.
- A new composite turbulence model is proposed in this work. A laser Doppler velocimeter (LDV) was used to obtain the velocity and turbulence intensity distributions in a two-dimensional IS set-up and comparison was made between the data and those obtained using the composite model. Heat transfer experiments were also conducted to obtain the temperature distributions in IS for verification of the predictive ability of the model. This represents the first attempt to develop a reliable model for turbulent transport processes in an IS configuration, and to verify it with appropriate experimental data. The model gives results, which are in reasonable agreement with the data. Also, it results in a much faster convergence than do the two other low-Reynolds number k - ϵ models tested. Clearly, more extensive testing of the model is needed for both IS flows and other impingement-type flows.

- Turbulent mixing in IS has been studied using the newly proposed composite model. The effects of various geometric as well as operating parameters (including the inlet jet turbulence intensity) on the mixing behavior have been investigated.
- A composite model has been extended and applied to the study of gas-particle flow and drying in IS; previous studies were conducted using the standard high-Reynolds number $k-\varepsilon$ model, which is known to inaccurately predict the turbulence behavior of the flow in IS. Reasonable agreement between the numerical and experimental results available in the literature is obtained using this new model.
- Drying characteristics of a two-dimensional flash dryer based on an IS flow configuration have been studied using the gas-particle transport model proposed in the present study. Effects of various operating parameters on the drying performance of this dryer have been illustrated.

6.3. RECOMMENDATIONS

The following tasks may be worth considering in the future studies of IS:

I. Laminar impinging streams

- Experiments should be performed to verify the validity of the flow regime diagram, Figure 3.5. Wider ranges of geometric and operating parameters should be explored
- Mixing of different (non-matched) Newtonian and/or non-Newtonian fluids in IS should be investigated either numerically or experimentally.
- Experimental verification of the novel conceptual design of an in-line mixer should be performed. The effect of the degree of jets offsetting on mixing should also be investigated. Other operations than mixing, e.g., chemical reactions, combustion, could also be attempted.

II. Turbulent impinging streams

- Detailed velocity, turbulence intensity as well as temperature distributions in the vicinity of the impingement region should be measured. This information will allow the further confirmation and/or modification of the turbulence model. Advanced flow measuring system, e.g., particle image velocimeter (PIV) would be very useful for this purpose.
- Higher-order models, e.g., Reynolds stress model (RSM), should be tested and results obtained with those models should be compared with the one presented here.
- The composite model should be verified against a wider range of flow problems in order to assess its usability as a general turbulence model.

III. Gas-particle impinging streams

- The turbulence modulation terms should be incorporated in the model. In addition, the particle-particle and more advanced particle-wall interactions should be considered. Again, the use of advanced flow measuring systems, e.g., PIV, would be very helpful.
- Wider ranges of geometric and operating parameters should be explored.
- Experiments should be performed to verify the numerical results presented in this study. Other drying media could be used. Multi-stage operation is also worth investigating.